EFFECTS OF THE ELECTRONIC SPIN TRANSITIONS OF IRON IN LOWER MANTLE MINERALS: IMPLICATIONS FOR DEEP MANTLE GEOPHYSICS AND GEOCHEMISTRY

Jung-Fu Lin,[1] Sergio Speziale,[2] Zhu Mao,[1] and Hauke Marquardt[2]

Received 5 September 2012; revised 27 March 2013; accepted 5 April 2013; published 17 June 2013.

[1] We have critically reviewed and discussed currently available information regarding the spin and valence states of iron in lower mantle minerals and the associated effects of the spin transitions on physical, chemical, and transport properties of the deep Earth. A high-spin to low-spin crossover of Fe^{2+} in ferropericlase has been observed to occur at pressure-temperature conditions corresponding to the middle part of the lower mantle. In contrast, recent studies consistently show that Fe^{2+} predominantly exhibits extremely high quadrupole splitting values in the pseudo-dodecahedral site (A site) of perovskite and post-perovskite, indicative of a strong lattice distortion. Fe^{3+} in the A site of these structures likely remains in the high-spin state, while a high-spin to low-spin transition of Fe^{3+} in the octahedral site of perovskite occurs at pressures of 15–50 GPa. In post-perovskite, the octahedral-site Fe^{3+} remains in the low-spin state at the pressure conditions of the lowermost mantle. These changes in the spin and valence states of iron as a function of pressure and temperature have been reported to affect physical, chemical, rheological, and transport properties of the lower mantle minerals. The spin crossover of Fe^{2+} in ferropericlase has been documented to affect these properties and is discussed in depth here, whereas the effects of the spin transition of iron in perovskite and post-perovskite are much more complex and remain debated. The consequences of the transitions are evaluated in terms of their implications to deep Earth geophysics, geochemistry, and geodynamics including elasticity, element partitioning, fractionation and diffusion, and rheological and transport properties.

Citation: Lin, J.-F., S. Speziale, Z. Mao, and H. Marquardt (2013), Effects of the electronic spin transitions of iron in lower mantle minerals: Implications for deep mantle geophysics and geochemistry, *Rev. Geophys.*, *51*, 244–275, doi:10.1002/rog.20010.

1. INTRODUCTION

[2] The Earth's lower mantle, as described in terms of a pyrolitic compositional model, is mainly composed of ferropericlase ((Mg,Fe)O; abbreviated as fp; approximately 20% in volume), aluminous silicate perovskite (Al-(Mg,Fe)(Si,Fe)O_3; hereafter called perovskite and abbreviated as Pv; approximately 75% in volume), and calcium silicate perovskite ($CaSiO_3$; approximately 5% in volume) (Figure 1) [e.g., *Ringwood*, 1982; *Irifune* 1994; *Irifune and Isshiki*, 1998; *Irifune et al.*, 2010]. Silicate perovskite transitions to silicate post-perovskite ((Mg,Fe)(Si,Fe)O_3; abbreviated as PPv) at pressure-temperature (*P-T*) conditions of the lowermost mantle and is expected to be stable only within the D″ layer just above the core-mantle boundary [e.g., *Murakami et al.*, 2004; *Oganov and Ono*, 2004; *Hirose*, 2006]. It should be cautiously noted that the exact mineral proportions of the lower mantle remain highly uncertain and debated [e.g., *Ricolleau et al.*, 2009; *Murakami et al.*, 2012]. Specifically, Mid-Ocean Ridge Basalt (MORB) assemblages at lower mantle P-T conditions are expected to contain high-pressure silica and Al-rich phases, and ferropericlase may be absent [*Irifune and Ringwood*, 1987, 1993].

[3] Physical and chemical properties of planetary materials directly reflect the electronic structures and bonding characters of the constituting atoms. The configuration and interaction of the outermost shell electrons of the atoms is of particular importance in understanding earth materials. Under the extreme high *P-T* conditions of the deep Earth, however, the electronic configurations can be significantly altered, causing an electronic spin-pairing transition. This transition

[1]Department of Geological Sciences, Jackson School of Geosciences, University of Texas at Austin, Austin, Texas, USA.
[2]Helmholtz Center Potsdam, German Research Center for Geosciences GFZ, Potsdam, Germany.

Corresponding author: J-F. Lin, Department of Geological Sciences, Jackson School of Geosciences, University of Texas at Austin, Austin, TX 78712, USA. (afu@jsg.utexas.edu)

8755-1209/13/10.1002/rog.20010
Paper number 2012RG000414

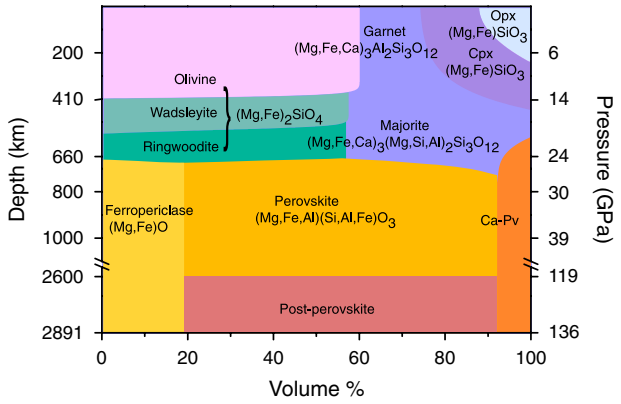

Figure 1. Mineralogical model of the Earth's interior as a function of depth (pressure). The mineral volume percentage is based on literature results for a pyrolite compositional model [e.g., *Ringwood*, 1982; *Irifune* and *Isshiki*, 1998; *Irifune et al*., 2010; *Hirose*, 2006]. Mineral abbreviation: Opx and cpx, orthopyroxene and clinopyroxene, respectively; CaPv, calcium silicate perovskite.

can, in turn, significantly affect the properties of the materials that compose the interior of our planet. Indeed, pressure-induced electronic spin-pairing transitions of iron and their associated effects, postulated nearly 50 years ago by *Fyfe* [1960] and later predicted by ab initio computations by *Cohen et al*. [1997], have recently been reported for lower mantle minerals at high pressures [e.g., *Badro et al*., 2003, 2004; *Li et al*., 2004; *Li et al*., 2005a; *Lin et al*., 2005]. Here we review what is known about the nature of the spin transitions, focusing on the effects of spin transitions on the thermoelastic, chemical, rheological, and transport properties of the lower mantle minerals at relevant *P-T* conditions.

[4] Iron is the most abundant transition metal within the Earth and features 3*d* electronic shells which can be partially filled, allowing for more complex structures than other major rock-forming elements. Iron exhibits two main valence states in lower mantle materials: ferrous iron (Fe^{2+}), with six 3*d* electrons, and ferric iron (Fe^{3+}), with five 3*d* electrons [e.g., *Cohen et al*., 1997; *McCammon*, 1997, 2006] (Figure 2). High *P-T* experimental results for pyrolitic compositions show that the concentration of iron is approximately 20 mol% in ferropericlase, where it exists mainly as ferrous iron (Fe^{2+}). Perovskite and post-perovskite each contain approximately 10 mol% iron, although both can contain very high amounts of ferric iron (in the case of perovskite, up to ~50–70% of total Fe) at lower mantle conditions [e.g., *Frost et al*., 2004; *McCammon*, 1997, 2006; *Irifune et al*., 2010]. The ionic radii and electronic configurations of the high-spin and low-spin states of iron ions in the same crystallographic site are intrinsically different [*Shannon and Prewitt*, 1969; *Shannon*, 1976; *Burns*, 1993]. For example, the ionic radius of the Fe^{2+} in the sixfold octahedral site is 0.78 Å for the high-spin state and 0.61 Å for the low-spin state. This difference is 0.17 Å (22%) in the ionic radius or 52% in volume between high-spin and low-spin states. On the other hand, all six 3*d* electrons of the low-spin Fe^{2+} are paired in the outer shell orbitals, whereas high-spin Fe^{2+} has four unpaired electrons occupying electronic orbitals. That is, the spin transition of iron in lower mantle minerals can result in significant changes in physical (e.g., density and bulk modulus), transport (e.g., electrical conductivity and radiative heat transfer), and chemical (e.g., element partitioning) properties (see further discussions below).

2. SPIN TRANSITIONS IN MANTLE MINERALS

[5] Classically, crystal field theory (CFT) has been successfully used to describe the electronic structure of transition metal compounds with the positively charged metal cation and the negative charge on the nonbonding electrons of the ligand [*Burns*, 1993]. The metal's five degenerate *d*-orbitals experience specific energy changes when surrounded by certain symmetries of ligands, which act as point charges. In combination with molecular orbital theory, CFT can be transformed to ligand field theory (LFT), which allows for a better understanding of the process of chemical bonding, electronic orbital structures, and other characteristics of coordination complexes.

[6] Take, for example, an octahedron in which six ligands, each positioned along a Cartesian axis, form an octahedral shape around a metal ion, such as the FeO_6 octahedron in the lower mantle ferropericlase (Figure 2a) [*Lin and Tsuchiya*, 2008a]. Based on CFT [*Burns*, 1993], the *d*-orbitals of the metal Fe^{2+} ion in this complex split into two sets with an energy difference Δc (the crystal-field octahedral splitting parameter). The d_{z^2} and $d_{x^2-y^2}$ orbitals lie along Cartesian axes and will therefore experience an increase in energy due to repulsion caused by their proximity to the ligands [*Burns*, 1993] (Figure 2a). The d_{xy}, d_{xz}, and d_{yz} orbitals do not lie directly along any Cartesian axes but lie instead in planes between the ligands and are thus lower in energy than the d_{z^2} and $d_{x^2-y^2}$, actually being stabilized. The three lower-energy orbitals are collectively referred to as t_{2g} and the two higher-energy orbitals as e_g. It should be noted, however, that the orbital splitting energies are directly related to the specific molecular coordination geometry of the complex. Thus, a tetrahedral ligand arrangement causes the t_{2g} orbitals to be higher in energy than the e_g orbitals and has a crystal-field splitting energy of Δc. The occupation of the 3*d* orbitals is defined by the surrounding environment of the iron ion and influenced by factors such as bond length, crystallographic site, pressure, and temperature, some of which can be interconnected.

[7] Based on the crystal field theory, the spin transition of iron in lower mantle phases is volume driven and results primarily from the competition between two quantities: the Δc and the exchange splitting energy (Λ) [e.g., *Burns*, 1993] (Figure 2b). For Fe^{2+} in the octahedral site of ferropericlase, for example, the 3*d* electrons of iron can occupy different degenerate sets of the 3*d* orbitals, namely the relatively lower-energy triplet t_{2g} orbitals and the relatively high-energy doublet e_g orbitals. Under ambient conditions in silicates and oxides, it is energetically favorable for the 3*d* electrons to occupy different orbitals with the same electronic spin, specifically the high-spin state with four unpaired electrons and two

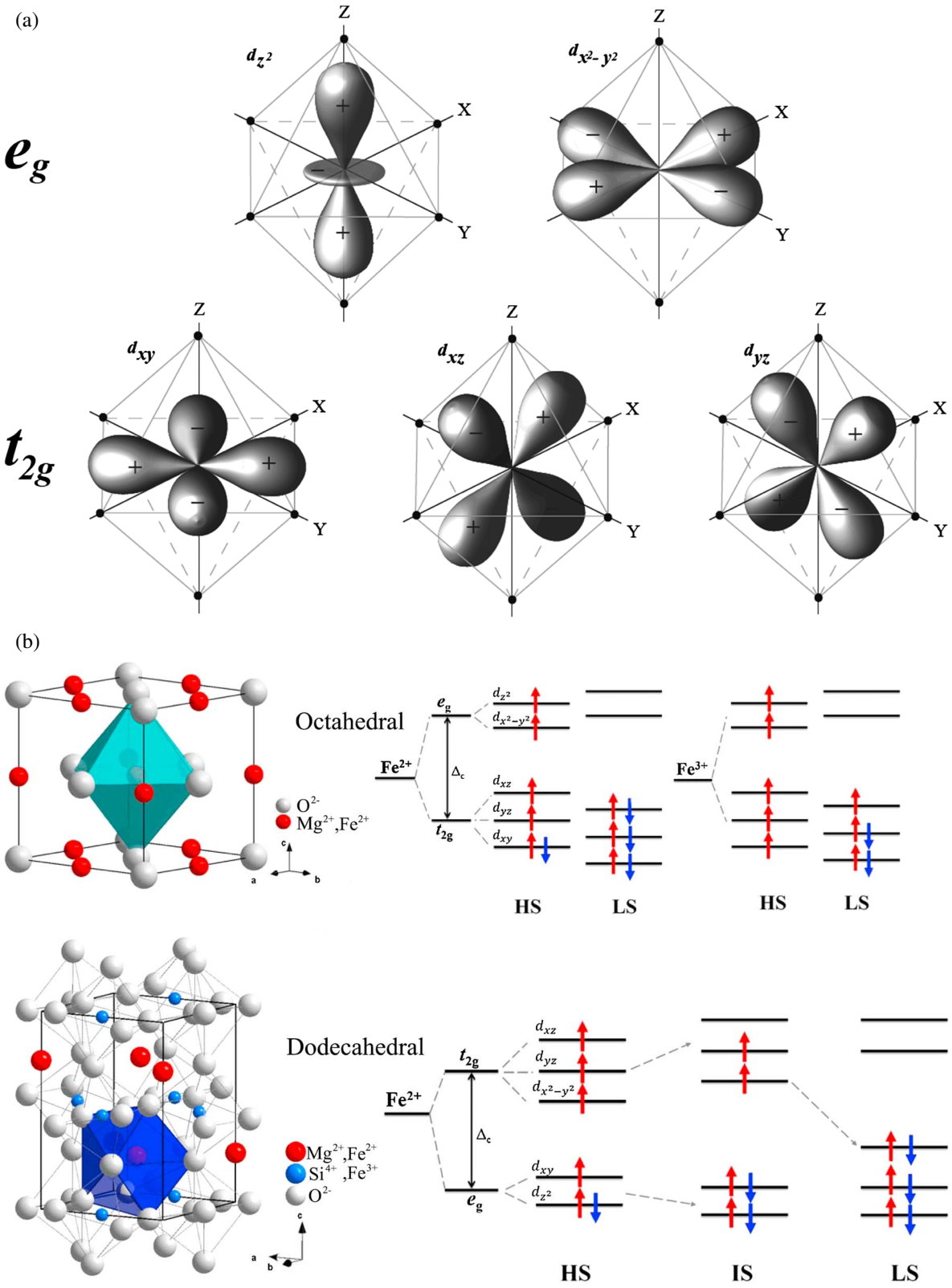

Figure 2. (a) *d*-orbital configurations in an octahedral site are shown to demonstrate the spatial organization of the ligands with respect to the orbitals along the Cartesian axes. (b) Crystal structures of lower mantle ferropericlase (upper left) and silicate perovskite (bottom left). Cubic ferropericlase is in the rock salt structure (space group: $Fm\bar{3}m$), whereas orthorhombic perovskite is in the *Pbnm* space group. Crystal field splitting diagrams with the crystal field splitting energy (Δc) for iron in the octahedral and dodecahedral sites are also shown for these structures (right figures). Iron is shown as Fe^{2+} in the high-spin, intermediate-spin, and/or low-spin electronic configurations in the octahedral and dodecahedral sites, respectively. Electronic configurations of Fe^{3+} can be understood by having five electrons in the 3*d* orbitals.

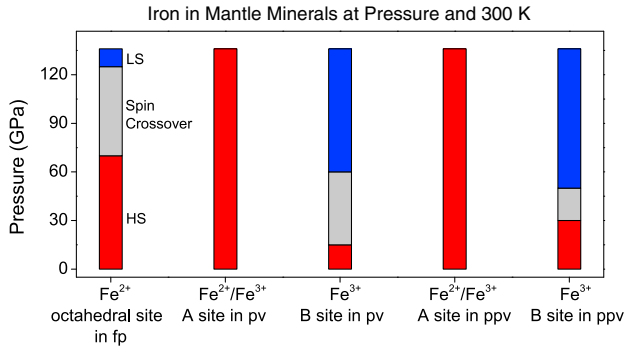

Figure 3. Spin states of iron in lower mantle phases as a function of pressure. Red: high-spin state; grey: spin crossover region; blue: low-spin state. Both theoretical and experimental results are used for the summary, whereas the high quadrupole component of the A-site Fe^{2+} in perovskite and post-perovskite is grouped together in the high-spin state. See Figures 4–6 and sections 2.1 and 2.2 for details.

paired electrons in Fe^{2+} (the total spin quantum number (S) is equal to 2 because each electron has $S=1/2$). In this case, the hybridized t_{2g} and e_g orbitals of the sixfold-coordinated Fe^{2+} are separated by the crystal-field splitting energy, which is lower than the electronic spin-pairing energy (Figure 2b). However, changes in *P-T*, site occupancy, and/or composition can have influences on the crystal-field splitting energy with respect to the spin-pairing energy. Under high pressures, the crystal-field splitting energy increases with respect to the spin-pairing energy, eventually leading to the pairing of the 3*d* electrons of the opposite spin, that is, the low-spin state with all six 3*d* electrons paired in the low-spin Fe^{2+} ($S=0$) (Figure 2b). The electronic density distribution of the 3*d* shell of the high-spin Fe^{2+} ions in the octahedral coordination is non-spherical with $S=2$ and $t_{2g\uparrow}^3 e_{g\uparrow}^2 t_{2g\downarrow}^1$, whereas Fe^{2+} ions in the low-spin state are more spherically symmetric with $S=0$ and $t_{2g\uparrow}^3 t_{2g\downarrow}^3$ (arrows indicate spin up or spin down, and superscripted numbers represent the orbitals' occupancies) [e.g., *Burns*, 1993]. In silicate perovskite and post-perovskite, this simplified crystal-field picture for the pressure-induced spin transition becomes more complex through crystallographic site distortion and electronic band overlap where occupancy degeneracy is lifted (Figure 2b) [e.g., *Burns*, 1993], complicating our understanding of the spin transition in these systems (see *Lin and Tsuchiya* [2008] and *Wentzcovitch et al.* [2012] for additional review). Figure 3 summarizes our current understanding of the spin states of iron in lower mantle phases as a function of pressure. Detailed discussions are presented below in sections 2.1 and 2.2.

2.1. Spin Transition in Ferropericlase

[8] Ferropericlase with a cubic rock-salt structure refers to a MgO-rich composition in the solid solution series between end-member periclase (MgO) and wüstite ($Fe_{1-X}O$) (X indicates the nonstoichiometric nature of the compound and typically has a value of 0.04–0.12). Lower mantle ferropericlase contains approximately 20% Fe^{2+} in the octahedral site of the crystal structure, and the presence of Fe^{3+} is typically lower than 1% [e.g., *McCammon et al.*, 1998]. A pressure-induced spin-pairing transition of Fe^{2+} in ferropericlase has been reported to occur over a narrow pressure range of 40–60 GPa at room temperature using a number of high-pressure diamond anvil cell (DAC) techniques in conjunction with X-ray and laser spectroscopies as well as theoretical calculations (Figure 3) [e.g., *Badro et al.*, 2003; *Lin et al.*, 2005] (see *Lin and Tsuchiya* [2008] for a review). However, a few high-pressure conventional Mössbauer studies report broader transition pressure ranges, probably due to the large sample size and the development of large pressure gradients (argon, ethanol-methanol pressure medium, or no medium was used) in the analyzed samples [*Speziale et al.*, 2005; *Kantor et al.*, 2006, 2009]. The disappearance of the quadrupole splitting in Mössbauer spectroscopy (MS) and the Kβ' satellite peak intensity in X-ray emission spectroscopy (XES) is indicative of the spin transition at high pressures.

[9] Most importantly, the spin transition broadens into a smooth crossover at relevant *P-T* conditions of the lower mantle; the respective region is referred to as the spin transition zone (STZ) (Figure 4) [e.g., *Sturhahn et al.*, 2005; *Tsuchiya et al.*, 2006; *Lin et al.*, 2007a; *Wentzcovitch et al.*, 2009; *Mao et al.*, 2011a]. The spin crossover arises from a condition in which the thermal energy at high *P-T* is sufficient to overcome the energy difference between the high-spin and low-spin states [e.g., *Sturhahn et al.*, 2005; *Tsuchiya et al.*, 2006]. The fraction of the low-spin state (n_{LS}) at a given *P-T* condition is shown theoretically and experimentally to be satisfactorily described by

$$n_{LS} = \frac{1}{1 + \exp(\Delta G(P,T)^*/T)} \quad (1)$$

where $\Delta G(P,T)^*$ is the difference of the Gibbs free energy between the low-spin and high-spin states [*Tsuchiya et al.*, 2006; *Speziale et al.*, 2007; *Wentzcovitch et al.*, 2009; *Mao et al.*, 2011a]. Along an expected lower mantle geotherm [*Brown and Shankland*, 1981], experimental results show that the crossover starts at approximately 70 GPa (1700 km depth) and 2200 K and completes at approximately 125 GPa (2700 km depth) and 2400 K (Figure 4) [*Lin et al.*, 2007a;

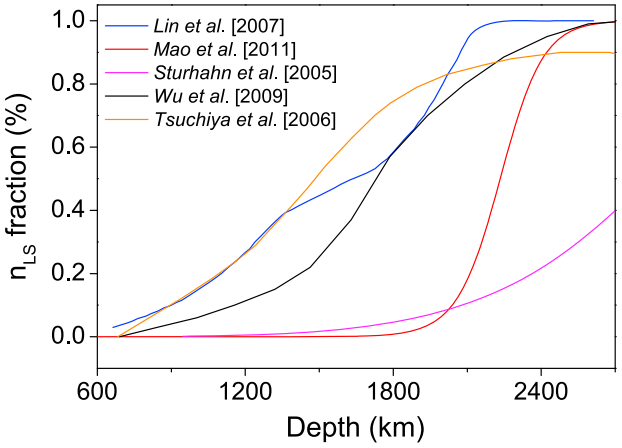

Figure 4. Electronic spin crossover of iron in ferropericlase (Mg,Fe)O along an expected lower mantle *P-T* path by *Brown and Shankland* [1981]. n_{LS}: low-spin fraction of Fe^{2+} in the octahedral site in ferropericlase.

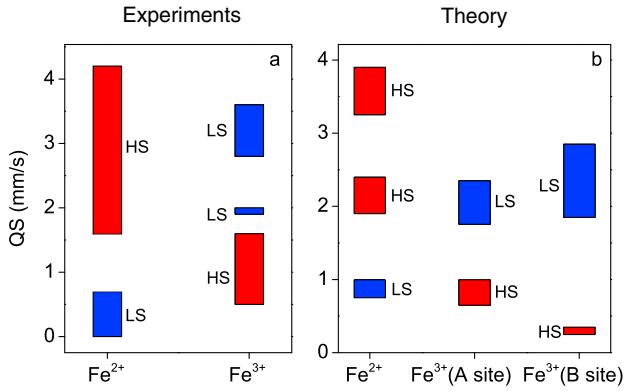

Figure 5. Quadrupole splitting (QS) of Fe^{2+} and Fe^{3+} in silicate perovskite from recent experimental and theoretical results at high pressures [e.g., *Jackson et al.*, 2005; *Li et al.*, 2006; *Lin et al.*, 2008, 2012a; *Grocholski et al.*, 2009; *Catalli et al.*, 2010a; *Hsu et al.*, 2010, 2011, *McCammon et al.*, 2008a, 2010; *Bengtson et al.*, 2008, 2009; *Narygina et al.*, 2009; *Mao et al.*, 2011a]. (a) Experimental results; (b) theoretical results. Red boxes: high-spin state; blue boxes: low-spin state. The QS range for a specific spin state reflects the effect of pressure and uncertainties in various studies. A and B represent A-site and B-site of Fe in perovskite, respectively. The extremely high QS component of Fe^{2+} is grouped and labeled as the HS state here (see section 2.2. for further discussions).

Mao et al., 2011a]. Thus, the spin crossover can occur in the middle to lower part of the lower mantle, and the high-spin and low-spin states of ferropericlase can exist in the uppermost and lowermost mantle, respectively [*Tsuchiya et al.*, 2006; *Lin et al.*, 2007a; *Wentzcovitch et al.*, 2009; *Mao et al.*, 2011a]. Due to the continuous nature of the spin crossover, the effects of the spin crossover of iron at relevant *P-T* of the lower mantle are expected to occur over a broader pressure range than those reported at ambient-temperature conditions. That is, the consequences of the spin crossover on geophysical and geochemical properties of the mantle may not be as evident, although a number of unexpected behaviors can also occur through the fluctuation of the fraction of the high-spin and low-spin states (see section 3, Effects of the Spin Transition, for details).

2.2. Spin and Valence States of Iron in Silicate Perovskite

[10] Aluminum-containing silicate perovskite stabilizes in the orthorhombic structure (space group: *Pbnm*) in the lower mantle (Figure 2), in which Al^{3+} substitutes for Si^{4+} in the octahedral site, requiring a charge-coupled substitution and/or a cation vacancy to retain charge neutrality. Experimental and theoretical studies suggest that iron in perovskite can exist in Fe^{2+} and Fe^{3+} states, and can possibly occupy one of two crystallographic sites: the large pseudo-dodecahedral Mg^{2+} site (A site) or the small octahedral Si^{4+} site (B site) (Figure 2) [e.g., *McCammon*, 2006; *Hsu et al.*, 2010, 2011]. Current consensus on the site occupancy holds that Fe^{2+} mainly substitutes for Mg^{2+} in the larger A site, while Fe^{3+} occupies both the A and B sites. The abundance of Fe^{3+} in the A and B sites appears to strongly depend on the Al content of perovskite and can also be affected by the thermodynamic history (e.g., heating or annealing) of the sample [*Hsu et al.*, 2010, 2011; *Fujino et al.*, 2012].

[11] Under ambient conditions, both Fe^{2+} and Fe^{3+} in perovskite exist in the high-spin state [e.g., *McCammon*, 2006; *McCammon et al.*, 2008a, 2008b; *Hsu et al.*, 2010, 2011; *Lin et al.*, 2012a]. Recently, electronic spin states of Fe^{2+} and Fe^{3+} in silicate perovskite have been extensively studied at high pressures [e.g., *Badro et al.*, 2004; *Li et al.*, 2004, 2006; *Jackson et al.*, 2005; *Stackhouse et al.*, 2006, 2007; *Bengtson et al.*, 2008, 2009; *Grocholski et al.*, 2009; *Catalli et al.*, 2010a, 2011; *Hsu et al.*, 2010, 2011, 2012; *McCammon et al.*, 2008a, 2008b; *Fujino et al.*, 2012; *Lin et al.*, 2012a; *Metsue and Tsuchiya*, 2012]. The interpretations of these results have been quite different, although some general trends have been identified in experimental Mössbauer and X-ray emission spectroscopic studies as well as in theoretical predictions. Both experimental and theoretical studies have reported extremely high hyperfine quadruple splitting (QS) values of Fe^{2+} (as high as ~4.4 mm/s) above approximately 30 GPa [e.g., *Jackson et al.*, 2005; *McCammon et al.*, 2008a; *Grocholski et al.*, 2009; *Hsu et al.*, 2010, 2011; *Bengtson et al.*, 2009; *Lin et al.*, 2012a] (Figure 5), while a reduced intensity of the Fe Kβ' satellite emission was observed with increasing pressure [*Badro et al.*, 2004; *Li et al.*, 2004, 2006; *Fujino et al.*, 2012]. Combined with previous X-ray emission spectroscopic analyses for the total spin momentum of iron in perovskite [*Badro et al.*, 2004; *Li et al.*, 2004, 2006], the extremely high QS has been interpreted as a result of the occurrence of the intermediate-spin Fe^{2+} with a total spin momentum of one ($S = 1$) in the A site starting at around 30 GPa [*Lin et al.*, 2008; *McCammon et al.*, 2008a, 2010; *Narygina et al.*, 2010]. First-principles theoretical calculations, however, show that the A-site Fe^{2+} is stable in the high-spin state at all mantle pressures and that the extremely high QS component is a result of a change of Fe-O distances related to the A site (redistribution of Fe^{2+} in the A site) [*Bengtson et al.*, 2009; *Hsu et al.*, 2010, 2011; *Metsue and Tsuchiya*, 2012], rather than the high-spin to the intermediate-spin transition [e.g., *McCammon et al.*, 2008a; *Narygina et al.*, 2010]. We note that the high QS value is not unique to the intermediate-spin state, as iron-bearing pyrope in the high-spin state exhibits the largest quadrupole splitting (QS) in Mössbauer spectra among all common Fe-bearing rock-forming silicate minerals at ambient conditions; garnet exhibits extremely high QS values of 3.47–3.58 mm/s [*Černá et al.*, 2000]. The collapse of the QS in the A-site Fe^{2+} was reported to take place at approximately 120 GPa as a result of the occurrence of the low-spin Fe^{2+} [*McCammon et al.*, 2010].

[12] It has been shown both experimentally and theoretically that Fe^{3+} in perovskite enters into both A and B sites, suggesting a charge-coupled substitution mechanism [e.g., *McCammon et al.*, 1998]. Recent experimental and theoretical studies show that a high-spin to low-spin transition of the B-site Fe^{3+} occurs at approximately 15–50 GPa, which is associated with an increased QS value in the low-spin state (Figure 5) [e.g., *Jackson et al.*, 2005;

Stackhouse et al., 2007; *Catalli et al*., 2010a; *Hsu et al*., 2011; *Lin et al*., 2012a]. The A-site Fe^{3+} remains in the high-spin state to at least 136 GPa, i.e., over the entire pressure range of the lower mantle. These studies also suggest that Fe^{3+} remains in the high-spin state in Al-bearing perovskite in the A site, although site exchange between Al^{3+} and Fe^{3+} occurring at high *P-T* has been proposed to promote Fe^{3+} in the B site [e.g., *Grocholski et al*., 2009; *Catalli et al*., 2010a; *Hsu et al*., 2012].

[13] Based on the aforementioned discussion on the spin and valence states of iron in perovskite, it is most likely that the B-site Fe^{3+} undergoes a spin transition while the A-site Fe^{2+} and Fe^{3+} remain in the high-spin state (Figure 3). These results can be understood in terms of a volume-driven spin transition of iron in the octahedral coordination, which is more favorable for the spin transition than any other coordination because of the alignment of negative charges (oxygen ions) along particular *d*-orbitals of iron ions. One possible explanation to reconcile recent Mössbauer and X-ray emission results is that some of the observed Kβ' intensity reduction may be affected by pressure-induced broadening effects [e.g., *Lin et al*., 2005], which have been previously neglected in the data processing. In the X-ray emission data analyses, it had been assumed that the Kβ emission line shape was not affected by applied pressures. Further examinations of literature X-ray emission spectra of ferropericlase, however, show that a slight reduction in the satellite intensity can be seen before the well-defined spin transition at 40–60 GPa and that the low-spin state has much broader Kβ main peaks than the high-spin state [e.g., *Lin et al*., 2005, 2006a]. It is thus conceivable that part of the inferred reduction of the total spin momentum as derived from XES spectra is indeed due to our currently limited understanding of the emission process as a function of pressure. This notion of the broadening effect may also help us to understand the spin states of iron in perovskite and post-perovskite (see section 2.3 below).

2.3. Spin and Valence States of Iron in Silicate Post-Perovskite

[14] Post-perovskite is found to be stable in the $CaIrO_3$-type structure (*Cmcm*) at the *P-T* conditions of the lowermost mantle region, the D″ zone [e.g., *Murakami et al*., 2004; *Oganov and Ono*, 2004], while iron-rich post-perovskite has also been reported to exist in the *Pmcm* and *Pmma* space groups due to an ordered cation distribution in the crystallographic sites [*Yamanaka et al*., 2012]. It has been reported to accommodate significant amounts of Fe^{3+}, similar to perovskite [*Sinmyo et al*., 2006; *Jackson et al*., 2009]; however, other studies contradict this view [*Sinmyo et al*., 2008, 2011; *Mao et al*., 2010], and the exact amount and the site occupancy of Fe^{3+} merits further investigation. A number of kinked structures, formed by sliding the {010} planes of the perovskite structure with variation in the stacking sequence of SiO_6 octahedral layers, have also been reported to exist in post-perovskite [*Oganov et al*., 2005; *Tschauner et al*., 2008; *Mao et al*., 2010]. The corresponding plane slips in post-perovskite might introduce more crystallographic defects favorable for the substitution of Si by Fe^{3+}.

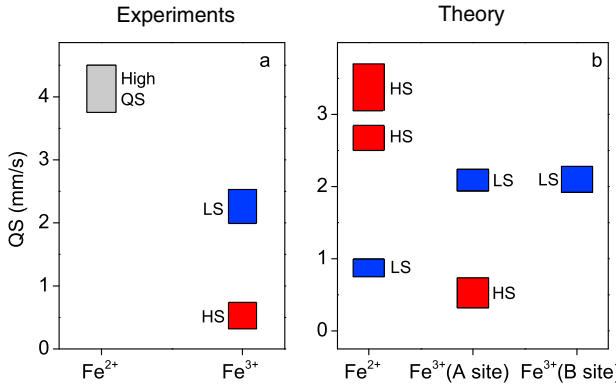

Figure 6. Quadrupole splitting of Fe^{2+} and Fe^{3+} and their assigned spin and valence states in post-perovskite [*Lin et al*., 2008; *Jackson et al*., 2009; *Catalli et al*., 2010b; *Mao et al*., 2010; *Yu et al*., 2012]. (a) Experiments; (b) theory. Red: high-spin state; blue: low-spin state. The extremely high QS component of Fe^{2+} is grouped and labeled as the high QS state in grey box here (see section 2.3 for further discussions).

[15] High-pressure Mössbauer spectroscopy results show that Fe^{2+} exhibits extremely high QS of 3.8–4.5 mm/s, indicating that Fe^{2+} likely substitutes Mg^{2+} in the bipolar-prismatic site (also called A site here for simplicity), similar to Fe^{2+} in the A site in perovskite [*Lin et al*., 2008; *Jackson et al*., 2009; *Mao et al*., 2010] (Figure 6). In conjunction with a complementary high *P-T* X-ray emission spectroscopic study, it has been suggested that iron predominantly exists in the intermediate-spin Fe^{2+} state with a total spin momentum of one in the *$CaIrO_3$*-type post-perovskite at relevant *P-T* conditions of the lowermost mantle [*Lin et al*., 2008; *Mao et al*., 2010]. Since the intermediate-spin Fe^{2+} is found in PPv with both 25 mol% and 40 mol% Fe, it is suggested that it is predominantly stable over a wide range of Fe content in post-perovskite relevant to the D″ region, where Fe-enrichment may be expected [*Mao et al*., 2004; *Lin et al*., 2008; *Mao et al*., 2010]. Analogous to the discussion for Fe^{2+} in perovskite, however, first-principles calculations suggest that Fe^{2+} in post-perovskite is in the high-spin state at all mantle pressures and that the intermediate-spin and low-spin states of the A-site Fe^{2+} are highly unfavorable energetically [*Stackhouse et al*., 2006; *Yu et al*., 2012]. Theoretical calculations also show that the A-site Fe^{2+} in the high-spin state can exhibit extremely high QS at lowermost mantle pressures [*Yu et al*., 2012], consistent with those observed in Mössbauer spectra [*Lin et al*., 2008; *Mao et al*., 2010]. That is, the extremely high QS component of the experimental Mössbauer spectra can be explained as a result of the lattice distortion similar to that of silicate perovskite. In this scenario, the reduction in the derived total spin momentum from the integration of the satellite intensity in the Fe Kβ emission spectra may be partially attributed to the pressure-induced broadening effect discussed earlier, together with the presence of the low-spin Fe^{3+} in the B site (Figures 3 and 6). It should be noted here that standard density-functional theory (DFT) does not describe the onsite Coulomb interactions between 3*d* electrons

of iron in iron-bearing minerals such as perovskite and post-perovskite properly, which can lead to difficulties in correctly predicting the electronic band gap as well as the stability of the spin and valence states of iron in the lower mantle phases. The DFT + Hubbard U (DFT + U) method, on the other hand, provides more reliable predictions and has been recently used to calculate hyperfine parameters of perovskite and post-perovskite that are consistent with experimental observations [*Hsu et al*., 2010, 2011; *Metsue and Tsuchiya*, 2012; *Yu et al*., 2012].

[16] High-pressure Mössbauer spectroscopic results on post-perovskite also suggest that Fe^{3+} exists in two different lattice sites of post-perovskite [*Jackson et al*., 2009; *Catalli et al*.,2010b; *Mao et al*., 2010]. The observed low QS is assigned to the high-spin Fe^{3+} in the bipolar-prismatic A site, whereas the high QS (~2 mm/s) is assigned to the low-spin Fe^{3+} in the octahedral B site [*Lin et al*., 2008; *Jackson et al*., 2009; *Catalli et al*., 2010b; *Mao et al*., 2010], consistent with theoretical calculations [*Yu et al*., 2012] (Figure 6). In this scenario, Fe^{3+} enters the sites through charge-coupled substitutions, which are also suggested by theoretical calculations [*Yu et al*., 2012]. Because the ionic radius of the low-spin Fe^{3+} is smaller than that of the high-spin Fe^{3+}, the low-spin Fe^{3+} is more stable in the smaller octahedral site in post-perovskite, consistent with a volume-driven spin transition behavior. The abundance of Fe^{3+} is observed to be affected by the presence of the kinked structures in post-perovskite [*Jackson et al*., 2009; *Mao et al*., 2010]. We note that anomalously high concentrations of Fe^{3+} could also be produced by thermal gradients in laser-heating syntheses as shown for perovskite [*Fialin et al*., 2009]. A small amount of metallic iron phase coexisting with Fe^{3+}-rich post-perovskite has been observed by *Jackson et al*. [2009], who proposed that the formation of metallic iron and Fe^{3+} in post-perovskite is achieved by disproportionation of Fe^{2+} to form iron metal and Fe^{3+}, similar to that in perovskite [*Frost et al*., 2004]. However, in a recent study, *Sinmyo et al*. [2011] did not observe metallic Fe associated with post-perovskite for a wide range of compositions.

[17] The notable difference between the Mössbauer parameters of the perovskite and post-perovskite phases is that the QS corresponding to the low-spin Fe^{3+} site is much smaller in post-perovskite. The smaller QS associated with the low-spin site in post-perovskite can be explained by a less distorted octahedral site, because distortion from a cubic environment around the iron nucleus results in an increased QS value [*Hawthorne*, 1988]. Since post-perovskite is the high-pressure polymorph of perovskite, the QS of Fe^{2+} in post-perovskite could be similar to that of Fe^{2+} in perovskite, as both phases exhibit extremely high QS values of approximately 4 mm/s (Figures 5 and 6).

2.4. Spin Transition in Magnesite-Siderite System

[18] Magnesite forms a continuous solid solution with siderite ($FeCO_3$) in the rhombohedral structure with the $R\bar{3}c$ space group. The electronic spin-pairing transition of Fe^{2+} in the magnesite-siderite system has been recently reported to occur at high pressures and room temperature experimentally and theoretically using high-pressure X-ray emission spectroscopy, X-ray diffraction, laser Raman spectroscopy, and first-principles calculations [*Mattila et al*., 2007; *Shi et al*., 2008; *Lavina et al*., 2009, 2010a, 2010b; *Nagai et al*., 2010; *Farfan et al*., 2012; *Lin et al*., 2012b]. These studies show that the transition at 42–50 GPa is accompanied by a volume reduction of approximately 6–10% and that the compositional effect on the transition pressure is small. It has been suggested that low-spin ferromagnesite with a smaller unit cell volume can become more stable than pure magnesite at relevant high *P-T* conditions of the mantle [e.g. *Lin et al*., 2012b]. Although high *P-T* experiments have shown that the solubility of iron in magnesite in rock assemblages is low, the low-spin ferromagnesite can become a potential deep carbon bearing mineral at mid-lower mantle conditions [*Dasgupta and Hirschmann*, 2010].

3. EFFECTS OF THE SPIN TRANSITION

[19] The geophysical relevance of the electronic spin transitions resides in their effects on the physical and chemical properties of lower mantle phases. Here we evaluate the consequences of the spin transitions on properties of lower mantle minerals. We have also evaluated literature data relevant to iron-bearing perovskite and post-perovskite in order to shed light on the potential effects of iron-magnesium substitution and the spin transition.

3.1. Thermal Equation of States

[20] Recent experimental and theoretical studies have shown that the pressure-induced electronic spin transition of iron results in a reduction in the unit cell volume of ferropericlase at high *P-T* conditions [e.g., *Lin et al*., 2005; *Fei et al*., 2007a; *Lin and Tsuchiya* 2008; *Wentzcovitch et al*., 2009] and may also cause changes in the unit cell volume of perovskite and post-perovskite [e.g., *Hsu et al*., 2010, 2011; *Catalli et al*., 2010a, 2010b, 2011; *Mao et al*., 2011b; *Yu et al*., 2012]. The obtained pressure-volume (*P-V*) relations are not only important to constrain the effect of the spin transitions on the thermoelastic properties of the host minerals but also critical to model the spin-crossover diagram in the lower mantle [*Lin et al*., 2005; *Sturhahn et al*., 2005; *Tsuchiya et al*., 2006; *Wu et al*., 2009; *Mao et al*., 2011a].

3.1.1. Ferropericlase

[21] The *P-V* relations of ferropericlase have been measured experimentally and been compared to those of pure end-member MgO in order to understand the effect of the spin transition of Fe on volume, density, and incompressibility of ferropericlase at high *P-T* conditions (Figure 7). High-spin ferropericlase has a larger unit cell volume than MgO due to the substitution of the larger Fe^{2+} cation for Mg^{2+}, but a volume reduction of a few percentage points occurs across the spin transition to the low-spin state. Once the spin transition is completed, the unit cell volume of ferropericlase with up to 39 mol% Fe has been found to be similar to or slightly lower than that of MgO at given *P-T* conditions of the lower mantle (Figure 7) [*Lin et al*., 2005; *Fei et al*., 2007a; *Speziale et al*., 2007; *Marquardt et al*.,

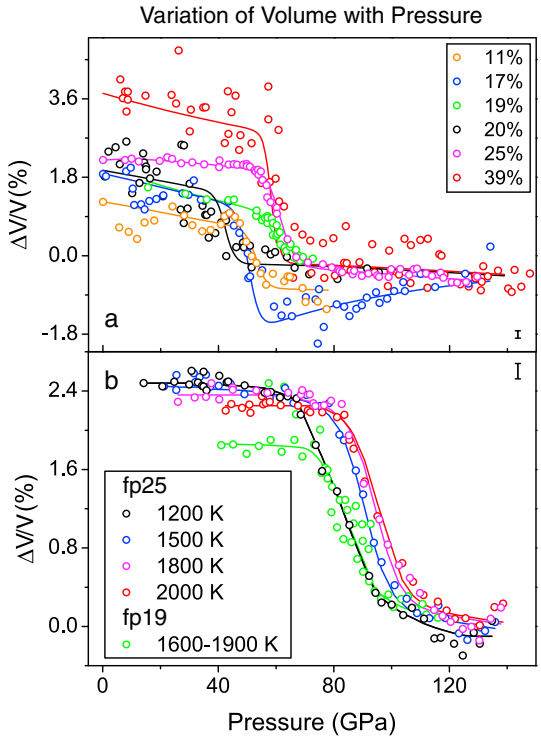

Figure 7. Relative volume deviation of ferropericlase with respect to MgO reference at high pressures. (a) 300 K. Orange circles: 10% Fe [*Marquardt et al*., 2009a, 2009b]; blue circles: 17% Fe [*Lin et al*., 2005; *Speziale et al*., 2007]; green circles: 19% Fe [*Komabayashi et al*., 2010]; black circles: 20% Fe [*Fei et al*., 2007a, 2007b]; magenta circles: 25 % Fe [*Mao et al*., 2011a]; red circles: 39% Fe [*Fei et al*., 2007a, 2007b]. (b) high temperatures. Black, blue, magenta, and red circles: 25% Fe at 1200 K, 1500 K, 1800 K, and 2000 K, respectively [*Mao et al*., 2011a]; green circles: 19% Fe at 1600–1900 K [*Komabayashi et al*., 2010]. Representative error bars are shown on the right bottom (a) and top (b) corners of the figure.

2009a; *Tange et al*., 2009; *Komabayashi et al*., 2010; *Mao et al*., 2011a]. The magnitude of the volume reduction is greater for ferropericlase with a higher Fe content but can be slightly reduced by elevating temperature at high pressures for a given composition [*Mao et al*., 2011a]. Overall, the volume reduction across the spin transition is in the order of 1.5 to 3% for ferropericlase with relevant lower mantle compositions (Figure 7), consistent with ~4% volume reduction predicted theoretically [*Tsuchiya et al*., 2006; *Wentzcovitch et al*., 2009].

[22] Comparison of the *P-V* relations of ferropericlase to those of MgO between the high-spin and low-spin states also provides constraints on the spin-crossover diagram of ferropericlase at high *P-T* conditions, as the unit cell volume change can be related to the high-spin and low-spin fractions (see Equation (1)) [*Mao et al*., 2011a]. Based on the experimentally measured *P-V* data, the onset of the spin transition at 300 K occurs at approximately 40–60 GPa (Figure 8a) [*Lin et al*., 2005; *Speziale et al*., 2007; *Marquardt et al*., 2009a; *Tange et al*., 2009; *Komabayashi et al*., 2010; *Mao et al*., 2011a], consistent with theoretical predictions [*Tsuchiya et al*., 2006; *Wentzcovitch et al*., 2009]. Nevertheless, *Fei et al*. [2007a, 2007b] reported a significantly lower onset pressure for ferropericlase with 20% Fe after thermal annealing. The onset and width of the spin transition does not exhibit any obvious compositional dependence at 300 K (Figure 8a) [*Lin et al*., 2005; *Fei et al*., 2007a, 2007b; *Speziale et al*., 2007; *Marquardt et al*., 2009a; *Komabayashi et al*., 2010; *Mao et al*., 2011a], in contrast to a theoretical study that showed an increase in the onset pressure with Fe content [*Persson et al*., 2006].

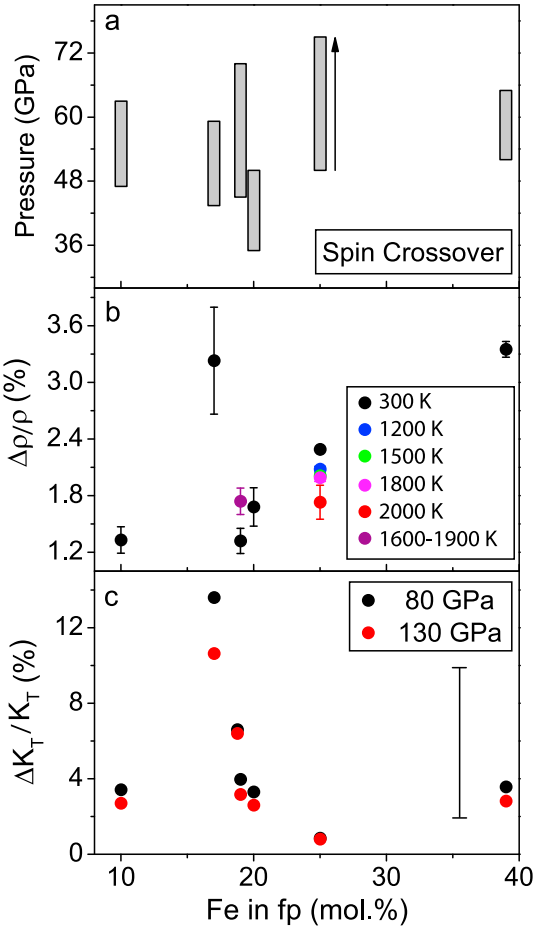

Figure 8. (a) Spin-crossover pressure, (b) change in density, and (c) isothermal bulk modulus of ferropericlase as a function of iron content. Arrow in Figure 8a shows the high-spin to low-spin transition of Fe in ferropericlase with increasing pressure. The variation of Fe content in ferropericlase is taken from *Lin et al*. [2005] (fp17), *Speziale et al*. [2005] (fp20), *Fei et al*., 2007a, 2007b (fp20 and fp39), *Marquardt et al*., 2009a, 2009b (fp10), *Komabayashi et al*. [2010] (fp19), and *Mao et al*. [2011a] (fp25). In Figures 8b and 8c, relative deviation in density (ρ) at various temperatures and isothermal bulk modulus (K_T) at 300 K is calculated using the high-spin state as the reference for each given composition. The calculated deviation in density at high temperature in Figure 8b is from *Komabayashi et al*. [2010] at 1600–1900 K and from *Mao et al*. [2011a] at 1200 K, 1500 K, 1800 K, and 2000 K. The density deviation is calculated at the pressure where the spin transition has been completed. Representative error bars are shown for $\Delta K_T/K_T$ on the right of Figure 8c. See Figure 7 for some of the data used here.

On the other hand, experimental *P-V-T* measurements, conducted under similar conditions by using same pressure calibrant material (Au) and pressure medium (NaCl) in conjunction with laser annealing, have shown an increase of both the onset pressure and the width of the spin transition with increasing temperature (Figure 7b) [*Komabayashi et al*., 2010; *Mao et al*., 2011a], although the temperatures in *Komabayashi et al*. [2010] were not well constrained. The experimentally determined width of the spin transition at high temperatures is narrower than the theoretical predictions [*Tsuchiya et al*., 2006; *Wentzcovitch et al*., 2009].

[23] Using the *P-V* relations of ferropericlase, we have evaluated the variation of density ($\Delta\rho$) and isothermal bulk modulus (ΔK_T) across the spin transition using the EoS of the high-spin state as the reference for each given composition (Figures 8b and 8c) [*Lin et al*., 2005; *Fei et al*., 2007a, 2007b; *Speziale et al*., 2005; *Marquardt et al*., 2009a; *Komabayashi et al*., 2010; *Mao et al*., 2011a]. For ferropericlase with 10% FeO, the spin transition of Fe^{2+} leads to a 1.4 (±0.1)% increase in density. Increasing FeO content in the system further increases the density contrast between the high-spin and low-spin states, reaching 3.4 (±0.1)% in the case of 39% FeO content (Figure 8b). *Mao et al*. [2011a] reported a systematic decrease in the $\Delta\rho$ with increasing temperature for ferropericlase with 25% FeO, consistent with theoretical calculations [*Wentzcovitch et al*., 2009]. In contrast, *Komabayashi et al*. [2010] found $\Delta\rho$ to be larger at high temperature than at 300 K for ferropericlase with 19% FeO. The spin transition of Fe^{2+} also causes a slight increase in the bulk modulus of ferropericlase (Figure 8c) [*Lin et al*., 2005; *Fei et al*., 2007a, 2007b; *Speziale et al*., 2007; *Marquardt et al*., 2009a; *Komabayashi et al*., 2010; *Mao et al*., 2011a]. A comparison between the high-spin and low-spin states of ferropericlase from most recent experimental works shows approximately 1 to 4% increase in K_T associated with the spin transition (Figure 8c) [*Lin et al*., 2005; *Fei et al*., 2007a, 2007b; *Marquardt et al*., 2009a; *Komabayashi et al*., 2010; *Mao et al*., 2011a], consistent with a ~6% increase in theoretical calculations when uncertainties are taken into account [*Wentzcovitch et al*., 2009]. It should be noted, however, since the spin transition occurs at 40–60 GPa, the EoS parameters of ferropericlase in the LS state are poorly constrained due to the limited pressure range in most of the experimental works [*Fei et al*., 2007a, 2007b; *Speziale et al*., 2005; *Marquardt et al*., 2009a, 2009b; *Komabayashi et al*., 2010], leading to large uncertainties in the derived K_T for the low-spin state and the ΔK_T across the spin transition.

[24] Reduction in the elastic moduli associated with the spin transition in ferropericlase has been reported experimentally and theoretically [*Crowhurst et al*., 2008; *Lin and Tsuchiya*, 2008; *Marquardt et al*., 2009b; *Wentzcovitch et al*., 2009] (see section 3.2, Sound Velocities, for more discussion). Using known *P-V* equations, the softening of the isothermal bulk modulus (K_T) in ferropericlase can be derived following the method by *Wentzcovitch et al*. [2009]. In the region of the spin transition, the K_T depends on the volume and the bulk modulus of both the high-spin and low-spin states and the pressure dependence of n_{LS}, which is responsible for the softening in K_T (Figure 9) [*Fei et al*., 2007a, 2007b; *Crowhurst et al*., 2008; *Lin and Tsuchiya*, 2008; *Lin et al*., 2009; *Marquardt et al*., 2009b]. Although most of the calculated K_T from the EoS of ferropericlase suffer from large uncertainties, comparison of literature results shows a positive effect of the spin transition on the elastic moduli.

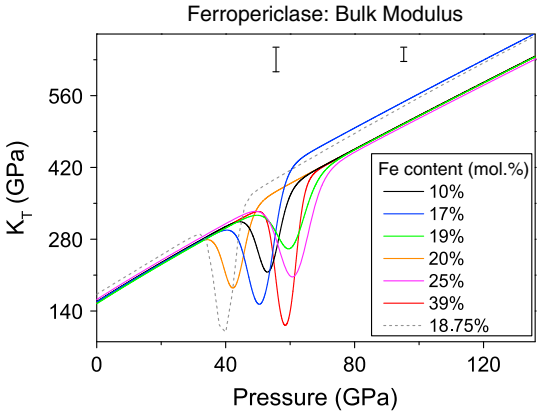

Figure 9. Isothermal bulk modulus (K_T) of ferropericlase as a function of pressure across the spin transition. A number of studies with different Fe contents are shown. Black line: 10% FeO [*Marquardt et al*., 2009a, 2009b]; blue line: 17% FeO [*Lin et al*., 2005; *Speziale et al*., 2007]; green line: 19% FeO [*Komabayashi et al*., 2010]; orange line: 20% FeO [*Fei et al*., 2007a, 2007b]; magenta line: 25 % FeO [*Mao et al*., 2011b]; red line: 39% FeO [*Fei et al*., 2007a, 2007b]; grey dashed line: 18.75% FeO [*Wentzcovitch et al*., 2009]. Representative error bars are shown on top of the K_T.

[25] *Mao et al*. [2011a] used thermal elastic modeling of the experimental *P-T-V* curves of ferropericlase to derive a density increase of 1.2%, an increase in thermal expansion coefficient by 200% over a range of 1000 km, and a maximum decrease of 37% and 13% in bulk modulus and bulk sound velocity, respectively, at ~2180 km depth across the spin crossover. The softening in K_T derived from experimental elastic parameters is less pronounced than that estimated from computational studies [e.g., *Wentzcovitch et al*., 2009].

3.1.2. Silicate Perovskite and Post-Perovskite

[26] As mentioned in section 2, the spin crossover behavior of Fe in silicate perovskite and post-perovskite is much more complex compared to ferropericlase due to the existence of different valence states and crystallographic site occupancies of Fe in both phases. However, current consensus is that a high-spin to low-spin transition of Fe^{3+} in the octahedral site occurs at pressures of 15–50 GPa (Figure 3) [*Hsu et al*., 2011; *Lin et al*., 2012a]. Using the EoS of end-member perovskite ($MgSiO_3$) as a reference [*Mao et al*., 2011b], we have evaluated the deviations of the unit cell volumes of Fe-bearing perovskite with pressure in various compositions and compared with theoretical calculations (Figure 10). For perovskite containing mainly Fe^{2+}, which occupies the large dodecahedral A site and likely remains in the high-spin state in the lower mantle (see section 1.2; Figures 2 and 3), the volume deviation as a function of pressure does not show any abrupt observable changes (Figure 10b) [*Lundin et al*., 2008; *Mao*

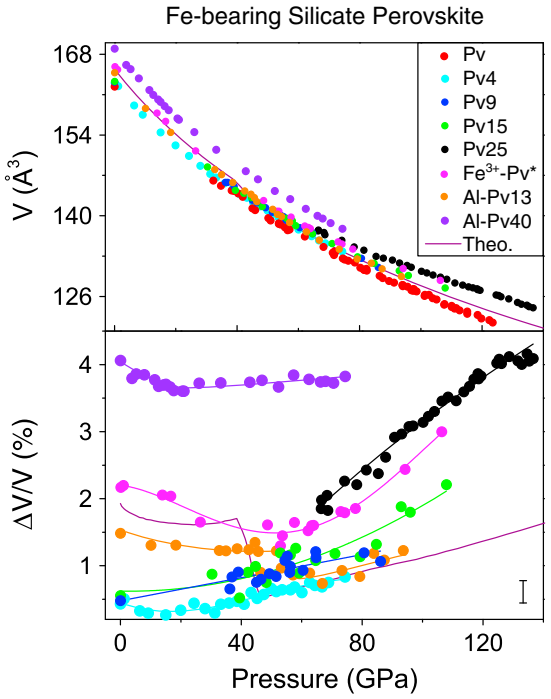

Figure 10. (a) Pressure-volume relations and (b) the unit cell volume deviation of Fe-containing perovskite from the $MgSiO_3$ counterpart at 300 K. The volume deviation was derived using $MgSiO_3$-perovskite as the reference. Red and black circles: *Mao et al.* [2011b]; blue, green circles: *Lundin et al.* [2008]; magenta circles: *Catalli et al.* [2010a] (the perovskite sample was synthesized from glass with starting composition, $0.9MgSiO \cdot 0.1Fe_2O_3$); orange circles: *Catalli et al.* [2011]; purple line: *Hsu et al.* [2011]; cyan and violet circles: *Boffa Ballaran et al.* [2012].

et al., 2011b; *Boffa Ballaran et al.*, 2012]. In contrast to the A-site Fe^{2+}, Fe^{3+} in the smaller octahedral site undergoes a high-spin to low-spin transition at lower mantle pressures, leading to a reduction of 0.5–1% in the unit cell volume between 40 and 60 GPa [*Catalli et al.*, 2011a; *Hsu et al.*, 2011; *Tsuchiya and Wang*, 2013]. Similar volume reductions have not been observed in Al-free Fe^{3+}-bearing perovskite. However, this could be due to the site occupancies, limited available data points, and limited data quality between 30 and 50 GPa in *Catalli et al.* [2010a]. The high-spin to low-spin transition of Fe^{3+} in Al-bearing perovskite has been shown to be sharper than that in the Al-free system based on synchrotron Mössbauer and X-ray emission measurements [*Catalli et al.*, 2011a]. The presence of low-spin Fe^{3+} makes the Fe-bearing perovskite stiffer than $MgSiO_3$-Pv with pressure [*Catalli et al.*, 2010a; *Hsu et al.*, 2011; *Mao et al.*, 2011b]. To date, we still lack the experimental constraints on the effect of temperature on the EoS of perovskite across the spin transition. Recent theoretical work by *Tsuchiya and Wang* [2013] has shown an increase in the onset pressure and width of the spin transition of Fe^{3+} in perovskite with increasing temperature, similar to the observation in ferropericlase.

[27] The EoS of post-perovskite is much less constrained compared to that of ferropericlase and perovskite, largely because of the experimental difficulties in studies conducted at extremely high *P-T* conditions. Post-perovskite becomes thermodynamically unstable in decompression due to synthesizing conditions, making the measured *P-V* curves less reliable at lower pressures. A survey of the literature data on the *P-V* relations shows that the unit cell volume of post-perovskite expands with the addition of Fe [*Mao et al.*, 2006; *Shieh et al.*, 2006, 2011; *Guignot et al.*, 2007; *Shim et al.*, 2008, *Nishio-Hamane and Yagi*, 2009; *Catalli et al.*, 2010b], although the incompressibilites of Fe-bearing and Fe-free post-perovskite appear to be similar over the limited experimental pressure range (Figure 11). Post-perovskite with much higher Fe-content (Fe/(Fe + Mg) = 73% and 90%), synthesized from almandine, has been reported to exhibit a slightly higher incompressibility than the $MgSiO_3$ counterpart [*Shieh et al.*, 2011]. Since most of the samples used in the EoS studies were not characterized for the spin and valence states of Fe, a quantitative and systematic understanding of the effects of Fe spin and valence states remains difficult. The study by *Catalli et al.* [2010b] has suggested that post-perovskite with low-spin Fe^{3+} exhibits a unit cell volume close to that of $MgSiO_3$ post-perovskite at similar pressures, indicating a reduction in the unit cell volume caused by the spin transition of Fe^{3+}. Future experimental and theoretical studies are needed to investigate the combined effect of temperature and spin transition of Fe on the EoS of post-perovskite.

3.2. Sound Velocities

[28] Studying sound velocities of candidate lower mantle minerals at relevant *P-T* conditions is critical in understanding mineralogical models, seismic profiles, and geodynamics of the region. Prior to the discovery of the spin transitions of iron in the lower mantle, sound velocities of lower mantle materials were commonly studied as functions of pressure, temperature, and composition, including the influence of minor elements such as iron and aluminum. The spin transition of iron additionally complicates our understanding of the elasticity of ferropericlase and perovskite and requires further investigations [e.g., *Lin et al.*, 2006b; *Crowhurst et al.*, 2008; *Marquardt et al.*, 2009a; *Antonangeli et al.*, 2011]. For example, increasing pressure typically increases the compressional wave velocity of ferropericlase, whereas increasing temperature decreases it. Nevertheless, it has been reported that the compressional wave velocity may be softened across the spin transition of ferropericlase with increasing pressure.

3.2.1. Ferropericlase

[29] The electronic spin-pairing transition of Fe in the minerals of the lower mantle causes a change on the topology of the 3*d* electronic charge density. The effect of the spin transition on the elasticity of ferropericlase can be understood through the change of the relative strength of the interactions between the Fe atom and the surrounding oxygen and magnesium (or iron) atoms in the crystal lattice of the Fe-bearing minerals of the lower mantle. *Wu et al.* [2009] gave a very "intuitive" account of the nature of this effect in the case of ferropericlase. The local shear interaction along the cubic face diagonal [110] weakens when Fe is in the low-spin configuration; this does

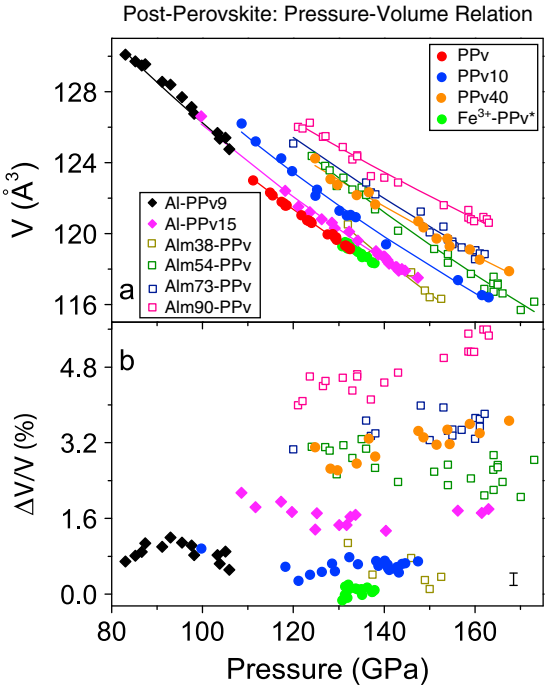

Figure 11. (a) Pressure-volume relations and (b) the volume deviation of Fe-containing post-perovskite (PPv) at 300 K. The volume deviation was derived using $MgSiO_3$ PPv as the reference. Circles: Mg-Fe PPv; diamonds: Mg-Fe PPv with Al; open squares: PPv synthesized from pyrope-almandine; red circles: *Guignot et al*. [2007]; blue circles: *Nishio-Hamane and Yagi* [2009]; orange circles: *Mao et al*. [2006]; green circles: *Catalli et al*. [2010b] (the perovskite sample was synthesized from glass with starting composition, 0.915MgSiO 0.085Fe_2O_3); black diamonds: *Shieh et al*. [2006]; magenta diamonds: *Nishio-Hamane and Yagi* [2009]; dark yellow, olive, navy, and pink squares: *Shieh et al*. [2011].

not happen for the shear interaction along the [100] direction. The result is a change of the shear anisotropy in case of the low-spin configuration with respect to the high-spin counterpart as observed experimentally [*Marquardt et al*., 2009b].

[30] Effects of the spin transition on sound velocities of ferropericlase were first reported using Nuclear Resonant Inelastic X-ray Scattering (NRIXS) in a DAC, in which significant changes in derived *Vp* and *Vs* across the spin transition were observed [*Lin et al*., 2006b]. However, it has since been shown that the *Vp* and *Vs* values derived from the Debye sound velocity of the measured partial phonon density of states of Fe in ferropericlase are lower than expected from results of complementary experimental methods for the studied composition. The first direct measurements on acoustic wave velocities of single-crystal ferropericlase ($(Mg_{0.94}Fe_{0.06})O$) using Impulsive Stimulated Light Scattering (ISLS) indicated that there is a reduction in elastic wave velocities across the iron spin transition [*Crowhurst et al*., 2008]. The results suggested a marked reduction in compressional wave velocity and a small decrease in shear velocity (Figure 12). One year later, Brillouin scattering results showed no substantial reduction in shear velocities in $(Mg_{0.9}Fe_{0.1})O$ but could not give direct information about the behavior of the compressional acoustic velocity due to experimental limitations [*Marquardt et al*., 2009b]. In contrast to ISLS, where the pseudo-surface shear velocity is measured and used to invert for the elastic shear constants, Brillouin scattering allows for a direct quantification of the bulk acoustic shear wave velocity. A very recent Brillouin scattering study by *Murakami et al*. [2012], which was performed on polycrystalline $(Mg_{0.92}Fe_{0.08})O$, confirmed that the iron spin crossover does not substantially lower the average shear

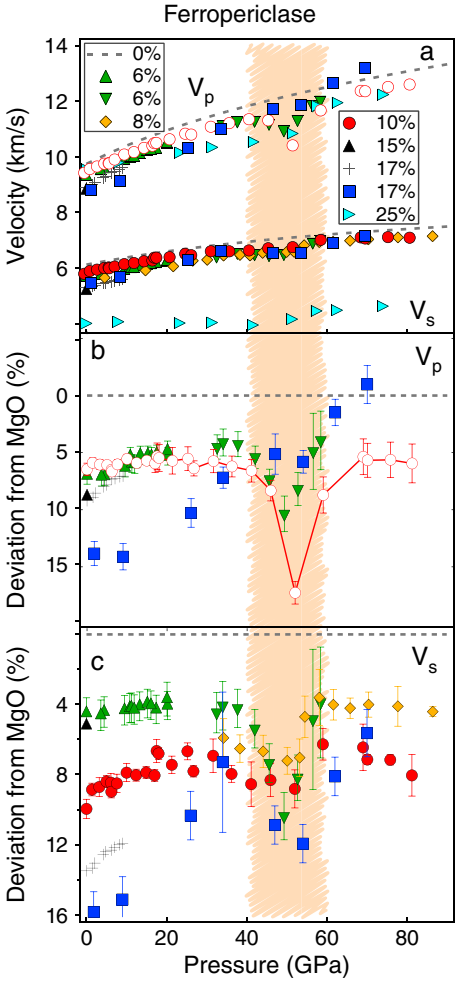

Figure 12. (a) Sound wave velocities of ferropericlase (MgFe)O and (b, c) their deviations from MgO at high pressures. Grey dashed lines: MgO, computational [*Karki et al*., 1999]; green triangles: $(Mg_{0.94}Fe_{0.06})O$, single-crystal Brillouin scattering [*Jackson et al*., 2006]; green reversed triangles: $(Mg_{0.94}Fe_{0.06})O$, single-crystal ISLS [*Crowhurst et al*., 2008]; orange diamonds, $(Mg_{0.92}Fe_{0.08})O$, polycrystalline Brillouin scattering [*Murakami et al*., 2012]; red circles: $(Mg_{0.9}Fe_{0.1})O$, single-crystal Brillouin scattering [*Marquardt et al*., 2009a, 2009b]; black triangles: $(Mg_{0.85}Fe_{0.15})O$, single-crystal gigahertz interferometry [*Jacobsen et al*., 2002); black crosses: $(Mg_{0.83}Fe_{0.17})O$, polycrystalline ultrasonics [*Kung et al*., 2002]; blue squares: $(Mg_{0.83}Fe_{0.17})O$, single-crystal IXS [*Antonangeli et al*., 2011]; light blue right-pointing triangles: $(Mg_{0.75}Fe_{0.25})O$, polycrystalline NRIXS [*Lin et al*., 2006a, 2006b; *Lin et al*., 2007a, 2007b]. Error bars as reported in the literature, sometimes smaller than symbol sizes. The shaded region denotes the pressure range where the iron spin crossover is expected to take place.

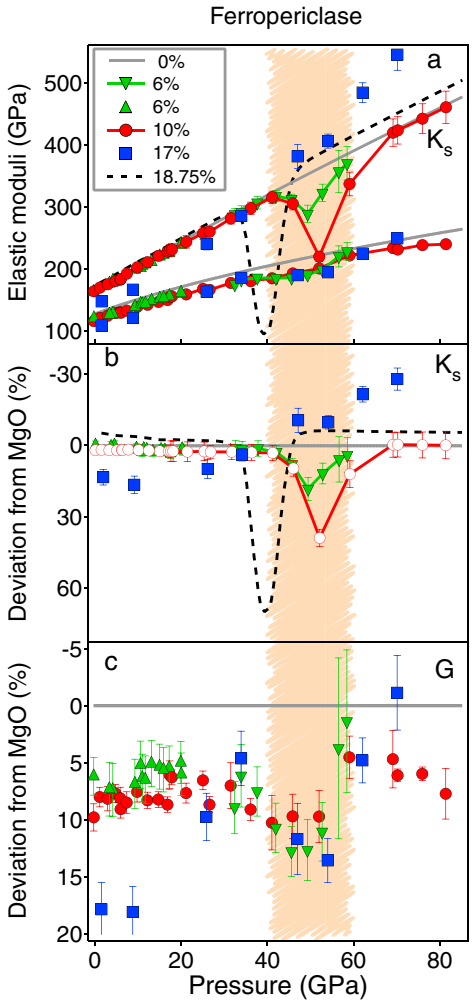

Figure 13. (a) Aggregate elastic moduli of (Mg,Fe)O and (b, c) their deviations from MgO. Symbols and references are the same as in Figure 12. The black dashed curves correspond to computational results on $(Mg_{0.8125}Fe_{0.1875})O$ [*Wentzcovitch et al.*, 2009].

velocities. Even though these recent results from polycrystalline Brillouin scattering experiments are promising, it should be noted that effort is still necessary to understand the quality and reliability of the bulk elastic properties determined by Brillouin scattering from polycrystalline materials at high pressures. The stress distribution in a diamond-anvil cell at high pressures is not uniform. Therefore, a major complication might arise from the development of a crystallographic lattice-preferred orientation (LPO) in the polycrystalline sample, in which case the measured aggregate velocity will be an average distribution function weighted by the grains' orientation and could strongly deviate from the isotropic average velocity. Further potential bias of measured velocities could arise from the anisotropic deformation behavior of the sample's crystals, leading to intergranular stresses and the anisotropic coupling between probing laser light and probed acoustic phonons. Additional care has to be taken to precisely characterize the average crystallite size, as small grain size can also have an impact on the measured bulk elastic properties [*Marquardt et al.*, 2011].

[31] Recently, *Antonangeli et al.* [2011] published inelastic X-ray scattering (IXS) results on single-crystal $(Mg_{0.83}Fe_{0.17})O$ and did not observe any reduction of compressional velocities. These results thus contradict the previous direct determination of compressional wave velocities across the spin transition [*Crowhurst et al.*, 2008] that reported a significant drop in the compressional velocity and the bulk modulus (Figure 13).

[32] A computational study on $(Mg_{0.8125}Fe_{0.1875})O$, however, found a marked reduction in the adiabatic bulk modulus and consequently in the bulk sound velocity [*Wentzcovitch et al.*, 2009]. This theoretical study thus qualitatively supports the work of *Crowhurst et al.* [2008]. Applying the thermodynamic definition of the bulk modulus to the *P-V* compression curve from high-pressure synchrotron X-ray diffraction data also leads to a reduction across the spin transition [*Crowhurst et al.*, 2008; *Lin and Tsuchiya*, 2008; *Lin et al.*, 2009; *Marquardt et al.*, 2009a; *Mao et al.*, 2011a] (see section 3.1.1 for details). This approach, however, does not provide direct constraints on the compressional velocity.

[33] In addition to aggregate elastic properties, the experimental studies that were performed on single-crystal ferropericlase allow for the determination of the elastic constants C_{ij} (Figure 14a). The discussed discrepancies between the extant data are reflected in these constants as well. The study of *Crowhurst et al.* [2008] indicates the reduction of all three cubic elastic constants, whereas *Antonangeli et al.* [2011] do not observe substantial reduction in any of the constants. A very interesting observation is that the change of the iron spin state seems to markedly enhance the elastic shear anisotropy of ferropericlase, in which the low-spin ferropericlase is substantially more anisotropic compared to its high-spin counterpart [*Marquardt et al.*, 2009b; *Antonangeli et al.*, 2011] (Figures 14b and 14c).

[34] Assuming that there are no systematic biases in the two experimental works that provide constraints on the behavior of the compressional velocity across the spin transition [*Crowhurst et al.*, 2008; *Antonangeli et al.*, 2011], reconciling both results remains a challenge. A possible explanation might be related to the differences in the frequency and the scattering vector (or inversely the "length scale") of the experimental probes (Figure 15). Phonon dispersion frequency probed by the IXS is a few orders higher than that in the ISLS and Brillouin scattering techniques, whereas its length scale is a few orders of magnitude shorter [*Robert et al.*, 2004]. The results of each method correspond to a certain frequency and length scale range and thus may not be comparable, as the spin transition involves dynamic electronic processes with ultrafast changes of the electron spins and orbital occupancies. It is therefore conceivable that its effect on the acoustic wave velocities critically depends on frequency and length scale (similar to a viscoelastic response) [see, for instance, *Abramson et al.*, 1999, Figure 19] such that the potential reduction within the transition would be seen quite differently in an ultra-high frequency probe like the IXS. In this case, the ISLS and Brillouin scattering results would be more meaningful regarding the implications of the measured elasticity across the spin transition for seismological observations [*Jackson*, 2008] (Figure 15). The currently available mineral physics studies

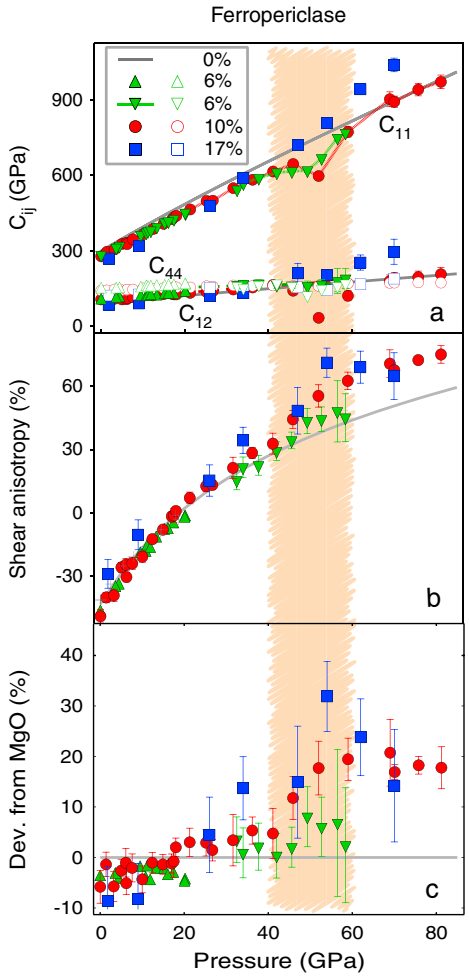

Figure 14. (a) Elastic constants of ferropericlase at high pressures. For clarity, C_{44} is shown by open symbols. (b) Shear anisotropy of ferropericlase and deviation from MgO (c) as derived from single-crystal studies. The experimentally determined shear anisotropy of MgO (grey crosses) [*Sinogeikin and Bass*, 2000] was extrapolated to high pressures by using the pressure derivative predicted theoretically [*Karki et al.* 1999]. Symbols and references are the same as Figure 12.

that directly probed compressional and shear velocities (ISLS and Brillouin spectroscopy, respectively) in single crystals indicate that the effect of the iron spin transition is that (1) the compressional velocities are markedly depressed across the spin transition, (2) the average shear velocity is less affected, and (3) the shear anisotropy is enhanced.

3.2.2. Perovskite and Post-Perovskite

[35] To our knowledge, there are no published experimental data relative to the sound wave velocities of Fe-bearing perovskite that provide direct information about the effect of the iron spin state. Computations on $(Mg,Fe)(Si,Al)O_3$-perovskite indicate that the effect of the iron spin state on the bulk and shear moduli is negligible [*Li et al.*, 2005b]. Another computational study on Fe-bearing perovskite [*Caracas et al.*, 2010] also found that there is no significant impact of the spin state on bulk elastic properties, but differences in the elastic anisotropy of the low- and high-spin $FeSiO_3$ end-member have been reported in this study.

[36] A study on Fe-rich post-perovskite using the NRIXS method provided the first experimental constraints on the bulk sound wave velocities of this phase but did not discuss the spin state of the respective sample [*Mao et al.*, 2006]. Importantly, in this study the Debye sound velocity was derived from the measured partial phonon density of states (DoS) of iron in post-perovskite [*Sturhahn*, 2004] and was then used to calculate the sound velocities using relevant bulk modulus and density values. However, it has been shown in other studies and been discussed above [*Lin et al.*, 2006b; *McCammon et al.*, 2008b] that the sound velocities of ferropericlase and perovskite derived by this approach are lower than observed by other techniques. A computational study on sound wave velocities of Fe-bearing post-perovskite [*Stackhouse et al.*, 2006] finds only small effects of the iron spin state on elastic properties. Based on our current understanding, the magnitude of the effects on the elastic properties associated with the high-spin and low-spin transition are stronger for ferropericlase than for $(Mg,Fe)SiO_3$ perovskite and post-perovskite.

3.3. Transport Properties

[37] Transport properties of iron-containing lower mantle minerals can be strongly affected by the electronic configurations in the partially filled 3*d*-electron orbitals that exhibit a band gap in the eV range, including the radiative component of thermal conduction [e.g., *Burns*, 1993] and electrical conductivity [e.g., *Dobson et al.*, 1997; *Dobson and Brodholt*, 2000; *Lin et al.*, 2007a, 2007b]. Specifically, increasing iron concentration generally enhances optical absorption and electrical conductivity and hence reduces radiative

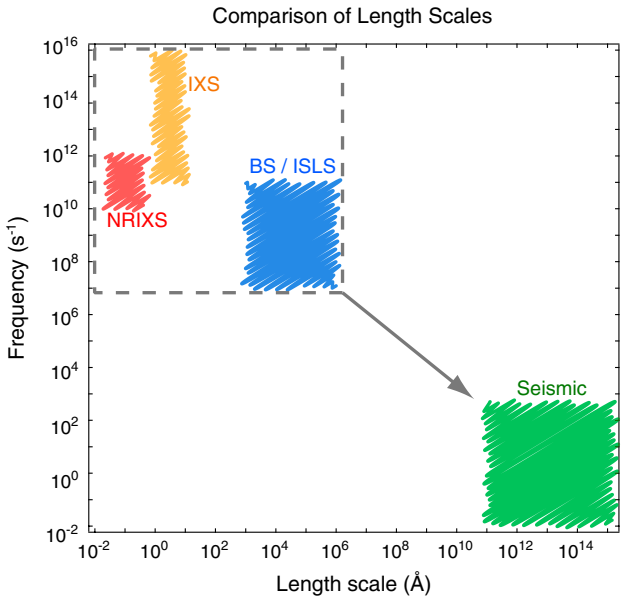

Figure 15. Illustration of the corresponding frequency and "length scales" that are typical of the experimental methods used to determine elastic wave velocities of materials at high pressures. See *Robert et al.* [2004] for details of the frequency-length scales of these techniques. The typical values for seismological studies [*Jackson*, 2008] are also shown to highlight the extrapolation that is required to translate between laboratory data and seismic observables.

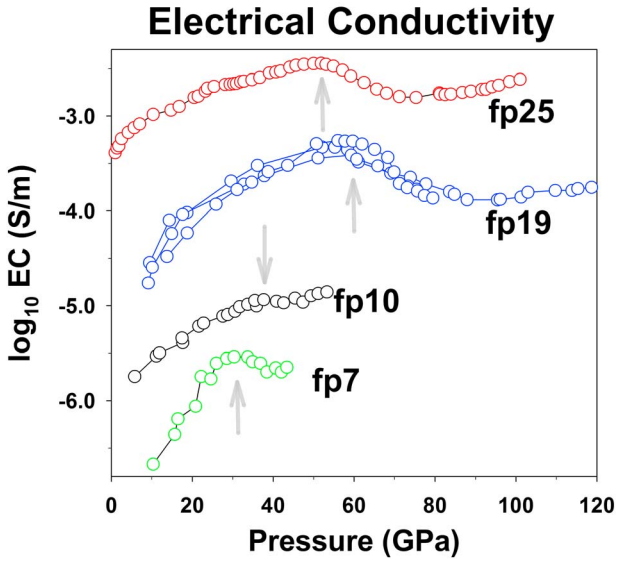

Figure 16. Electrical conductivity of ferrpericlase at high pressures and 300 K. fp7 and fp10: *Yoshino et al.* [2011]; fp19: *Ohta et al.* [2007]; fp25: *Lin et al.* [2007b]. Grey arrow indicates the occurrence of the decreased electrical conductivity as a result of the spin transition. Error bars for these measurements are likely large (~30–50%).

thermal conductivity and electrical resistance in high-spin ferropericlase and silicate perovskite [e.g., *Burns*, 1993; *Dobson et al.*, 1997; *Yoshino et al.*, 2011]. The electronic configurations of Fe^{2+} and Fe^{3+} in the crystallographic sites of ferropericlase and silicate perovskite change significantly across the spin transition (Figure 2) (e.g., see *Lin and Tsuchiya* [2008] for a review), indicating that the spin transition can affect the transport properties of lower mantle crystals. Here we discuss the effects of the spin transition on transport properties, focusing on the spin transition of Fe^{2+} in ferropericlase and the B-site Fe^{3+} in perovskite (Figure 3).

3.3.1. Electrical Conductivity

[38] Previous studies have shown that the electrical conductivity of ferropericlase is very sensitive to iron content, Fe^{2+} to Fe^{3+} ratio, and point defects [e.g., *Dobson et al.*, 1997; *Dobson and Brodholt*, 2000]. The electrical resistance, activation energy, and activation volume of (Mg,Fe)O decrease with increasing iron content in the high-spin state. Electrical conductivity of ferropericlase across the spin transition has been studied using DACs and Kawai-type multi-anvil apparatus to pressures over 100 GPa and temperatures up to 500–600 K (Figure 16) [*Lin et al.*, 2007b; *Ohta et al.*, 2007; *Yoshino et al.*, 2011]. The electrical conductivity of ferropericlase gradually rises by 1 order of magnitude with increasing pressure up to approximately 50 GPa but decreases by a factor of approximately 3 between 50 and 70 GPa for samples with approximately 20–25% FeO (Figure 16) [*Lin et al.*, 2007a, 2007b; *Ohta et al.*, 2007]. For samples with lower iron content (7–10% FeO), the electrical conductivity remains almost constant between 25 and 40 GPa and then increases slightly with increasing pressures [*Yoshino et al.*, 2011]. The observed decrease or flattening of the electrical conductivity is consistent with the reported pressure range of the spin transition in ferropericlase and has been attributed to the isosymmetric high-spin to low-spin transition of iron. Low-spin ferropericlase is observed to exhibit lower electrical conductivity than high-spin ferropericlase at high pressures as a result of the decreased electron mobility and/or density of the charge carriers across the spin transition [*Lin et al.*, 2007b]. The measured activation energy of the low-spin ferropericlase is consistent with small polaron conduction (electronic hopping, charge transfer), although the conduction mechanisms at relevant *P-T* conditions of the lower mantle still require investigation. Using the decreased electrical conductivity as an indicator, the spin transition appears to occur at relatively low pressures for MgO-rich ferropericlase (Figure 16) [*Yoshino et al.*, 2011], suggesting a compositional effect on the onset pressure of the transition. At temperatures up to 600 K, the pressure range of the decreased electrical conductivity broadens for ferropericlase containing 7% FeO, indicating a spin crossover behavior. An extrapolation of the electrical conductivity of the low-spin ferropericlase to lower mantle *P-T* conditions (~2500 K and ~100 GPa) yields an electrical conductivity in the order of tens of *S/m* [*Lin et al.*, 2007b], consistent with model values for the lower mantle [e.g., *Olsen*, 1999]. Such a value is apparently too low to account for the possible existence of a highly conductive layer with the conductance of $>10^8$ *S* at the base of the lower mantle, although the conductance depends on the thickness of the layer as well.

[39] Electrical conductivity measurements designed specifically for understanding the effect of the spin transition in perovskite and post-perovskite are rather scarce [e.g., *Ohta et al.*, 2008, 2010a, 2010b]. It has been shown that the electrical conductivity of $Mg_{0.9}Fe_{0.1}SiO_3$ perovskite increases with pressure up to 70 GPa, decreases to around 85 GPa, and again increases mildly to 135 GPa [*Ohta et al.*, 2008, 2010a, 2010b]. It was suggested that the reduction in the conductivity of perovskite at 70–85 GPa is related to the high-spin to low-spin transition of iron in perovskite [e.g., *Ohta et al.*, 2008, 2010a, 2010b]; however, as summarized in the discussion of the spin transition in perovskite (Figures 3 and 5), consensus on current experimental and theoretical results point to a spin transition of the B-site Fe^{3+} at 15–50 GPa and a low-spin transition of the A-site Fe^{2+} at approximately 120 GPa. Therefore, the abrupt decrease in the electrical conductivity does not appear to be consistent with the current understanding of the spin transition in perovskite.

[40] Electrical conductivity has been measured in silicate post-perovskite ($Mg_{0.9}Fe_{0.1}SiO_3$) in a laser-heated DAC at *P-T* conditions relevant for the lowermost mantle [*Ohta et al.*, 2008]. The results indicate that the electrical conductivity of post-perovskite is about 3 orders of magnitude higher than that of perovskite with a similar chemical composition. However, this is probably due to the layered crystal structure of post-perovskite, with short Fe-Fe distances normal to the layers rather than to spin transition of Fe^{3+}.

Finally, although the measured sample resistances are fairly accurate, conductivities converted from the resistances are expected to have systematic errors of up to 30% [*Nellis et al.*, 1999], mainly due to uncertainties in the sample geometry and thickness.

3.3.2. Thermal Conductivity

[41] Thermal conductivity of the lower mantle phases is a key parameter controlling the heat transfer and hence the evolution and style of deep Earth dynamics. Specifically, the thermal conductivity of lower mantle materials affects how heat flows from the outer core into the lowermost mantle, which in turn affects the inner working of the geodynamo and the solidification of the inner core. The thermal conductivity consists of the lattice and radiative thermal components. An effect of the spin transition on the lattice thermal conductivity is expected due to the increase in density and the possible modification of the vibrational spectrum (both on acoustic phonon velocities and density of states) associated with the transition.

3.3.2.1. Lattice Thermal Conductivity

[42] Measurement of the lattice (phonon) contribution to thermal diffusivity ($D = \kappa/(\rho C_P)$ where κ is thermal conductivity, ρ is density, and C_P is specific heat at constant pressure) at high pressures is extremely challenging. However, very recent results have been published for both perovskite and ferropericlase to maximum *P-T* of 26 GPa and 1273 K in large-volume press experiments [*Manthilake et al.*, 2011]. Lattice thermal conductivity of silicate perovskite $(Mg_{0.9}Fe_{0.1})SiO_3$ has been measured in a DAC at a given pressure of 125 GPa (a pressure relevant to understand the effects of Fe spin-transition) with pulse laser heating and time-resolved optical radiometry [*Beck et al.*, 2007; *Goncharov et al.*, 2010]. Preliminary results suggest a value of $\kappa = 25$ (± 10) $W\,m^{-1}K^{-1}$ [*Goncharov et al.*, 2010], broadly consistent with an extant estimate of $\kappa = 12\ W\,m^{-1}K^{-1}$ based on ambient pressure measurements of $MgSiO_3$ perovskite [*Osako*, 1991]. However, this technique is still in an early development stage, and the results and their interpretations have been disputed [*Beck et al.*, 2007, 2009; *Hofmeister*, 2009].

[43] Density-Functional Theory (DFT)-based ab initio computational approaches have also been recently developed to determine the lattice thermal conductivity of lower mantle phases at relevant *P-T* conditions, thus supplementing the very few available experimental results. Due to the technical challenges involved with the incorporation of Fe, the published results are relative to the lattice thermal conductivity of MgO [*de Koker*, 2010; *Stackhouse et al.*, 2010; *Tang and Dong*, 2010] and recently for MgO perovskite and $MgSiO_3$ post-perovskite [*Haigis et al.*, 2012]. However, recent rapid progress in determining thermoelastic properties and hyperfine electronic structures of Fe-bearing mantle oxides and silicates at high *P-T*, including the effects of the spin transition of iron [*Tsuchiya et al.*, 2006; *Caracas and Cohen*, 2008; *Bengtson et al.*, 2009; *Wentzcovitch et al.*, 2009; *Hsu et al.*, 2010, 2011], suggest that the effect of the spin-pairing transition on thermal transport properties will be accessible by *ab initio* computations in the near future.

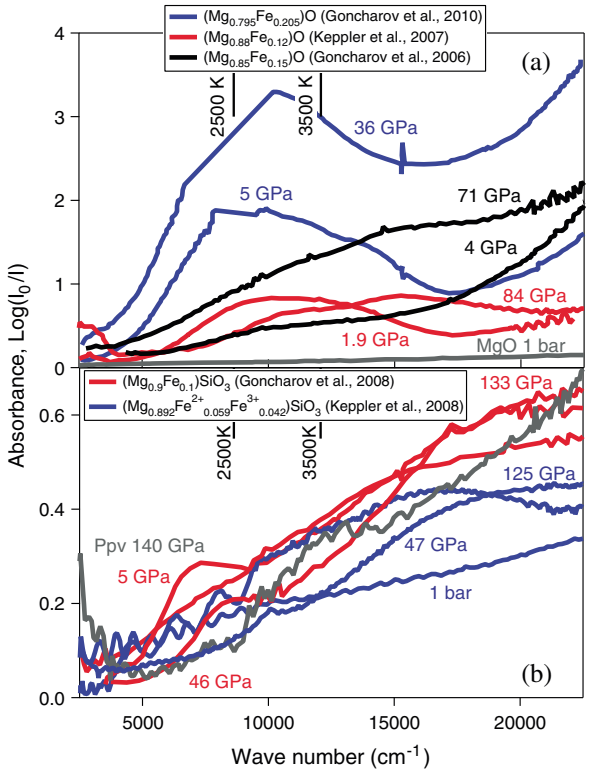

Figure 17. Absorption spectra of ferrpericlase, perovskite, and post-perovskite at high pressures and 300 K. The vertical black lines at the top indicate the maximum of the black-body radiation curve at 2500 and 3500 K. (a) The sample of $(Mg_{0.795}Fe_{0.205})O$ has an initial thickness of 16 μm; the sample of $(Mg_{0.88}Fe_{0.12})O$ has an initial thickness of 40 μm (the spectrum at 84 GPa has been scaled to a thickness of 40 μm); the sample of $(Mg_{0.85}Fe_{0.15})O$ has an initial thickness of 15 μm. The spectrum for MgO (data from *Hofmeister et al.* [2003] and *Skvortsova et al.* [2008] scaled to a thickness of 300 μm) is plotted for comparison. (b) The sample of $(Mg_{0.9}Fe_{0.1})SiO_3$ has an initial thickness of 30 μm (the spectrum at 133 GPa has been scaled to a thickness of 30 μm); the sample of $(Mg_{0.892}Fe^{2+}_{0.059}Fe^{3+}_{0.042})SiO_3$ has an initial thickness of 30 μm; the sample of post-perovskite has a composition $(Mg_{0.9}Fe_{0.1})SiO_3$ and an initial thickness of 5.75 μm [*Goncharov et al.*, 2010].

3.3.2.2. Radiative Thermal Conductivity

[44] More results are available regarding the radiative component of the thermal conductivity in both ferropericlase and perovskite, which has been estimated from ultraviolet (UV) optical and near-infrared (IR) absorption spectroscopy measured in the DAC across the whole pressure range of the lower mantle (Figure 17).

3.3.3. Ferropericlase

[45] Measurements performed on $(Mg_{0.88}Fe_{0.12})O$ to 84 GPa at ambient temperature show that the spin transition of Fe^{2+} is associated to the appearance of two new absorption bands in the regions of 10,000 and 15,000 cm^{-1} that can be assigned to the $^1A_{1g} \rightarrow {}^1T_{1g}$ and $^1A_{1g} \rightarrow {}^1T_{2g}$ transitions of the low-spin Fe^{2+} (Figure 17a); however, the estimated effect is to decrease the radiative thermal conductivity only by about 15% at temperatures between 2000 and 3000 K

[*Keppler et al*., 2007]. Additional experimental results for $(Mg_{0.79}Fe_{0.21})O$ up to 36 GPa are in qualitative agreement but, due to the larger iron content, show a 10-fold increase of the linear absorption coefficient [*Goncharov et al*., 2010]. This implies a significant decrease of conductivity as a result of iron addition, as radiative thermal conductivity (κ_{rad}) is given by

$$\kappa_{rad} \propto \int_{\upsilon} \frac{E(\upsilon)}{A(\upsilon)} d\upsilon \quad (2)$$

where υ is frequency, $E(\upsilon)$ is the emissivity of the black body, and $A(\upsilon)$ is the absorption coefficient in the near-IR frequency corresponding to the maximum of the black-body radiation curve in the 2000–3000 K range expected in the lowermost mantle [*Goncharov et al*., 2010]. These results suggest that the spin transition in ferropericlase does not have a major effect on the average radiative thermal conductivity of the lower mantle but that the absolute value of the radiative thermal conductivity of ferropericlase is sensitive to its iron content.

[46] Optical absorption measurements performed on samples of $(Mg_{1-x}Fe_x)O$ with $0.06 < x < 0.25$ characterized by high Fe^{3+} contents show that the oxidation state of iron has a strong effect on the absorption spectrum of ferropericlase across the whole near-IR to UV region, making it substantially opaque in the region of the maximum black-body radiation at temperatures of the lower mantle (Figure 17a). In this case, however, the effect of the spin transition is to slightly decrease the radiative thermal conductivity [*Goncharov et al*., 2006, 2010]. Additional measurements of UV, optical, and near-IR absorption of ferropericlase $(Mg_{0.85}Fe_{0.15})O$ with high Fe^{3+} content at simultaneous high *P-T* up to 55 GPa and 800 K show a minor temperature effect at high pressures, suggesting that the results obtained at ambient temperatures can be extended to the temperature regime of the lower mantle [*Goncharov et al*., 2008].

3.3.3.1. Perovskite and Post-Perovskite

[47] Measurements of UV, optical, and near-IR absorption of perovskite with a composition $(Mg_{0.892}Fe^{2+}_{0.059}Fe^{3+}_{0.042})(Si_{0.972}Al_{0.028})O_3$ compressed to 125 GPa (Figure 17b) show negligible absorption in the near-IR region (7000 cm^{-1}), which is characteristic of the crystal-field bands of Fe^{2+}, while the Fe^{2+}-Fe^{3+} inter-valence optical transition bands (at 15000–20000 cm^{-1}) dominate the spectra due to the very large amount of Fe^{3+} caused by the presence of Al in the perovskite structure [*Keppler et al*., 2008]. *Goncharov et al*. [2008, 2010] investigated $(Mg_{0.9}Fe_{0.1})SiO_3$ with 11% Fe^{3+} content. Experiments performed to a maximum pressure of 46 GPa show a substantial absorption in the spectral region of the Fe^{2+} crystal-field bands (Figure 17b), in agreement with results at room pressure for $(Mg_{0.94}Fe_{0.06})SiO_3$ by *Keppler et al*. [1994] with a pressure-induced blue-shift and a decrease in intensity attributed to the spin crossover of Fe^{2+} in the A-site [*Goncharov et al*., 2008]. These observations are in apparent disagreement with the most currently accepted interpretation that the B-site Fe^{3+} undergoes a spin-pairing transition in the pressure range between 15 and 50 GPa. The decreased absorption in the near-IR region is accompanied by an increase in the absorption in the 15,000 to 20,000 cm^{-1} region due to intense Fe^{2+}-Fe^{3+} inter-valence absorption bands (Figure 17b). Additional measurements up to 133 GPa indicate a progressive increase of the absorption, especially in the 15,000 to 20,000 cm^{-1} range [*Goncharov et al*., 2008, 2010]. Both studies on Al-bearing and Al-free perovskite suggest that the occurrence of the spin-pairing transition of Fe does not substantially affect the radiative thermal conductivity of perovskite [*Keppler et al*., 2008; *Goncharov et al*., 2008, 2009, 2010]. However, these results show that the absolute value of the radiative thermal conductivity of perovskite is substantially affected by the valence state of iron that is in turn controlled by the presence of Al^{3+} in substitution of Si^{4+}. With a fixed total Fe content of approximately 9 mol %, the radiative thermal conductivity estimated at lower-mantle conditions at 130 GPa and 2500 K increases 5 times from 0.4 to 2 $W\,m^{-1}K^{-1}$ from Al-free perovskite with Fe^{3+}/Fe^{2+} ratio equal to 0.12 to Al-bearing perovskite with Fe^{3+}/Fe^{2+} ratio of 0.81 [*Keppler et al*., 2008; *Goncharov et al*., 2009].

[48] To our knowledge, only one set of measurements of IR, optical, and UV absorption has been performed for Al-free post-perovskite with 10, 20, and 30 mol% iron to 140 GPa and ambient temperature [*Goncharov et al*., 2010]. That study shows, as expected, that increasing iron content from 10 to 30 mol%, the absorption coefficient increases by a factor of 8 in the whole frequency range between 5000 and 25000 cm^{-1}. Weak absorption bands at 8000 cm^{-1} and a strong band at 12,000 cm^{-1} were also observed. The strong band at 12,000 cm^{-1} is absent in Al-free perovskite, however, and the difference is most likely due to a different Fe^{3+}/Fe^{2+} ratio with respect to perovskite with identical total Fe content [*Goncharov et al*., 2010]. This very limited information does not allow us to make any inferences about the effect of the spin-pairing transition on the thermal conductivity of post-perovskite.

3.3.3.2. Rheology and Textures

[49] Understanding the potential effects of the spin transition on lattice preferred orientation, plastic flow, and flow-induced fabrics in ferropericlase, perovskite, and post-perovskite is of great importance to understanding geophysics and geodynamics of the lower mantle. Although ferropericlase constitutes only approximately one third of this region by volume, it exhibits weaker creep strength and higher elastic anisotropy than the more abundant perovskite and post-perovskite and likely plays an important role in the deformation of the lower mantle [e.g., *Karato*, 1998, 2008]. Recent radial X-ray diffraction results on ferropericlase show that the {001} texture is the dominant lattice-preferred orientation across the spin transition as well as in the low-spin state at high pressures and room temperature [*Lin et al*., 2009]. This preferred orientation pattern is predicted to be produced by $\{110\}\langle 1\bar{1}0\rangle$ slip. Since the slip system does not change across the spin transition, it is likely that the spin transition would not affect the lattice-preferred orientation in ferropericlase over a wide range of pressure-temperature conditions of the lower mantle. It has also been suggested that the spin transition results in a reduced differential stress and/or elastic strength along with

the volume reduction [*Lin et al*., 2009]. The high-spin to low-spin transition causes a density increase of about 3%, which would allow the sample to relax and accommodate to the extrinsic stress field, resulting in a reduced differential stress. The drastic reduction of the differential stress supported by ferropericlase in the mixed-spin, where high-spin and low-spin states coexist, and low-spin states indicates that the strength of this mineral decreases across the spin transition. Thus, the low-spin ferropericlase should exhibit lower strength than what is expected by extrapolation of the high-spin state. The influence of the spin transition on differential stress and the strength of ferropericlase is expected to be less dominant across the spin crossover at high *P-T* conditions relevant to the lower mantle (Figure 2) [e.g., *Tsuchiya et al*., 2006; *Lin et al*., 2007a, 2007b; *Mao et al*., 2011a], making this phenomenon less significant in geophysical implications. Theoretical calculations predicted a reduction in the effective activation energy for diffusion creep and a viscosity minimum across the spin transition in ferropericlase in the mid-lower mantle [*Wentzcovitch et al*., 2009]. These calculations combine ab initio energy calculations and a classical model to treat the elastic strain contribution to the activation energy for diffusion creep [*Sammis et al*., 1981]. The cause of the viscosity weakening is the anomalous bulk modulus softening associated with the Fe spin-transition [*Crowhurst et al*., 2008; *Mao et al*., 2011a].

[50] The effect of the spin transition on the rheology of the Fe-bearing lower mantle minerals may be related to the possibility that the transition of Fe can affect the diffusivity of both iron and magnesium, which probably control the viscosity of these minerals in the different creep regimes in the lower mantle. In the case of ferropericlase, it has been demonstrated that the spin-pairing transition is associated with weakening of the bulk modulus and such weakening can cause a minimum of viscosity at mid-lower mantle depths [*Wentzcovitch et al*., 2009]. The effect of the bulk modulus reduction across the spin-transition on diffusivity of iron in ferropericlase has been quantitatively investigated in a computational study [*Saha et al*., 2013]. A strain-induced layering with the formation of interconnected ferropericlase-rich bands in the lower mantle could cause local low viscosity regions associated with plumes and deep subducted slabs. *Saha et al*. [2013] also point out that the bulk modulus softening can affect the diffusivity of magnesium as well. A test of the global consequences of compressibility weakening induced by the Fe spin-pairing on the global dynamics of the mantle and the generation of "low viscosity channels" in the lower mantle is presented by *Matyska et al*. [2011]. Potential effects of the spin transitions in perovskite and post-perovskite remain to be investigated.

3.4. Iron Partitioning

[51] Ever since the initial experimental observation of the spin-pairing transition of Fe^{2+} in ferropericlase [*Badro et al*., 2003], researchers have focused their attention on the effects of the spin transition on the partitioning of iron between the major phases of the lower mantle. Indeed, the possibility that the spin-pairing transition causes anomalies in the partitioning of Fe between ferropericlase and perovskite or post-perovskite has the potential to strongly affect a wide range of properties of lower mantle materials including density, mechanical and rheological behavior, and transport properties.

[52] In the simplest case, the exchange reaction $MgSiO_3 + FeO \leftrightarrow FeSiO_3 + MgO$ is characterized by an equilibrium exchange partition constant:

$$K_D = \left(X_{Fe}/X_{Mg}\right)^{sil} / \left(X_{Fe}/X_{Mg}\right)^{fp} \quad (3)$$

where X is the molar fraction, *sil* indicates the silicate perovskite or post-perovskite and *fp* indicates ferropericlase. As defined in thermodynamics, the value of K_D is related to the change of Gibbs free energy (ΔG) associated with the exchange reaction:

$$\begin{aligned}\Delta G &= \Delta H - T\Delta S = -k_B T \ln K_D \\ &= -k_B T\left\{\ln\left[\left(X_{Fe}/X_{Mg}\right)^{sil}\right] - \ln\left[\left(X_{Fe}/X_{Mg}\right)^{fp}\right]\right\} \quad (4)\end{aligned}$$

where G is Gibbs free energy, H is enthalpy, S is entropy, and k_B is Boltzmann constant. At the spin-pairing transition of Fe, the change of the electronic contributions to enthalpy and entropy can be estimated by the crystal field theory and optical spectroscopic results [*Burns*, 1993]. Based on the theory and thermodynamic arguments, *Badro et al*. [2003, 2005] predicted a substantial enrichment of Fe in ferropericlase as a consequence of the spin-pairing transition with a more than ten times decrease of K_D (to a value of $K_D \approx 0.03$), which was only slightly mitigated by the corresponding spin transition in the silicate perovskite phase. However, this prediction represents a lower bound to the partition coefficient because it does not consider temperature effects that broaden the spin transitions into a progressive crossover [*Tsuchiya et al*., 2006].

[53] Partitioning of iron between Mg-rich silicate perovskite (post-perovskite) and ferropericlase in an Al-free system, using olivine $(Mg_{1-x}Fe_x)_2SiO_4$ with $0.1 < x < 0.15$ as starting material, has been investigated in the DAC across the entire lower mantle pressure regime at temperatures ranging from 1500 to 2450 K [*Kobayashi et al*., 2005; *Auzende et al*., 2008; *Sinmyo et al*., 2008; *Sakai et al*., 2009, 2010]. These studies have been performed by combining in situ X-ray diffraction with chemical characterization of recovered samples using energy-dispersive X-ray spectroscopy (EDS) of the transmission electron microscope (TEM). The resulting overall picture is that Fe is preferentially accommodated in ferropericlase with a weak decrease of K_D with increasing pressure at deep lower mantle conditions [*Kobayashi et al*., 2005]. The effect of temperature is moderate (Figure 18a), with an increase of K_D with increasing temperature up to 0.26 at 60 GPa and 2450 K. The effect of pressure is larger at high temperature, with K_D decreasing from 0.17 at 76 GPa and 2200 K down to 0.08 at 100 GPa and 2150 K [*Auzende et al*., 2008]. *Auzende et al*. [2008] suggest that the spin transition in ferropericlase is the main cause of the decreased K_D at pressures above 70–80 GPa. *Sinmyo et al*. [2008] observed a larger temperature effect and smaller

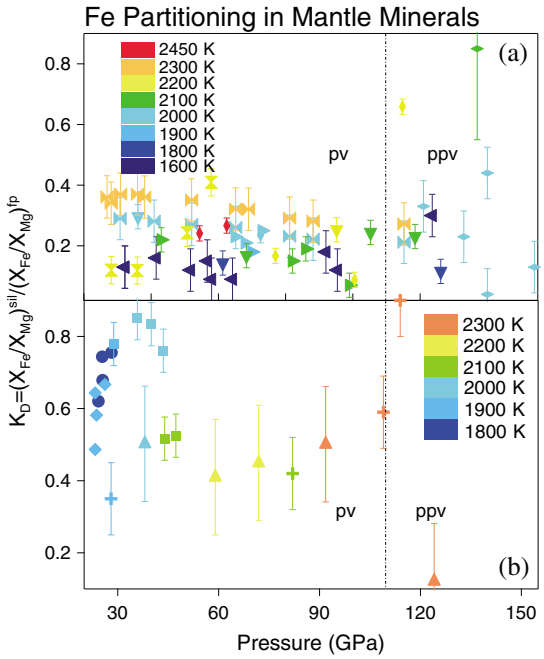

Figure 18. Pressure and temperature dependence of the partition coefficient $K_D = (X_{Fe}/X_{Mg})^{sil}/(X_{Fe}/X_{Mg})^{fp}$ (see text for details). (a) K_D in the system $(Mg_{1-x}Fe_x)_2SiO_4$ with $0.1 < x < 0.15$. Vertical hourglasses: *Andrault* [2001]; left-pointing triangles: *Kobayashi et al*. [2005]; vertical rhombs: *Auzende et al*. [2008]; down-pointing triangles: *Sinmyo et al*. [2008]; right-pointing triangles: *Sakai et al*. [2009]; horizontal rhombs: *Sakai et al*. [2010]; horizontal hourglasses: *Narygina et al*. [2011]. (b) K_D in the pyrolite (Al-bearing) system. Circles: *Irifune* [1994]; diamonds: *Wood* [2000]; squares: *Irifune et al*. [2010]; triangles: *Murakami et al*. [2005]; crosses: *Sinmyo and Hirose* [2013].

pressure dependence than *Auzende et al*. [2008], with almost constant K_D of 0.25 between 95–105 GPa and 2130–2170 K (Figure 18a). *Sinmyo et al*. [2008] explained the difference as an effect of thermally induced diffusion of Fe (Soret effect) caused by laser heating of the samples by *Auzende et al*. [2008]. The Soret effect can indeed cause a net decrease of the overall Fe content at the locations heated by IR laser absorption [*Heinz and Jeanloz*, 1987; *Sinmyo and Hirose*, 2010]. *Sinmyo et al*. [2008] tried to minimize this effect by thermally insulating their sample with NaCl, whereas *Auzende et al*. [2008] did not use an insulating layer. A study by *Sakai et al*. [2009] is consistent with the results of *Auzende et al*. [2008] finding a negative pressure dependence and a positive temperature dependence of K_D. In their study, *Sakai et al*. [2009] performed experiments in single-crystal samples thermally insulated with NaCl as well as powder samples. Their results are consistent between the different setups. In addition, *Sakai et al*. [2009] showed a slight decrease of K_D with increasing X_{Fe} in ferropericlase.

[54] In a recent study at pressures from 30 to 120 GPa and temperatures between 1950 and 2300 K, *Narygina et al*. [2011] have combined X-ray diffraction in the laser-heated DAC with in situ XANES (X-ray absorption near edge structure) at the Fe *K*-edge to determine the speciation and distribution of Fe in the coexisting oxide and silicate phases. Their results show a very weak pressure dependence of K_D and a more visible dependence on temperature (Figure 18a). Separate measurements performed after temperature quenching from 2300 K are consistent with the high-temperature results, suggesting that the distribution of Fe between the coexisting ferropericlase and perovskite phases is preserved across temperature quenching.

[55] Partitioning of Fe between Mg-rich silicate post-perovskite and ferropericlase at pressures above 110 GPa has been determined in the Al-free system $(Mg_{1-x}Fe_x)_2SiO_4$ with $0.1 < x < 0.15$ [*Kobayashi et al*., 2005; *Auzende et al*., 2008; *Sinmyo et al*., 2008; *Narygina et al*., 2011]. However, these available results are often inconsistent, showing either a moderate to large increase of K_D [*Kobayashi et al*., 2005; *Auzende et al*., 2008] or a decrease [*Sinmyo et al*., 2008; *Narygina et al*., 2011] with respect to the ferropericlase/perovskite counterpart (Figure 18a). *Sakai et al*. [2010] studied the Fe partitioning between post-perovskite and ferropericlase in a wide range of *P-T* and total Fe contents. Their results indicate that K_D increases with increasing temperature and also exhibits negative pressure dependence. In addition, K_D increases with decreasing total Fe content approaching unity for total X_{Fe} ($X_{Fe} = FeO/(FeO + MgO)$ mol) contents well below 0.1, which are of limited relevance for the deep Earth. The results of *Sakai et al*. [2010] can reconcile the disagreement between the previous works by other groups if one considers that the high K_D at the location of the heating "hot-spot" could be due to substantial Fe loss by Soret diffusion [e.g., *Auzende et al*., 2008), while measurements performed in areas that preserved a pristine X_{Fe} would show lower K_D [e.g., *Sinmyo et al*., 2008].

[56] The presence of Al in the lower mantle can have a large effect on the site occupancy and the valence state of iron in perovskite due to Al^{3+}-Si^{4+} substitution [*McCammon*, 1997; *Richmond and Brodholt*, 1998]. In order to evaluate the effect of Al on the partitioning of Fe between perovskite (and post-perovskite) and ferropericlase in the lower mantle, experimental studies have been carried out on the pyrolite system as a representative composition of the average bulk Earth mantle [*Ringwood*, 1982] (Figure 18b). A recent study performed in the multi-anvil press [*Irifune et al*., 2010] shows that starting from 40 GPa, the value of K_D decreases from 0.85 at 1973 K to 0.52 at 47 GPa and 2073 K. The new results extend and confirm previous studies at very shallow lower mantle conditions [*Irifune*, 1994; *Wood*, 2000] and suggest an effect caused by the onset of the spin transition in ferropericlase. Additional data relative to the pyrolite system are reported by *Murakami et al*. [2005], who investigated a wide range of pressures from 40 to 90 GPa and temperatures from 2000 to 2300 K. Their results show a positive temperature dependence of K_D and slight negative pressure dependence with values ranging between 0.4 and 0.5 (Figure 18b). A very recent study by *Sinmyo and Hirose* [2013] investigated Fe partitioning between silicate perovskite and ferropericlase in pyrolite up to 114 GPa and 2300 K. The new study confirms the results by *Murakami et al*. [2005] in the pressure range up to 90 GPa, and it shows an increase of the partition coefficient

above 100 GPa to a value of 0.9 at their maximum experimental pressure (Figure 18b). The relationship between the change of the pressure dependence of K_D above 100 GPa and spin transitions of Fe is not completely clear because Fe^{3+} in the B site of silicate perovskite is predicted to undergo spin-pairing at pressures between 15 and 50 GPa.

[57] *Murakami et al*. [2005] also measured iron partitioning between post-perovskite and ferropericlase in the pyrolite system at 2250 K and 124 GPa. The value of K_D that they determined is 0.12, which corresponds to a 75% decrease with respect to the K_D determined between perovskite and ferropericlase at 90 GPa and 2300 K. The presence of Al_2O_3 apparently causes an increase of fractionation of Fe in perovskite, indicating a coupled substitution of the Al^{3+} and Fe^{3+} for the B-site Si^{4+} in perovskite. In addition, it has been observed that Fe^{2+} disproportionates into metallic Fe^0 and Fe^{3+} [*Frost and Langenhorst*, 2002], with Fe^{3+} being accommodated in perovskite but almost absent in ferropericlase. The large decrease of K_D between post-perovskite and ferropericlase observed by *Murakami et al*. [2005] could be due to a large decrease of the absolute Fe and Al content in post-perovskite with respect to perovskite (Figure 18b).

[58] The picture emerging from these different studies is that Fe partitioning between the silicate and ferropericlase phases of the lower mantle is strongly affected by the presence of Al in the system, which favors the presence of Fe^{3+} in perovskite and effectively increases K_D at pressures below 40 GPa up to 0.85. This is consistent with the interpretation that the spin transition of B-site Fe^{3+} in perovskite occurs below 40 GPa. With the onset of the spin-pairing transition of Fe^{2+} in ferropericlase, the value of K_D decreases quickly reaching to a value of 0.5 at pressures as high as 90 GPa and then increases again up to 0.9 at 114 GPa in the temperature range between 2000 and 2300 K. In absence of Al, the value of K_D is almost constant from 30 GPa to about 70 GPa and varies with temperature from 0.13 at 1600 K to 0.36 at 2300 K. At higher pressure, probably also due to the occurrence of the spin crossover in ferropericlase, K_D decreases with pressure, although the exact pressure dependence is not resolved by the available results (Figure 18).

[59] In addition to the studies of partitioning behavior of Fe between ferropericlase and the silicate phases, *Hirose et al*. [2008] focused on the experimental determination of the partition of Fe between coexistent perovskite and post-perovskite with overall composition $(Mg_{0.9}Fe_{0.1})SiO_3$, showing that sample material recovered from 100 GPa and 1700–1800 K presented a systematic enrichment of Fe in the perovskite phase. A recent study in the laser-heated DAC focused on the partitioning of Fe between coexisting perovskite and post-perovskite at lower mantle conditions determined by combining X-ray diffraction and X-ray absorption techniques [*Andrault et al*., 2010]. The results indicate a systematic depletion of Fe in post-perovskite with a $K_D = 0.42$ (here $K_D = (X_{Fe}/X_{Mg})^{ppv}/(X_{Fe}/X_{Mg})^{pv}$ where *ppv* indicates the silicate post-perovskite and *pv* indicates perovskite). A careful evaluation of the effect of the valence state of Fe on its partitioning into the two polymorphs at lowermost-mantle conditions has been carried out by *Sinmyo et al*. [2011] by combined X-ray diffraction and electron energy-loss near-edge spectroscopy (ELNES) analyses. *Sinmyo et al*. [2011] show that post-perovskite is depleted in Fe^{3+} with respect to perovskite, independent of the Al content in systems characterized by $Fe^{3+}/\Sigma Fe$ ratios between 0.04 and 0.22, compatible with the lower mantle. They propose that Fe^{3+} in perovskite and metallic Fe recombine to form Fe^{2+} upon the perovskite to post-perovskite transition, which also causes a strongly partition of Fe^{2+} into ferropericlase. However, additional experiments performed by *Sinmyo et al*. [2011] on anomalously oxidized samples show that the oxidation state of Fe in post-perovskite is strongly influenced by the oxidation state present in the source material.

[60] The overall picture emerging from experimental studies is still contradictory, with studies that suggest either Fe enrichment in perovskite [*Murakami et al*., 2005; *Sinmyo et al*., 2008; *Narygina et al*., 2011] or in post-perovskite [*Kobayashi et al*., 2005; *Auzende et al*., 2008]. *Caracas and Cohen* [2007, 2008] determined the pressure-composition phase diagram of the $(Mg,Fe)SiO_3$ system based on static DFT calculations and adding a temperature shift calibrated on high temperature computation performed on the Fe-free system [*Tsuchiya et al*., 2004]. They also presented the vibrational entropic and thermal expansion contributions to the computed static enthalpies and configurational entropies. Their results indicated that at conditions of the lower mantle, Fe^{2+}, which is in the high-spin configuration in both the polymorphs and at any condition, preferentially partitions in post-perovskite and expands the coexistence loop, such that a perovskite with 7 mol% Fe content (typical of pyrolite compositions) would start to transform first producing a post-perovskite with 13 mol% Fe. *Caracas and Cohen* [2008] examined the disagreement between computational studies and several experimental studies and suggested that one source of disagreement (together with the approximations in their calculation of the vibrational entropic contribution) could be that some experimental results are not representative of equilibrium conditions.

[61] The attainment of the thermodynamic equilibrium in temperature and composition is extremely complicated in high *P-T* DAC experiments. The presence of temperature heterogeneities and thermally induced Fe diffusion can complicate the interpretation of the results. In addition, the thin foil sample preparation for TEM analyses can generate artifacts [e.g. *Barna et al*., 1999; *Wirth*, 2009]. As a consequence, the uncertainty associated to the K_D determined at deep lower mantle conditions oscillates between 0.05 and 0.1, and the large majority of the results are marginally consistent within their reciprocal uncertainties.

[62] In addition to the studies performed on the solid phases, *Nomura et al*. [2011] have experimentally investigated the partitioning of Fe between melt and coexisting liquidus solid (the first crystallizing solid) in the $(Mg_{0.89}Fe_{0.11})_2SiO_4$ system at relevant lower mantle *P-T* conditions from 20 to 159 GPa using electron microprobe analyses of the *P-T* quenched and recovered samples. Their results show that $K_D = (X_{Fe}/X_{Mg})^{sol}/(X_{Fe}/X_{Mg})^{liq}$

(where X is the molar fraction, *sol* indicates solid silicate perovskite, post-perovskite or ferropericlase, and *liq* indicates the melt) is almost constant with a value of 0.22 to 0.29 at shallower lower mantle conditions up to 75 GPa. At higher pressures it drops to 0.07 and remains almost constant to 159 GPa. Additional X-ray emission spectroscopy performed on $(Mg_{0.95}Fe_{0.05})SiO_3$ glass indicates the presence of the spin-pairing transition of Fe^{2+} in the pressure regime between 59 and 77 GPa, and the authors suggest that the same effect is causing the large change of K_D observed in the $(Mg_{0.89}Fe_{0.11})_2SiO_4$ system [*Nomura et al*., 2011]. However, such a transition in Fe-containing glass may not be representative of the potential spin transition in silicate melts because melts can display behaviors distinct from those of glasses. Furthermore, the reported pressure range of the spin transition is inconsistent with our current understanding of the spin transition in perovskite (Figure 5).

[63] The results by *Nomura et al*. [2011] supported the hypothesis that the spin-pairing transition of iron in the lower mantle played a crucial role on iron partitioning between solids and deep silicate melts by stabilizing dense silicate liquids at the bottom of the lower mantle through the progressive cooling of the whole mantle magma ocean in the primordial Earth [*Labrosse et al*., 2007]. This pristine basal magma ocean (BMO) could probably be present in the large low-shear-velocity provinces (LLSVPs) and in the ultra-low-velocity zones (ULVZs) [*Labrosse et al*., 2007]. However, a very recent study by *Andrault et al*. [2012], who investigated Fe partitioning between solid and melt in an Al-bearing simplified pyrolite system in a range of pressures between 40 and 120 GPa, showed that $K_{Fe}=X^{sol}_{Fe}/X^{liq}_{Fe}$ (where X is the molar fraction, *sol* indicates the solid, and *liq* indicates the melt) is almost constant at a value of 0.55 ($\pm$0.1) across the whole lower mantle. The results of *Andrault et al*. [2012] clearly contradict those of *Nomura et al*. [2011] and the hypothesis of the segregation of a Fe-rich, high density basal magma ocean.

[64] Spin-pairing transitions can affect the isotopic fractionation of iron between minerals of the lower mantle and also between minerals and metallic Fe at deep mantle conditions. Theoretical ab initio computations with representative Fe^{2+} clusters in both ferropericlase and perovskite have been performed at conditions corresponding to the very deep mantle (120 GPa and up to 4000 K). These studies show that heavy Fe^{2+} is favored in the low-spin configuration in ferropericlase, while no preferential enrichment exists for the low-spin Fe^{2+} in the A site in perovskite [*Rustard and Yin*, 2009]. *Polyakov* [2009] evaluated the isotopic fractionation of Fe between metallic iron and ferropericlase and between iron and post-perovskite from measured partial phonon density of states (DoS) of ^{57}Fe in silicate, oxide, and metallic Fe at high pressures using nuclear inelastic X-ray scattering data in the DAC [*Mao et al*., 2001; *Lin et al*., 2006b; *Mao et al*., 2006]. The results show that ^{57}Fe is enriched in both oxides and silicates with respect to metallic iron at core-mantle boundary conditions, and this behavior is the opposite to that observed for the corresponding solid phases at ambient pressure. The studies by *Rustard and Yin* [2009] and *Polyakov* [2009] are compatible with scenarios of strong isotopic fractionation and stratification at early stages of the Earth history. The Fe isotopic signatures of different physical reservoirs in the deep mantle should be traceable in modern Earth volcanic products, and the isotopic ratio of volcanic rocks in planetary bodies should be indicative of the *P-T* conditions of the core formation.

3.5. Iron Diffusion

[65] Elemental diffusion is a key parameter in determining the rheology of materials. In both diffusion and dislocation creep, deformation is controlled by the diffusion rates of the different chemical species and vacancies [e.g., *Karato*, 2008]. In this respect, the spin crossovers of Fe in ferropericlase and silicate perovskite and post-perovskite may produce important effects on diffusion rates and ultimately on the rheology of the deep mantle. Chemical diffusion rates in deep mantle materials have been investigated up to uppermost lower mantle pressures, including Mg-Fe inter-diffusion in ferropericlase up to 35 GPa by *Yamazaki and Irifune* [2003]. Pressure regimes relevant for the spin-pairing transition in lower mantle minerals are still experimentally inaccessible for diffusion studies.

[66] Very recently, two different groups have addressed the effect of the spin transition on the absolute diffusion rate of Fe^{2+} across the whole pressure range of the lower mantle using ab initio computations [*Ammann et al*., 2011; *Saha et al*., 2011]. These studies determine the absolute diffusivity D of Fe^{2+} as a dilute impurity whose migration is mediated by Mg vacancies; the migration energetics are determined using ab initio density functional theory calculations including an effective Hubbard-U energy term to accurately describe electron correlation effects in Fe. Both studies consider the case of $(Mg_{0.97}Fe_{0.03})O$, which ensures dilute-limit conditions for the system.

[67] However, the two studies use different approaches to determine diffusivity. *Ammann et al*. [2011] explicitly included the rates of all the four possible exchanges involving the impurity and the vacancy and the exchange rate in the pure iron-free crystal. *Saha et al*. [2011] simplified the analysis of the rates of the different exchange processes by treating the hopping frequency (except for the exchange between impurity and vacancy) as a function of the exchange rate between vacancy and neighboring Fe and the exchange rate for hopping of Mg in the pure Fe-free lattice. Another important source of the differences between the two models is the choice of the vacancy concentration: it is fixed to 1 (dilute limit) by *Ammann et al*. [2011], while *Saha et al*. [2011] modeled it based on an estimated extrinsic vacancy concentration corresponding to 100 ppm Al content [*van Orman et al*., 2009]. Furthermore, *Ammann et al*. [2011] did not consider mixed high-spin and low-spin state conditions, while *Saha et al*. [2011] developed a thermodynamic model to describe the behavior of Fe^{2+} in an extended mixed-spin region.

[68] Nevertheless, one important conclusion of both studies is that in the vacancy-mediated diffusion, the low-spin Fe configuration is always energetically unfavorable in the

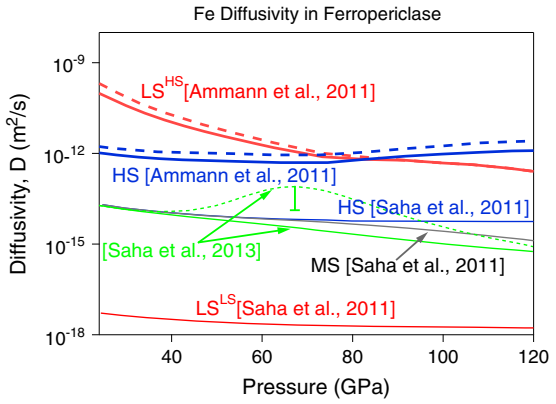

Figure 19. Pressure dependence of Fe^{2+} diffusivity (D) in ferropericlase along a representative geotherm [*Stacey and Davis*, 2004]. Red and blue continuous curves are relative to the dilute limit, while dashed curves refer to an empirical model for 20 mol% FeO content [*Ammann et al.*, 2011]. HS: high spin; MS: mixed spin; LS^{LS}: low spin with the low-spin configuration in the activated state (see text); LS^{HS}: low spin with the high-spin configuration in the activated state. The green curves are relative to ferropericlase with 18 mol% FeO content [*Saha et al.*, 2013]. The continuous curve does not include elastic softening, while the dashed curve includes the effect of elastic softening. The error bar represents the range of values of the diffusivity including softening between the classical strain energy model and a lower bound based on ab initio computations (for details, see *Saha et al.* [2013]).

activated state for hopping to a neighboring Mg vacancy. That is, even the low-spin Fe^{2+} switches to the high-spin configuration during a successful hop and returns to the low-spin configuration after the exchange. This result confirms recent experimental observations for Cr^{3+} and Ga^{3+} in periclase [*Crispin and van Orman*, 2010] and implies that crystal field effects are stronger than the constraints imposed by ionic radii in determining the diffusivities of transition metals during their migration to neighboring magnesium vacancies in periclase. One interesting result by *Ammann et al.* [2011] suggested that the spin configuration of Fe can change also as a consequence of nearby Mg jumps. This effect has the important consequence of accelerating the diffusion of Mg.

[69] Figure 19 shows the diffusivities modeled by the two studies along a representative geothermal path [*Stacey and Davis*, 2004]. The two models are in qualitative agreement, indicating that the spin-pairing transition of Fe^{2+} affects diffusivity by less than one order of magnitude in the dilute limit. However, the diffusivity computed by *Saha et al.* [2011] is about 2 orders of magnitude lower due to the smaller vacancy concentration used in their model.

[70] *Ammann et al.* [2011] did not consider a mixed-spin region. At pressures below the sharp spin-transition, the low-spin Fe^{2+} has a higher diffusivity than the high-spin state if the migration mechanism involves switching to the activated high-spin Fe^{2+} state. The results of *Saha et al.* [2011] showed that the diffusivity of dilute Fe^{2+} in the mixed-spin regime is dominated by the high-spin species, and the low diffusivity of the low-spin species starts to influence the overall Fe diffusivity only in the lowermost mantle (in this matter the models of the two groups are very similar). *Saha et al.* [2011] also computed the diffusivity of the pure low-spin Fe^{2+} without switching to the high-spin configuration in the activated state (see Figure 19). Such a migration mechanism could be relevant at extremely high pressures such as those in super-Earth planets.

[71] In addition to the dilute limit, *Ammann et al.* [2011] presented a model to estimate Fe diffusivity as a function of Fe content and found qualitatively similar results for an Fe content of 20%, with a negligible increase of the diffusion coefficient (Figure 19). In a more recent paper, *Saha et al.* [2013] also presented a model which includes the elastic softening induced by Fe spin crossover (which is a function of the finite Fe content in ferropericlase). *Saha et al.* [2013] combined ab initio modeling of the energetics of iron migration with the elastic strain energy model by *Sammis et al.* [1981] to incorporate the contribution to Fe diffusivity due to the bulk modulus softening across the spin-pairing transition. The effect of the anomalous softening of the bulk modulus is that of increasing the diffusivity of Fe up to 30 times in part of the lower mantle for $(Mg_{0.82}Fe_{0.18})$ O along a geothermal *P-T* path [*Saha et al.*, 2013]. In addition, the anomalous softening due to Fe spin crossover would largely affect the diffusivity of Mg, with additional consequences for ferropericlase rheology [*Saha et al.*, 2013].

[72] In conclusion, the models by both *Ammann et al.* [2011] and *Saha et al.* [2011] indicate that in the dilute limit, the Fe^{2+} diffusivity in ferropericlase is weakly affected by the spin crossover except for the very bottom of the lower mantle, where it can decrease by about one order of magnitude. At relevant *P-T* conditions of the lower mantle, Mg diffuses much more slowly than Fe^{2+} in ferropericlase. The effect of the Fe concentration at levels compatible with a lower mantle ferropericlase composition (approximately 20% FeO) can be as high as one order of magnitude increase of the diffusivity [*Saha et al.*, 2013] (Figure 19). Based on the available experimental and computational results, ferropericlase is mechanically weaker than perovskite, although Fe diffusion (and its partitioning) as well as the viscosity of lower mantle rocks is dominated by the behavior of perovskite. However, due to the fact that the ferropericlase content is close to the percolation threshold of the lower mantle materials, it is possible that in environments subject to large strains, such as deep subducted slabs and large-upwelling regions (super-plumes), ferropericlase grains may become interconnected such that layered ferropericlase might become more dominant in controlling Fe mobility, rheology and associated mechanical anisotropy. Overall, Fe diffusivity in mantle minerals is too slow to produce large-scale homogenization in geologic times; however, if enhanced by 2 to 4 orders of magnitude (based on the diffusivities calculated by *Ammann et al.* [2011] and *Saha et al.* [2011], respectively) at grain boundaries, it could still be compatible with slab homogenization in one hundred million years [*Kellogg and Turcotte*, 1987] and allow for substantial core-mantle mixing [*Hayden and Watson*, 2007].

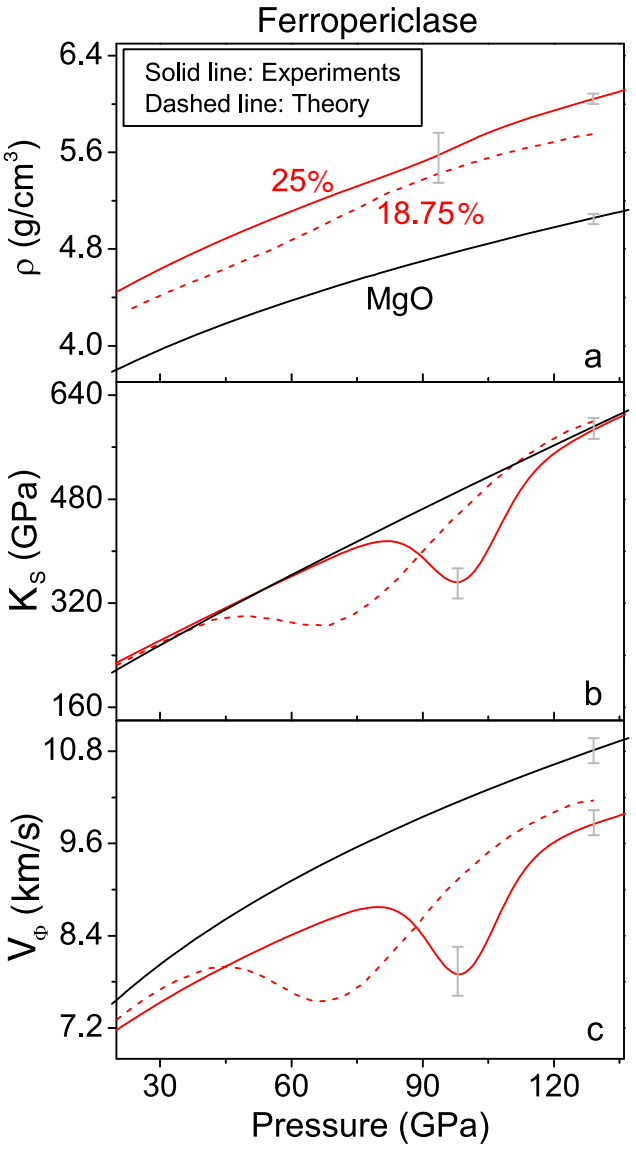

Figure 20. Thermal elastic parameters of ferropericlase along an expected lower mantle geotherm [*Brown and Shankland*, 1981]. Black line: MgO [*Tange et al.*, 2009]; red solid line: 25% FeO in ferropericlase [*Mao et al.*, 2011a]; red dashed line: 18.75% FeO in ferropericlase from theoretical calculations [*Wentzcovitch et al.*, 2009].

4. GEOPHYSICAL IMPLICATIONS

[73] To understand the geophysical consequences of the spin transition in the lower mantle, we have modeled the density, bulk modulus (K_S), and bulk sound velocity (V_Φ) of ferropericlase along an expected lower mantle geotherm using the experimental EoS and a spin crossover model (Figures 20 and 21) [*Brown and Shankland*, 1981; *Mao et al.*, 2011a]. The results for $(Mg_{0.75}Fe_{0.25})O$ are compared with a computational model for $(Mg_{0.8125}Fe_{0.1875})O$ [*Wentzcovitch et al.*, 2009]. Here pure MgO is used as the reference for deriving the deviations [*Tange et al.*, 2009]. We note that the width of the spin crossover determined from the experimental results for ferropericlase with 25% FeO [*Mao et al.*, 2011a] is much narrower than what was predicted by computations for ferropericlase with ~19% FeO [*Wentzcovitch et al.*, 2009], and the spin crossover occurs at a much higher pressure (Figures 20 and 21). On the other hand, both experimental and theoretical models consistently show a reduction in the bulk modulus and the bulk sound velocity within the spin crossover (Figure 20). Using MgO as the EoS reference [*Tange et al.*, 2009], high-spin ferropericlase with 25% FeO is ~17% denser than MgO, whereas the low-spin state becomes ~19% denser (Figure 21a). Within the spin crossover region, K_S and V_Φ of ferropericlase are 28% and 22% lower than those of MgO. These anomalous behaviors in the thermal elastic

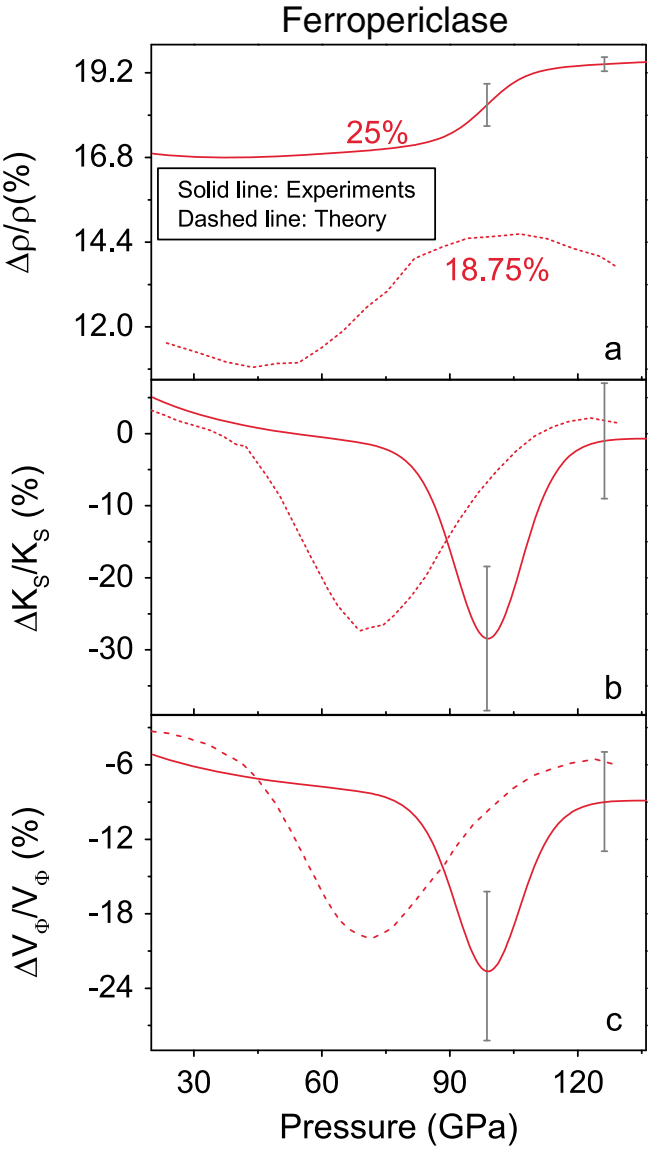

Figure 21. Deviations of the thermal elastic parameters of ferropericlase along a representative lower mantle geotherm [*Brown and Shankland*, 1981]. MgO EoS parameters were used as the reference [*Tange et al.*, 2009]. Red solid line: 25% FeO in ferropericlase [*Mao et al.*, 2011a]; red dashed line: 18.75% FeO in ferropericlase from theoretical calculations [*Wentzcovitch et al.*, 2009].

properties of ferropericlase across the spin crossover must be taken into account in order to understand the seismic signatures and geodynamics of the lower mantle.

[74] It has been shown that the spin transition affects sound wave propagation characteristics of (MgFe)O [*Lin et al*., 2006b; *Crowhurst et al*., 2008; *Marquardt et al*., 2009a; *Wentzcovitch et al*., 2009; *Antonangeli et al*., 2011] as well as perovskite [*McCammon et al*., 2008a] and post-perovskite [*Caracas et al*., 2010]. However, scarce data and existing inconsistencies between the available data sets preclude an adequate evaluation of the implications of the spin transitions for the interpretation of seismic observables and our understanding of global geodynamics [e.g., *Speziale et al*., 2007; *Lin and Tsuchiya*, 2008; *Cammarano et al*., 2010; *Morra et al*., 2010]. In addition, published studies of the acoustic wave propagation across the spin transition in ferropericlase have exclusively been conducted at mantle pressures and ambient temperature. In general, it has been shown both theoretically and experimentally that temperature broadens the pressure range over which the spin transition occurs in ferropericlase [*Sturhahn et al*., 2005; *Tsuchiya et al*., 2006; *Lin et al*., 2007a; *Komabayashi et al*., 2010; *Mao et al*., 2011a]. This makes it unlikely that the spin transition causes abrupt changes but rather favors gradual changes in the elastic properties throughout the lower mantle.

[75] Most of our current knowledge on the effect of the spin transition on seismic velocities is limited to ferropericlase, and its implications have been modeled in different studies. *Cammarano et al*. [2010] tested different mineral physics models against radial one-dimensional seismic profiles in order to assess the implications of the spin crossover in ferropericlase on the interpretation of the seismic data. The authors concluded that including a reduction of the compressional velocity across the spin crossover leads to a better fit of seismic data in the upper part of the lower mantle but requires a thermal, chemical, or thermochemical transition in the central part of the lower mantle. The iron spin crossover also affects *P-T* derivatives of the acoustic velocities of ferropericlase [e.g., *Marquardt et al*., 2009a] and might therefore be responsible for the observations of lateral seismic heterogeneity [e.g., *Kennett et al*., 1998; *Masters et al*., 2000; *Romanowicz* 2008]. In addition, there appears to be consensus that the spin crossover affects the elastic shear anisotropy in ferropericlase [*Crowhurst et al*., 2008, *Marquardt et al*., 2009b, *Antonangeli et al*., 2011]. *Marquardt et al*. [2009b] estimated the maximum elastic shear anisotropy of low-spin ferropericlase throughout the Earth's lower mantle to be about three times that of perovskite and post-perovskite, making it a strong candidate to explain seismic observations of shear anisotropy in the lowermost mantle.

[76] In a nutshell, the electronic spin transition has the potential to substantially impact our understanding of the deep Earth structure and dynamics. Unfortunately, as discussed in the section 3.2, Sound Velocities, the effect of the spin crossover on the compressional velocity of ferropericlase is still unclear. Certainly, multidisciplinary experiments and/or calculations are critical to enhance our current understanding about the elastic properties of the low-spin ferropericlase and their behaviors in the spin transition zone of the lower mantle. The knowledge on spin-affected and frequency-dependent elasticity of lower mantle minerals is prerequisite to adequately interpreting seismic observables in terms of the structure, mineralogy, and dynamic state of the Earth's deep interior [*Jackson*, 2008].

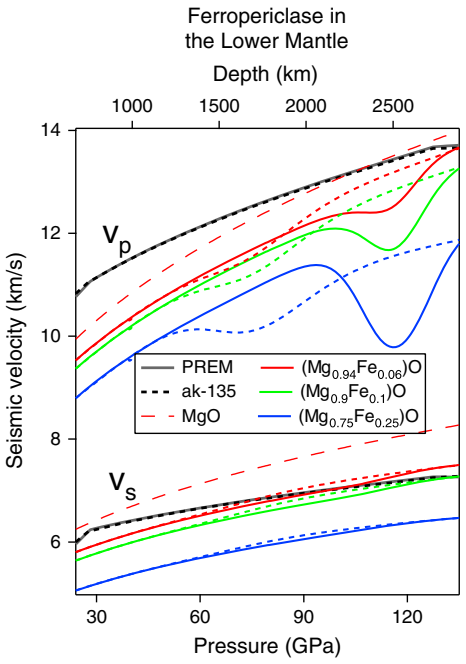

Figure 22. Aggregate longitudinal and shear acoustic velocities of ferropericlase along a geothermal *P-T* path [*Brown and Shankland*, 1981]. The *P-T* dependences of density and the elastic moduli are determined by Eulerian strain equations and an extended Grüneisen equation of state approach [*Stixrude and Lithgow-Bertelloni*, 2005]. The compositional dependences of density and elastic moduli are based on *Jacobsen et al*. [2002]. The pressure dependences of the elastic moduli are based on *Jacobsen et al*. [2004], *Jackson et al*. [2006], *Fei et al*. [2007a], *Crowhurst et al*. [2008], *Marquardt et al*. [2009a], *Mao et al*. [2011a], and *Murakami et al*. [2012]. Two models of the temperature effect on the breadth of the mixed spin region are plotted as continuous curves [*Mao et al*., 2011a] or dashed curves [*Marquardt et al*., 2009a; *Tsuchiya et al*., 2006]. Curves for MgO are based on *Karki et al*. [1999] and *Sinogeikin and Bass* [2000]. PREM: Preliminary Reference Earth Model [*Dziewonski and Anderson*, 1981]; ak-135: Reference Earth Model [*Kennett et al*., 1995].

[77] In addition to the contradictory results on ferropericlase at room temperature and the scarce information on any other major lower mantle phase, the understanding of the effect of spin transitions on seismic wave propagation in the lower mantle is hampered by the lack of any simultaneous high *P-T* data. With the limitations imposed by our incomplete knowledge of the combined *P-T* effects, the currently available experimental and computational results regarding the elastic properties of ferropericlase across the spin transition [*Tsuchiya et al*., 2006; *Fei et al*., 2007a; *Crowhurst et al*., 2008; *Marquardt et al*., 2009a; *Wentzcovitch et al*., 2009;

Antonangeli et al., 2011; *Mao et al*., 2011a] can be utilized to construct velocity-depth profiles along an expected geothermal path [*Brown and Shankland*, 1981] for compositions relevant for the lower mantle (Figure 22). Based on two models for the broadening of the mixed-spin region at high temperatures [*Marquardt et al*., 2009b; *Mao et al*., 2011a], the maximum decrease of the compressional wave velocity induced by the spin-pairing transition in ferropericlase with relevant mantle composition $(Mg_{0.75}Fe_{0.25})O$ can be as large as 15% at 110 GPa, which corresponds to 2500 km depth. Such a large decrease would produce an effect of 3% decrease for a pyrolite mantle composition (which contains about 20 vol% ferropericlase at lower mantle conditions) (Figure 1). Regions with anomalously high Fe content could be affected by an even larger velocity decrease, though the location and the width of the mixed spin region are poorly constrained at present. Most importantly, it is evident that the role played by perovskite and post-perovskite is dominant in determining the average elastic properties of the deep mantle for realistic compositions such as pyrolitic or if the effect of Fe incorporation in the silicate phases is treated as a small perturbation of the shear properties of the Fe-free end members [*Murakami et al*., 2012], but data relative to the Fe-bearing silicate phases of the lower mantle are mostly lacking.

[78] The effect of Fe spin crossover on the elastic properties of ferropericlase and of perovskite has a potential impact on the overall dynamics of the deep mantle. In fact, the anomalous softening of the bulk modulus that has been widely observed in ferropericlase [*Crowhurst et al*., 2008; *Tsuchiya et al*., 2006] causes anomalies in the thermoelastic properties and induces a reduction of the activation energies for diffusion of Fe and Mg [*Wentzcovitch et al*., 2009; *Mao et al*., 2011a, 2011b; *Saha et al*., 2013]. This can affect the rheology of a pyrolitic mantle in the case of textural layering that allows weak ferropericlase grains to be interconnected [*Lin*, *et al*., 2009]. Some experimental results and preliminary computations suggest that spin crossover in perovskite is also associated with elastic softening [*Catalli et al*., 2011; *Hsu et al*., 2011]. As a consequence, it is possible that the depth dependence of the viscosity of the lower mantle is nonmonotonic and low viscosity layers can be present in the deep mantle with strong effects on the global mantle convection [*Matyska et al*., 2011].

[79] Fe diffusion within ferropericlase is affected by spin transitions, and the effect is amplified if the reduction of the activation energy due to elastic softening is taken into account [*Ammann et al*., 2011; *Saha et al*., 2011, 2013]. If diffusivity at grain-boundaries is 2 to 4 orders of magnitude higher than in crystals, the spin crossover would regulate the chemical homogenization of compositional anomalies at the bottom of the mantle [*Saha et al*., 2011, 2013].

[80] Finally, Fe spin crossover also affects the acoustic velocity and the anisotropy of ferropericlase [*Wentzcovitch et al*., 2009; *Marquardt et al*., 2009b]. The combination of density anomaly and change in the phonon spectrum has a potential impact on possible anomalies in lattice thermal conductivity of ferropericlase. If similar effects are confirmed for silicate perovskite, this could produce a new, more complex picture of dynamic behavior and energy flow across the deep mantle. New experimental and computational studies of the effect of Fe spin configuration changes on thermal conductivity are necessary to understand and quantify the relevance of these potential anomalies.

5. CONCLUSIONS

[81] The occurrence of the spin-pairing transitions in ferropericlase, perovskite, and post-perovskite visibly affects a range of physical and chemical properties that are crucial in determining several aspects of the geophysical, geochemical, and geodynamic behaviors of the Earth. Experimental and computational studies of the thermal and electrical conductivities, diffusion coefficients, and element fractionation and partitioning at the extreme *P-T* conditions of the lower mantle are still in their early stages. However, a number of general trends can be identified based on the extant results and aforementioned discussions in section 3, especially in the case of ferropericlase:

[82] 1. The spin-pairing transition of Fe^{2+} results in an increase in density, incompressibility, and shear wave anisotropy from the high-spin to low-spin ferropericlase, and a decrease in bulk modulus and compressional wave velocity occurs within the spin transition. The effects are significantly reduced at expected lower mantle *P-T* conditions because of the broad spin crossover behavior. The spin-pairing transition of the B-site Fe^{3+} in perovskite likely causes an increase in density from the high-spin to the low-spin state.

[83] 2. The spin-pairing transition of Fe^{2+} is responsible for a decrease of the electrical conductivity of ferropericlase, while no clear connection can be made between the spin transition in Fe^{3+} in the B site and the electrical conductivity of perovskite. The effect of the spin pairing of Fe in lower mantle minerals is probably less relevant than the anisotropic (electronic) structure of post-perovskite in a scenario of a highly conductive layer at the core-mantle boundary that can interact with the liquid core, affecting the length of the day [*Ohta et al*., 2008].

[84] 3. The electronic spin-pairing transitions of Fe in major lower mantle solids have the potential to produce anomalies in the depth-dependent thermal conductivity with consequences on the mantle convection. There are not yet experimental or computational constraints on the effect of the spin transition on the lattice thermal conductivity of the lower mantle materials. Based on the available optical and IR absorption experiments, radiative thermal conductivities of ferropericlase and perovskite are weakly affected by the spin transitions of Fe. Instead, radiative heat transfer is very sensitive to the Fe^{3+}/Fe^{2+} ratio. Available results on ferropericlase at simultaneous high *P-T* up to 55 GPa and 800 K measured in the DAC [*Goncharov et al*., 2008] indicate that temperature effects are moderate. The interpretation of the absorption spectra in terms of the thermal conductivity is controversial, especially in case of perovskite. Due to intrinsic experimental difficulties, different groups report variable values including up to one order of magnitude difference in the radiative thermal conductivity at lower mantle

conditions, with marked effects on our interpretation of the actual thermal structure of the deep Earth and its evolution through time [*Keppler et al*., 2008; *Goncharov et al*., 2009]. High radiative thermal conductivity comparable or exceeding the lattice contribution would help stabilize large-scale plumes arising from the core-mantle region [*Keppler et al*., 2008].

[85] 4. In the absence of direct experimental results, the effect of the spin transition on the diffusion of Fe in ferropericlase has been determined by ab initio computations [*Ammann et al*., 2011; *Saha et al*., 2011, 2013]. The absolute theoretical diffusion coefficient of Fe^{2+} in low-spin configuration also in the activated state, computed with *ab initio* methods, would be 4 orders of magnitude lower than the high-spin configuration at lower mantle conditions [*Saha et al*., 2011]. A thermodynamic model suggests that in the mixed spin regime, the diffusion of Fe^{2+} is 10 times slower compared to the high-spin state. Including the effect of elastic softening induced by the spin crossover, the diffusivity of Fe in ferropericlase would increase up to 30 times at lower mantle depths [*Saha et al*., 2013]. If grain-boundary diffusivity is 2 to 4 orders of magnitude larger than within the crystals, the predicted diffusion lengths of Fe^{2+} in ferropericlase and perovskite at lowermost-mantle *P-T* conditions would overlap the characteristic length for convective mixing, allowing chemical homogenization at length scale of 10 km in few hundred million years [*Saha et al*., 2011].

[86] 5. Deformation experiments conducted on ferropericlase show that the spin transition in ferropericlase does not change the most active slip systems. The transition is accompanied by a decrease of the deviatoric stress and/or the elastic strength [*Lin et al*., 2009]. *Wentzcovitch et al*. [2009], using an elastic strain energy model, predict a large reduction of viscosity associated with the spin transition in ferropericlase. Based on recent first-principles calculations [*Ammann et al*., 2011; *Saha et al*., 2011], Fe^{2+} diffuses faster than Mg in ferropericlase at any condition in the lower mantle. In addition to this, the diffusion in perovskite is predicted to be substantially lower than that of ferropericlase. This implies that the spin transition in ferropericlase does not play a major role in determining the rheology of the lower mantle [*Ammann et al*., 2011], with the possible exception of regions where ferropericlase is interconnected. However, the elastic softening induced by the spin transition increases the diffusivity of Fe in ferropericlase and has the potential to affect the diffusion of Mg as well [*Saha et al*., 2013], with consequences for its viscosity. The presence of elastic softening in silicate perovskite associated with spin pairing transition [*Catalli et al*., 2011; *Hsu et al*., 2011] could be associated with similar effects of its viscosity and open scenarios of a large-scale low viscosity layer in the deep mantle [*Matyska et al*., 2011].

[87] 6. The results of several experimental studies suggest that the spin transition directly affects Fe-Mg partitioning between perovskite and ferropericlase $K_D^{pv/fp}$. Both in Al-free and Al-bearing systems, the onset of the Fe^{2+} spin transition is accompanied by a decrease of $K_D^{pv/fp}$, with a total reduction of 20 to 25% between 60 and 110 GPa. Furthermore, the effect of temperature is to increase the $K_D^{pv/fp}$, although this has yet been clearly resolved. A rapid increase of the K_D is observed between 20 and 40 GPa in the Al-bearing pyrolite system [*Irifune*, 1994; *Wood*, 2000; *Irifune et al*., 2010]. This increase is related to the coupled Al^{3+}-Fe^{3+} substitution for Si^{4+} in perovskite, although it could also be connected to the spin transition of the B-site Fe^{3+}. Iron is strongly depleted in post-perovskite with respect to ferropericlase and coexisting perovskite [*Andrault et al*., 2010; *Sinmyo et al*., 2011]. The effect of the spin transition of iron in deep silicate melts coexisting with liquidus solid phases is not yet clear. *Nomura et al*. [2011] proposed that it causes a strong fractionation into the liquid, opening scenarios of substantial chemical heterogeneity in basal remnants of a primordial mantle-wide magma ocean. A more recent study by *Andrault et al*. [2012] contradicts Nomura's results. However, the occurrence of the spin transition in melts needs to be validated in situ. In addition to this, ab initio computations suggest a strong effect of the spin transition on the isotopic fractionation of Fe between ferropericlase and metallic iron, with an enrichment of the heavier low-spin Fe^{2+} in ferropericlase that is contrary to room pressure behavior of the high-spin state [*Polyakov*, 2009; *Rustard and Yin*, 2009]. In summary, the effects of the spin transitions of iron on the Fe-Mg partitioning between ferropericlase and perovskite, the incorporation of Al in the silicate phases, the valence state changes of Fe, the disproportionation of Fe^{2+} into $Fe^0 + Fe^{3+}$, and the partitioning of iron in coexisting deep partial silicate melt could produce signatures relevant to the transport properties and the rheology of the mantle.

[88] Future studies on the spin transitions and their associated effect should focus on measuring physical, chemical, rheological, and transport properties of lower mantle minerals with well-characterized spin and valence states at relevant *P-T* conditions in order to provide more definite answers on their consequences on the properties of the deep Earth. In particular, the temperature effects on the spin and valence states of silicate perovskite and post-perovskite, which are the main components in the Earth's lower mantle and the lowermost mantle, respectively, are critical to address their effects on the physics, chemistry, and dynamics of the Earth's lower mantle. Multidisciplinary approaches, including theoretical calculations and the combination of different experimental techniques, are needed to uncover many of the existing unresolved issues.

GLOSSARY

Brillouin Spectroscopy: A spectroscopic technique used to measure phonon energies by measuring the frequency (energy) shift of the scattered light due to the interaction of an incident electromagnetic wave from a laser and an acoustic wave of the lattice vibration (photon-phonon interaction). The energy shift is associated with either the creation (loss of energy) or the annihilation (gain of energy) of a phonon. The technique has been used to measure sound velocities of materials at high pressures and temperatures in a diamond anvil cell.

Crystal Field Theory: A model used to describe electron energy levels in the presence of a ligand. A ligand is an ion or molecule that binds to a central metal atom. The strength of these outer ligands influences the electronic properties

of the overall molecule through the interaction of electron orbitals and varying degrees of repulsion between the electrons in those orbitals. The 3*d*-electrons close to the ligands have a higher energy than those further away, resulting in a split in 3*d*-orbital energy levels. The way in which the energy levels split is dependent on the direction and angle with which the ligand electrons approach the central atom.

Crystal-Field Splitting Energy: The energy difference in between the highest and lowest 3*d*-orbital energy levels caused by the electron orbital interaction of a central metal atom and a ligand.

D″ Zone: The approximately 200 km lowermost layer of the mantle extending to the core-mantle boundary. This layer has specific seismic signatures that are distinct from the rest of the lower mantle. Silicate post-perovskite is believed to be present in the layer and to be the cause of the seismic anomalies.

Diamond Anvil Cell (DAC): A device used to generate the high-pressure conditions present in the deep Earth and allow the study of material properties when coupled with laser optical and/or synchrotron X-ray spectroscopies. A DAC consists of two opposing diamonds with a sample compressed between the flat tip surfaces of the diamonds (called culets). Pressure in a DAC is typically monitored using a reference calibrant with known pressure-behavior of a measureable property, such as the ruby fluorescence pressure scale. Brillouin scattering, X-ray diffraction, and other measurements can be obtained by illuminating the sample with either X-rays or visible light. The combination of DAC with resistive heaters or with infrared laser allows one to produce simultaneous high-pressure and high-temperature conditions.

Equation of State: A thermodynamic pressure-volume-temperature (*P*-*V*-*T*) relationship describing the state of matter under a given set of physical conditions. These relationships are independent of path. Equations of state are useful in describing the transition of solids from one crystalline state to another, and are used to understand incompressibility (bulk modulus) of matter in the Earth's interior.

Elastic Constants: Elastic constants relate the external stress and the responding strain for materials that obey Hooke's law. The stress is the mechanical action exerted on a material whereas the elastic strain is the infinitesimal change in the length and volume in respond to the exerted stress. Elastic constants are used to calculate a material's sound velocities and elastic moduli, notably the bulk modulus, shear modulus, and Young's modulus.

Electronic Spin: A quantum property of every electron associated with its intrinsic angular momentum. Though there are no suitable physical analogies to describe the spin quantum number, there are two possibilities called spin "up" and spin "down". Each electron has a spin momentum (S) of $\frac{1}{2}$.

Ferropericlase: A magnesium-rich magnesium/iron oxide ((MgFe)O). Ferropericlase is one of the main constituents of the Earth's lower mantle, together with silicate perovskite. Among the minerals of the lower mantle it is the one in which changes in the spin state of valence electrons in iron have been most extensively studied.

Gibbs Free Energy: A thermodynamic state function that describes the likelihood that a reaction will occur. It is defined as the enthalpy (H) of the system minus the product of the temperature (T) times the entropy (S) of the system ($G = H - ST$).

Hund's Rules: A set of rules that describe electronic states with the least amount of repulsion between electrons. For a set of degenerate orbitals, the lowest energy electron configuration of an atom is the one with the largest number of unpaired outer shell electrons. The rules assume that the repulsion between the outer electrons is much greater than the spin-orbit interaction, which is in turn stronger than any other remaining interactions.

Lower Mantle Geotherm: The pressure and temperature profile of the Earth's lower mantle as a function of depth. Lower mantle geotherm models are typically derived measured thermodynamic parameters, together with phase transition boundaries as anchor points.

High-Spin State: Crystal field theory state in which an electron will fill an empty orbital before pairing with another electron in a lower energy orbital. Each unpaired electron in the high-spin state has an orbital spin momentum (S) of ½.

Impulsive Stimulated Light Scattering (ISLS): A noncontact laser optical method used to characterize a high-frequency acoustic behavior. A sample is stimulated by pulses of light from an IR laser, allowing the observation of wave velocities by a green laser based on the acoustic response to the sudden laser stimulation and consequent acoustic decay time.

Inelastic X-ray Scattering (IXS): A nondestructive analytical technique based on the inelastic scattering of an X-ray beam after hitting a sample. The scattered angle, polarization, and wavelength, and energy of the intensity can be used to characterize a number of physical, chemical, and transport properties of a material.

Intermediate-Spin State: Crystal field theory state in which a compound is transitioning between high-spin and low-spin states. The state in perovskite is described as Fe^{2+} having only two unpaired electrons ($S = 1$).

Low-Spin State: Crystal field theory state in which all possible electrons are paired with other surrounding electrons in lower energy orbitals before occupying an empty higher-energy orbital.

Mössbauer spectroscopy: A spectroscopic technique used to analyze changes in and around the nucleus, including oxidation state changes, the effects of different ligands on an atom, and the magnetic environment of a sample. Solid samples are exposed to a beam of gamma radiation, and the intensity remaining after transmission through the sample is plotted against velocity of the accelerated source. A drop in intensity at velocities corresponding to resonant energy levels will produce a dip (quantum beat) in the Mössbauer spectrum. Applying a magnetic field will cause interactions between nuclei and the field, which produces a measurable hyperfine splitting in the Mössbauer spectrum.

Partition Coefficient: The ratio of concentrations of a given compound in the two phases of a mixture of two immiscible phases at equilibrium. These coefficients are a measure of the difference in solubility of the element in two phases.

Pyrolite: A hypothetical rock that is used to explain the chemical and mineralogical composition of the upper mantle of the Earth. The chemical composition of pyrolite is obtaining by a linear combination of the compositions of primitive basalt and refractory (residual) peridotite in a 1 : 3 mass ratio.

Quadrupole Splitting: A nuclear interaction that reflects the interaction between nuclear energy levels and the surrounding electric charge distribution. These interactions produce a doublet in the Mössbauer spectrum when the nucleus' field is non-spherical, and the separation between the states can be used to measure the sign and strength of this electric field gradient.

Radiative Thermal Conductivity: A measure of a substance's ability to transfer radiative heat. Thermal radiation is energy emitted by matter as electromagnetic waves as a direct result of the random movements of atoms and molecules in matter.

Rietveld Refinement: A method of analyzing a powdered sample's diffraction data to refine the crystal structure. The structural parameters are refined by fitting the entire profile of the diffraction pattern to a calculated profile using a least-squares approach.

Silicate Perovskite: An aluminum-containing magnesium iron (or calcium) silicate (Al-$MgSiO_3$) which has a perovskite structure. It is thought to form the main mineral phases in the lower mantle, together with ferropericlase. Magnesium silicate perovskite may form up to 75% of the lower mantle, making it the most abundant mineral in the Earth.

Silicate Post-Perovskite: A high-pressure polymorph of silicate perovskite. Silicate perovskite transitions to post-perovskite at the high pressure-temperature conditions of the D″ layer.

Spin-Pairing Energy: The energy needed to force an electron to fill an orbital that is already occupied with a single electron. If the crystal field splitting energy overcomes the spin-pairing energy, the electron will pair with a lower energy orbital rather than fill an empty higher-energy orbital. If the crystal field splitting energy is less than the spin-pairing energy, greater stability is maintained by keeping the electrons unpaired.

Spin Transition: The transition of electrons between a high-spin and low-spin state. The most common way to induce a spin transition is to change thermodynamic variables (pressure or temperature) of the system. The transition may be abrupt, occurring within a few kelvins range, smooth, occurring over a large temperature range (spin crossover), or incomplete.

X-ray Emission Spectroscopy (XES): An element-specific experimental technique used to determine the electronic structure of materials, especially as a means of probing the density of partially occupied electronic states of a material. An X-ray beam passes through a sample, during which time the X-ray photons may suffer an energy loss. This energy loss reflects an internal excitation of the atomic system.

[89] **ACKNOWLEDGMENTS.** J.F.L. and Z.M. acknowledge supports from the US National Science Foundation (NSF Geophysics: EAR-1056670 and NSF Instrumentation and Facility: EAR-1053446) and the Carnegie/DOE Alliance Center (CDAC). H.M. acknowledges support from the German Science Foundation (SP 1216/3-1). The authors thank T. Katsura, J. Brodholt, and C. McCammon for constructive comments and discussions, J. Yang for helping with the figures, and N. Seymour for editing the manuscript. The Editor on this paper was Fabio Florindo. He thanks John Brodholt and two anonymous reviewers for their review assistance on this manuscript.

REFERENCES

Abramson, E. H., J. M. Brown, and L. J. Slutsky (1999), Applications of impulsive stimulated scattering in the earth and planetary sciences, *Annu. Rev. Phys. Chem.*, *50*, 279–313.

Ammann, M. W., J. P. Brodholt, and D. P. Dobson (2011), Ferrous iron diffusion in ferro-periclase across the spin transition, *Earth Planet. Sci. Lett.*, *302*, 393–402.

Andrault, D. (2001), Evaluation of (Mg,Fe) partitioning between silicate perovskite and magnesiowüstite up to 120 GPa and 2300 K, *J. Geophys. Res.*, *106*, 2079–2087.

Andrault, D., M. Muñoz, N. Bolfan-Casanova, N. Guignot, J.-P. Perillat, G. Aquilanti, and S. Pascarelli (2010), Experimental evidence for perovskite and post-perovskite coexistence throughout the whole D″ region, *Earth Planet. Sci. Lett.*, *293*, 90–96.

Andrault, D., S. Petitgirard, G. Lo Nigro, J.-L. Devidal, G. Veronesi, and G. Garbarino (2012), Solid-liquid iron partitioning in Earth's deep mantle, *Nature*, *487*, 354–357.

Antonangeli, D., J. Siebert, C. M. Aracne, D. L. Farber, A. Bosak, M. Hoesch, M. Krisch, Frederick J. Ryerson, G. Fiquet, and J. Badro (2011), Spin crossover in ferropericlase at high pressure: A seismologically transparent transition?, *Science*, *331*, 64–67.

Auzende, A.- L., J. Badro, F. J. Ryerson, P. K. Weber, S. J. Fallon, A. Addad, J. Siebert, and G. Fiquet (2008), Element partitioning between magnesium silicate perovskite and ferropericlase: New insights into bulk lower-mantle geochemistry, *Earth Planet. Sci. Lett.*, *269*, 164–174.

Badro, J., G. Fiquet, F. Guyot, J. P. Rueff, V. V. Struzhkin, G. Vankó, and G. Monaco (2003), Iron partitioning in Earth's mantle: Toward a deep lower mantle discontinuity, *Science*, *300*, 789–791.

Badro, J., J. P. Rueff, G. Vankó, G. Monaco, G. Fiquet, and F. Guyot (2004), Electronic transitions in perovskite: Possible nonconvecting layers in the lower mantle, *Science*, *305*, 383–386.

Badro, J., G. Fiquet, and F. Guyot (2005), Thermochemical state of the lower mantle: New insights from mineral physics, in *Earth's Deep Mantle: Structure, Composition, and Evolution, Geophys. Monogr. Ser.*, vol. *160*, edited by R. D. van der Hilst, J. D. Bass, J. Matas, and J. Trampert, pp. 241–260, AGU, Washington, D. C.

Barna, Á, B. Pécz, and M. Menyhard (1999), TEM sample preparation by ion milling/amorphization, *Micron*, *30*, 267–276.

Beck, P., A. F. Goncharov, V. V. Struzhkin, B. Militzer, H.- K. Mao, and R. J. Hemley (2007), Measurement of thermal diffusivity at high pressure using a transient heating technique, *Appl. Phys. Lett.*, *91*, 181914.

Beck, P., A. F. Goncharov, J. A. Montoya, V. V. Struzhkin, B. Militzer, R. J. Hemley, and H.- K. Mao (2009), Response to "Comment on 'Measurement of thermal diffusivity at high pressure using a transient heating technique'" [Appl. Phys. Lett., 95, 096101 (2009)], *Appl. Phys. Lett.*, *95*, 096102.

Bengtson, A., K. Persson, and D. Morgan (2008), Ab initio study of the composition dependence of the pressure induced spin crossover in perovskite $(Mg_{1-x},Fe_x)SiO_3$, *Earth Planet. Sci. Lett.*, *265*, 535–545.

Bengtson, A., J. Li, and D. Morgan (2009), Mössbauer modeling to interpret the spin state of iron in $(Mg,Fe)SiO_3$ perovskite, *Geophys. Res. Lett.*, *36*, L15301, doi:10.1029/2009GL038340.

Boffa Ballaran, T., A. Kurnosov, K. Glazyrin, D. J. Frost, M. Merlini, M. Hanfland, and R. Caracas (2012), Effect of chemistry on the compressibility of silicate perovskite in the lower mantle, *Earth Planet Sci. Lett.*, *333–334*, 181–190.

Brown, J. M., and T. J. Shankland (1981), Thermodynamic parameters in the Earth as determined from seismic profiles, *Geophys. J. R. Astron. Soc.*, *66*, 579–596.

Burns, R. G. (1993), *Mineralogical Applications of Crystal Field Theory*. Cambridge Univ. Press, Cambridge, U. K.

Cammarano, F., H. Marquardt, S. Speziale, and P. J. Tackley (2010), Role of iron-spin transition in ferropericlase on seismic interpretation: A broad thermochemical transition in the mid mantle?, *Geophys. Res. Lett.*, *37*, L03308, doi:10.1029/2009GL041583.

Caracas, R., and R. E. Cohen (2007), Effect of chemistry on the physical properties of perovskite and post-perovskite in *Post-Perovskite: The Last Mantle Phase Transition, Geophys. Monogr. Ser.*, vol. 174, edited by K. Hirose et al., pp. 115–128, AGU, Washington, D. C.

Caracas, R., and R. E. Cohen (2008), Ferrous iron in post-perovskite from first-principles calculations, *Phys. Earth Planet. Inter.*, *168*, 147–152.

Caracas, R., D. Mainprice, and C. Thomas (2010), Is the spin transition in Fe^{2+}-bearing perovskite visible in seismology?, *Geophys. Res. Lett.*, *37*, L13309, doi:10.1029/2010GL043320.

Catalli, K., S. H. Shim, V. B. Prakapenka, J. Zhao, W. Sturhahn, P. Chow, Y. Xiao, H. Liu, H. Cynn, and W. J. Evans (2010a), Spin state of ferric iron in $MgSiO_3$ perovskite and its effect on elastic properties, *Earth Planet. Sci. Lett.*, *289*, 68–75.

Catalli, K., S. H. Shim, V. B. Prakapenka, J. Zhao, and W. Sturhahn (2010b), X-ray diffraction and Mössbauer spectroscopy of Fe^{3+}-bearing Mg-silicate post-perovskite at 128–138 GPa, *Am. Mineral.*, *95*, 418–421.

Catalli, K., S.-H. Shim, P. Dera, V. B. Prakapenka, J. Zhao, W. Sturhahn, P. Chow, Y. Xiao, H. Cynn, and W. J. Evans (2011), Effects of the Fe^{3+} spin transition on the properties of aluminous perovskite—New insights for lower-mantle seismic heterogeneities, *Earth Planet. Sci. Lett.*, *310*, 293–302.

Černá, K., M. Mašláň, and P. Martinec (2000), Mössbauer spectroscopy of garnets of almandine-pyrope series, *Materials Structure*, *7*, 6–9.

Cohen, R. E., I. I. Mazin, and D. G. Isaak (1997), Magnetic collapse in transition metal oxides at high pressure: Implications for the Earth, *Science*, *275*, 654–657.

Crispin, K. L., and J. A. van Orman (2010), Influence of the crystal field effect on chemical transport in Earth's mantle: Cr^{3+} and Ga^{3+} diffusion in periclase, *Phys. Earth Planet. Inter.*, *180*, 159–171.

Crowhurst, J. C., J. M. Brown, A. F. Goncharov, and S. D. Jacobsen (2008), Elasticity of (Mg,Fe)O through the spin transition of iron in the lower mantle, *Science*, *319*, 451–453.

Dasgupta, R., and M. M. Hirschmann (2010), The deep carbon cycle and melting in Earth's interior, *Earth Planet. Sci. Lett.*, *298*, 1–13.

de Koker, N. (2010), Thermal conductivity of MgO periclase at high pressure: Implications for the D″ region, *Earth Planet. Sci. Lett.*, *292*, 392–398.

Dobson, D. P., and J. P. Brodholt (2000), The electrical conductivity of the lower mantle phase magnesiowüstite at high temperatures and pressures, *J. Geophys. Res.*, *105*, 531–538.

Dobson, D. P., N. C. Richmond, and J. P. Brodholt (1997), A high-temperature electrical conduction mechanism in the lower mantle phase $(Mg,Fe)_{1-x}O$, *Science*, *275*, 1779–1781.

Dziewonski, A., and D. L. Anderson (1981), Preliminary earth reference model, *Phys. Earth Planet. Inter.*, *25*, 297–356.

Farfan, G., S. Wang, H. Ma, R. Caracas, and W. L. Mao (2012), Bonding and structural changes in siderite at high pressure, *Am. Miner.*, *97*, 1421–1426.

Fei, Y., L. Zhang, A. Corgne, H. C. Watson, A. Ricolleau, Y. Meng, and V. B. Prakapenka (2007a), Spin transition and equations of state of (Mg, Fe)O solid solutions, *Geophys. Res. Lett.*, *34*, L17307, doi:10.1029/2007GL030712.

Fei, Y., A. Ricolleau, M. Frank, K. Mibe, G. Shen, and V. Prakapenka (2007b), Towards an internally consistent pressure scale, *Proc. Natl. Acad. Sci. U.S.A.*, *104*, 9182–9186.

Fialin, M., G. Catillon, and D. Andrault (2009), Disproportionation of Fe^{2+} in Al-free silicate perovskite in the laser heated diamond anvil cell as recorded by electron probe microanalysis of oxygen, *Phys. Chem. Miner.*, *36*, 183–191.

Fyfe, W. S. (1960), The possibility of *d*-electron uncoupling in olivine at high pressures, *Geochim. Cosmochim. Acta*, *19*, 141–143.

Frost, D. J., and F. Langenhorst (2002), The effect of Al_2O_3 on Fe-Mg partitioning between magnesiowüstite and magnesium silicate perovskite, *Earth Planet. Sci. Lett.*, *199*, 227–241.

Frost, D. J., C. Liebske, F. Langenhorst, C. A. McCammon, R. G. Tronnes, and D. C. Rubie (2004), Experimental evidence for the existence of iron-rich metal in the Earth's lower mantle, *Nature*, *428*, 409–412.

Fujino, K., et al. (2012), Spin transition of ferric iron in Al-bearing Mg-perovskite up to 200 GPa and its implication for the lower mantle, *Earth Planet. Sci. Lett.*, *317–318*, 407–412.

Goncharov, A. F., V. V. Struzhkin, and S. D. Jacobsen (2006), Reduced radiative thermal conductivity of low-spin (Mg,Fe)O in the lower mantle, *Science*, *312*, 1205–1208.

Goncharov, A. F., B. D. Haugen, V. V. Struzhkin, P. Beck, and S. D. Jacobsen (2008), Radiative thermal conductivity in the Earth's lower mantle, *Nature*, *456*, 231–234.

Goncharov, A. F., P. Beck, V. V. Struzhkin, B. D. Haugen, and S. D. Jacobsen (2009), Thermal conductivity of lower-mantle minerals, *Phys. Earth Planet. Inter.*, *174*, 24–32.

Goncharov, A. F., V. V. Struzhkin, J. A. Montoya, S. Kharlamova, R. Kundargi, J. Siebert, J. Badro, D. Antonangeli, F. J. Ryerson, and W. Mao (2010), Effect of composition, structure, and spin state on the thermal conductivity of the Earth's lower mantle, *Phys. Earth Planet. Inter.*, *180*, 148–153.

Grocholski, B., S. H. Shim, W. Sturhahn, J. Zhao, Y. Xiao, and C. Chow (2009), Spin and valence states of iron in $(Mg_{0.8}Fe_{0.2})SiO_3$ perovskite, *Geophys. Res. Lett.*, *36*, L24303, doi:10.1029/2009GL041262.

Guignot, N., D. Andrault, G. Morard, N. Bolfan-Casanova, and M. Mezouar (2007), Thermoelastic properties of post-perovskite phase $MgSiO_3$ system, *Earth Planet Sci. Lett.*, *256*, 162–168.

Haigis, V., M. Salanne, and S. Jahn (2012), Thermal conductivity of MgO, $MgSiO_3$ perovskite and post-perovskite in the Earth's deep mantle, *Earth Planet. Sci. Lett.*, *355–356*, 102–108.

Hawthorne, F. C. (1988), Mössbauer spectroscopy, *Rev. Mineral.*, *18*, 255–340.

Hayden, L. A., and E. B. Watson (2007), A diffusion mechanism for core-mantle interaction, *Nature*, *450*, 709–711.

Hirose, K., N. Takafuji, K. Fujino, S. R. Shieh, and T. S. Duffy (2008), Iron partitioning between perovskite and post-perovskite: A transmission electron microscope study, *Am. Mineral.*, *93*, 1678–1681.

Hofmeister, A. M., E. Keppel, and A. K. Speck (2003), Absorption and reflection infrared spectra of MgO and other diatomic compounds, *Mon. Not. R. Astron. Soc.*, *345*, 16–38.

Hofmeister, A. M. (2009), Comment on "Measurement of thermal diffusivity at high pressure using a transient heating technique" [Appl. Phys. Lett., 91, 181914 (2007)], *Appl. Phys. Lett.*, *95*, 096101.

Hsu, H., K. Umemoto, P. Blaha, and R. M. Wentzcovitch (2010), Spin states and hyperfine interactions of iron in $(Mg,Fe)SiO_3$ perovskite under pressure, *Earth Planet. Sci. Lett.*, *294*, 19–26.

Hsu, H., P. Blaha, M. Cococcioni, and R. M. Wentzcovitch (2011), Spin-state crossover and hyperfine interactions of ferric iron in $MgSiO_3$ perovskite, *Phys. Res. Lett.*, *106*, 118501.

Hsu, H., Y. G. Yu, and R. M. Wentzcovitch (2012), Spin crossover of iron in aluminous $MgSiO_3$ perovskite and post-perovskite, *Earth Planet. Sci. Lett.*, *294*, 19–26.

Irifune, T. (1994), Absence of an aluminous phase in the upper part of the Earth's lower mantle, *Nature*, *370*, 131–133.

Irifune, T., and M. Isshiki (1998), Iron partitioning in a pyrolite mantle and the nature of the 410-kmseismic discontinuity, *Nature*, *370*, 131–133.

Irifune, T., and A. E. Ringwood (1987), Phase transformation in a harzburgite composition to 26 GPa: Implications for dynamical behaviour of the subducting slab, *Earth Planet. Sci. Lett.*, *86*, 365–376.

Irifune, T., and A. E. Ringwood (1993), Phase transformations in subducted oceanic crust and buoyancy relationships at depths of 600–800 km in the mantle, *Earth Planet. Sci. Lett.*, *117*, 101–110.

Irifune, T., T. Shinmei, C. A. McCammon, N. Miyajima, D. C. Rubie, and D. J. Frost (2010), Iron partitioning and density changes of pyrolite in Earth's lower mantle, *Science*, *327*, 193–195.

Heinz, D. L., and R. Jeanloz (1987), Measurements of the melting curve of $Mg_{0.9}Fe_{0.1}SiO_3$ at lower mantle conditions and its geophysical implications, *J. Geophys. Res.*, *92*, 11,437–11,444.

Hirose, K. (2006), Postperovskite phase transition and its geophysical implications, *Rev. Geophys.*, *44*, RG3001, doi:10.1029/2005RG000186.

Jackson, I. (2008), Physical origins of anelasticity and attenuation in rock, in *Treatise on Geophysics*, vol. 2, *Properties of Rocks and Minerals*, pp. 493–525, Elsevier, Boston, Mass.

Jackson, J. M., W. Sturhahn, G. Shen, J. Zhao, M.Y. Hu, D. Errandonea, J. D. Bass, and Y. Fei (2005), A synchrotron Mössbauer spectroscopy study of $(Mg,Fe)SiO_3$ perovskite up to 120 GPa, *Amer. Miner.*, *90*, 199–205.

Jackson, J. M., S. V. Sinogeikin, S. D. Jacobsen, H. J. Reichmann, S. J. Mackwell, and J. D. Bass (2006), Single-crystal elasticity and sound velocities of $(Mg_{0.94}Fe_{0.06})O$ ferropericlase to 20 GPa, *J. Geophys. Res.*, *111*, B09203, doi:10.1029/2005JB004052.

Jackson, J. M., W. Sturhahn, O. Tschauner, M. Lerche, and Y. Fei (2009), Behavior of iron in post-perovskite assemblages at Mbar pressures, *Geophys. Res. Lett.*, *36*, L10301, doi:10.1029/2009GL037815.

Jacobsen, S. D., H.-J. Reichmann, H. A. Spetzler, S. J. Mackwell, J. R. Smyth, R. J. Angel, and C. A. McCammon (2002), Structure and elasticity of single-crystal (Mg,Fe)O and a new method of generating shear waves for gigahertz ultrasonic interferometry, *J. Geophys. Res.*, *107*(B2), 2037, doi:10.1029/2001JB000490.

Jacobsen, S. D., H. A. Spetzler, H. S. Reichmann, and J. R. Smyth (2004), Shear waves in the diamond-anvil cell reveal pressure-induced instability in (Mg,Fe)O, *Proc. Natl. Acad. Sci. U.S.A.*, *101*, 5867–5871.

Kantor, I. Y., L. S. Dubrovinsky, and C. A. McCammon (2006), Spin crossover in (Mg,Fe)O: A Mössbauer effect study with an alternative interpretation of X-ray emission spectroscopy data, *Phys. Rev. B*, *73*, 100101(R).

Kantor, I., L. Dubrovinsky, C. McCammon, G. Steinle-Neumann, A. Kantor, N. Skorodumova, S. Pascarelli, and G. Aquilanti (2009), Short-range order of Fe and clustering in $Mg_{1-x}Fe_xO$ under high pressure, *Phys. Rev. B*, *80*, 014204.

Karato, S.-I. (1998), Seismic anisotropy in the deep mantle and the geometry of mantle convection, *Pure Appl. Geophys.*, *151*, 565–587.

Karato, S.-I. (2008), *Deformation of Earth Materials*, 463 pp., Cambridge Univ. Press, New York.

Karki, B. B., R. M. Wentzcovitch, S. de Gironcoli, and S. Baroni (1999), First-principles determination of elastic anisotropy and wave velocities of MgO at lower mantle conditions, *Science*, *286*, 1705–1707.

Kellogg, L. H., and D. L. Turcotte (1987), Homogenization of the mantle by convective mixing and diffusion, *Earth Planet. Sci. Lett.*, *81*, 371–388.

Kennett, B. L. N., E. R. Engdahl, and R. Buland (1995), Constraints on seismic velocities in the earth from travel times, *Geophys. J. Int.*, *122*, 108–124.

Kennett B. L. N., S. Widiyantoro and R. D. van der Hilst (1998), Joint seismic tomography for bulk sound and shear wave speed in the Earth's mantle, *J. Geophys. Res. 103*, 12,469–12,493

Keppler, H., C. A. McCammon, and D. C. Rubie (1994), Crystal-field and charge-transfer spectra of $(Mg,Fe)SiO_3$ perovskite, *Am. Miner.*, *79*, 1215–1218.

Keppler, H., I. Kantor, and L. S. Dubrovinski (2007), Optical absorption spectra of ferropericlase to 84 GPa, *Am. Miner.*, *92*, 433–436.

Keppler, H., L. S. Dubrovinski, O. Narygina, and I. Kantor (2008), Optical absorption and radiative thermal conductivity of silicate perovskite to 125 gigapascals, *Science*, *322*, 1529–1532.

Kesson, S. E., H. S. O'Neill, and J. M. G. Shelley (2002), Partitioning of iron between magnesian silicate perovskite and magnesiowüstite at about 1 Mbar, *Phys. Earth Planet. Inter.*, *131*, 295–310.

Kobayashi, Y., T. Kondo, E. Ohtani, N. Hirao, N. Miyajima, T. Yagi, T. Nagase, and T. Kikegawa (2005), Fe-Mg partitioning between $(Mg, Fe)SiO_3$ post-perovskite, perovskite, and magnesiowüstite in the Earth's lower mantle, *Geophys. Res. Lett.*, *32*, L19301, doi:10.1029/2005GL023257.

Komabayashi, T., K. Hirose, Y. Nagaya, E. Sugimura, and Y. Ohishi (2010), High temperature compression of ferropericlase and the effect of temperature on iron spin transition, *Earth Planet. Sci. Lett.*, *297*, 691–699.

Kung, J., B. Li, D. L. Weidner, J. Zhang, and R. C. Liebermann (2002), Elasticity of $(Mg_{0.83}Fe_{0.17})O$ ferropericlase at high pressure: Ultrasonic measurements in conjunction with X-radiation techniques, *Earth Planet. Sci. Lett.*, *203*, 557–566.

Labrosse, S., J. W. Hernlund, and N. A. Coltice (2007), A crystallizing dense magma ocean at the base of the Earth's mantle, *Nature*, *450*, 866–869.

Lavina, B., P. Dera, R. T. Downs, V. Prakapenka, M. Rivers, S. Sutton, and M. Nicol (2009), Siderite at lower mantle conditions and the effects of the pressure-induced spin-pairing transition, *Geophys. Res. Lett.*, *36*, L23306, doi:10.1029/2009GL039652.

Lavina, B., P. Dera, R. T. Downs, O. Tschauner, W. Yang, O. Shebanova, and G. Shen (2010a) Effect of dilution on the spin pairing transition in rhombohedral carbonates, *High Pressure Res.*, *30*, 224–229.

Lavina, B., P. Dera, R. T. Downs, W. Yang, S. Sinogeikin, Y. Meng, G. Shen and D. Schiferl (2010b) Structure of siderite $FeCO_3$ to 56 GPa and hysteresis of its spin-pairing transition, *Phys. Rev. B*, *82*, 064110.

Li, J., V. V. Struzhkin, H. K. Mao, J. Shu, R. J. Hemley, Y. Fei, B. Mysen, P. Dera, V. Prakapenka, and G. Shen (2004), Electronic spin state of iron in lower mantle perovskite, *Proc. Natl. Acad. Sci. U.S.A.*, *101*, 14027–14030.

Li, J., W. Sturhahn, J. M. Jackson, V. V. Struzhkin, J. F. Lin, J. Zhao, H. K. Mao, and G. Shen (2006), Pressure effect on the electronic structure of iron in $(Mg,Fe)(Si,Al)O_3$ perovskite: A combined synchrotron Mössbauer and X-ray emission spectroscopy study up to 100 GPa, *Phys. Chem. Miner.*, *33*, 575–585.

Li, L., J. P. Brodholt, S. Stackhouse, D. J. Weidner, M. Alfredsson, and G. D. Price (2005a), Electronic spin state of ferric iron in Al-bearing perovskite in the lower mantle, *Geophys. Res. Lett.*, *32*, L17307, doi:10.1029/2005GL023045.

Li, L., J. P. Brodholt, S. Stackhouse, D. J. Weidner, M. Alfredsson, and G. D. Price (2005b), Elasticity of $(Mg,Fe)(Si,Al)O_3$-perovskite at high pressure, *Earth Planet. Sci. Lett.*, *240*, 529–536.

Lin, J. F., and T. Tsuchiya (2008), Spin transition of iron in the Earth's lower mantle, *Phys. Earth Planet. Inter.*, *170*, 248–259.

Lin, J. F., V. V. Struzhkin, S. D. Jacobsen, M. Hu, P. Chow, J. Kung, H. Liu, H. K. Mao, and R. J. Hemley (2005), Spin transition of iron in magnesiowüstite in Earth's lower mantle, *Nature*, *436*, 377–380.

Lin, J. F., A. G. Gavriliuk, V. V. Struzhkin, S. D. Jacobsen, W. Sturhahn, M. Y. Hu, P. Chow, and C.-S. Yoo (2006a), Pressure-induced electronic spin transition of iron in magnesiowüstite-(Mg,Fe)O, *Phys. Rev. B*, *73*, 113107.

Lin, J. F., S. D. Jacobsen, W. Sturhahn, J. M. Jackson, J. Zhao, and C. S. Yoo (2006b), Sound velocities of ferropericlase in the Earth's lower mantle, *Geophys. Res. Lett.*, *33*, L22304, doi:10.1029/2006GL028099.

Lin, J. F., G. Vankó, S. D. Jacobsen, V. Iota, V. V. Struzhkin, V. B. Prakapenka, A. Kuznetsov, and C.-S. Yoo (2007a), Spin transition zone in Earth's lower mantle, *Science*, *317*, 1740–1743.

Lin, J. F., S. T. Weir, D. D. Jackson, W. J. Evans, and C. J. Yoo (2007b), Electrical conductivity of the lower-mantle ferropericlase across the electronic spin transition, *Geophys. Res. Lett.*, *34*, L16305, doi:10.1029/2007GL030523.

Lin, J. F., H. C. Watson, G. Vankó, E. E. Alp, V. B. Prakapenka, P. Dera, V. V. Struzhkin, A. Kubo, J. Zhao, C. McCammon, and W. J. Evans (2008), Intermediate-spin ferrous iron in lowermost mantle post-perovskite and perovskite, *Nat. Geosci.*, *1*, 688–691.

Lin, J. F., H-R. Wenk, M. Voltolini, S. Speziale, J. Shu, and T. S. Duffy (2009), Deformation of lower-mantle ferropericlase (Mg,Fe)O across the electric spin transition, *Phys. Chem. Minerals*, *36*, 582–592.

Lin, J. F., E. E. Alp, Z. Mao, T. Inoue, C. McCammon, Y. Xiao, P. Chow, and J. Zhao (2012a), Electronic spin and valence states of iron in the lower-mantle silicate perovskite by synchrotron Mössbauer spectroscopy, *Am. Miner.*, *97*, 592–597.

Lin, J. F., J. Liu, C. Jacobs, and V. B. Prakapenka (2012b), Vibrational and elastic properties of ferromagnesite across the electronic spin-pairing transition of iron, *Am. Miner.*, *97*, 583–591.

Lundin, S., K. Catalli, J. Santillán, S.-H. Shim, V. B. Prakapenka, M. Kunz, and Y. Meng (2008), Effect of Fe on the equation of state of mantle silicate perovskite over 1 Mbar, *Phys. Earth Planet Inter.*, *168*, 97–102.

Manthilake, G. M., N. de Koker, D. J. Frost, and C. A. McCammon (2011), Lattice thermal conductivity of lower mantle minerals and heat flux from Earth's core, *Proc. Natl. Acad. Sci. U.S.A.*, *108*, 17901–17904.

Mao, H.-K., et al. (2001), Phonon density of states of iron up to 153 Gigapascals, *Science*, *292*, 914–916.

Mao, W. L., G. Shen, V. B. Prakapenka, Y. Meng, A. J. Campbell, D. L. Heinz, J. Shu, R. J. Hemley, and H. K. Mao (2004), Ferromagnesian postperovskite silicates in the D″ layer of the Earth, *Proc. Natl. Acad. Sci. U.S.A.*, *101*, 15867–15869.

Mao, W. L., H. K. Mao, W. Sturhahn, J. Zhao, V. B. Prakapenka, Y. Meng, J. Shu, Y. Fei, and R. J. Hemley (2006), Iron-rich post-perovskite and the origin of ultralow-velocity zones, *Science*, *312*, 564–565.

Mao, Z., J. F. Lin, C. Jacobs, H. Watson, Y. Xiao, P. Chow, E. E. Alp, and V. B. Prakapenka (2010), Electronic spin and valence states of Fe in $CaIrO_3$-type post-perovskite in the Earth's lowermost mantle, *Geophys. Res. Lett.*, *37*, L22304, doi:10.1029/2010GL045021.

Mao, Z., J. F. Lin, J. Liu, and V. B. Prakapenka (2011a), Thermal equation of state of lower-mantle ferropericlase across the spin crossover, *Geophys. Res. Lett.*, *38*, L23308, doi:10.1029/2011GL049915.

Mao, Z., J. F. Lin, H. P. Scott, H. Watson, V. B. Prakapenka, Y. Xiao, and P. Chow (2011b), Stiff iron-rich silicate perovskite in the large low shear velocity provinces, *Earth Planet. Sci. Lett.*, *309*, 179–184.

Marquardt, H., S. Speziale, H. J. Reichmann, D. J. Frost, and F. R. Schilling (2009a), Single-crystal elasticity of $(Mg_{0.9}Fe_{0.1})O$ to 81 GPa, *Earth Planet. Sci. Lett.*, *287*, 345–352.

Marquardt, H., S. Speziale, H. J. Reichmann, D. J. Frost, F. R. Schilling, and E. J. Garnero (2009b), Elastic shear anisotropy of ferropericlase in Earth's lower mantle, *Science*, *324*, 224–226.

Marquardt, H., A. Gleason, K. Marquardt, S. Speziale, L. Miyagi, G. Neusser, H. R. Wenk and R. Jeanloz (2011), Elastic properties of MgO nano-crystals and grain boundaries to high pressures, *Phys. Rev. B*, *84*, 064131.

Masters G., G. Laske, H. Bolton and A. Dziewonski (2000), The relative behavior of shear velocity, bulk sound speed, and compressional velocity in the mantle: Implications for chemical and thermal structure, in *Earth's Deep Interior: Mineral Physics and Tomography From the Atomic to the Global Scale, Geophys. Monogr. Ser.*, vol *117*, edited by S. Karato et al., pp. 63–87, AGU, Washington, D. C.

Mattila, A., T. Pylkkänen, J. P. Rueff, S. Huotari, G. Vankó, M. Hanfland, M. Lehtinen, and K. Hämäläinen (2007), Pressure induced magnetic transition in siderite $FeCO_3$ studied by x-ray emission spectroscopy, *J. Physics: Con. Matt.*, *19*, 386206.

Matyska, C., D.A. Yuen, R.M. Wentzcovitch, H. Čížková (2011), The impact of variability in rheological activation parameters on lower-mantle viscosity stratification and its dynamics, *Phys. Earth Planet. Inter.*, *188*, 1–8.

McCammon, C. A. (1997), Perovskite as a possible sink for ferric iron in the lower mantle, *Nature*, *387*, 694–696.

McCammon, C. (2006), Microscopic properties to macroscopic behavior: The influence of iron electronic states. *J. Miner. Petro. Sci. 101*, 130–144.

McCammon, C., J. Peyronneau, and J.-P. Poirier (1998), Low ferric iron content of (Mg,Fe)O at high pressures and temperatures, *Geophys. Res. Lett.*, *25*, 1589–1592.

McCammon, C., I. Kantor, O. Narygina, J. Rouquette, U. Ponkratz, I. Sergueev, M. Mezouar, V. B. Prakapenka, and L. Dubrovinsky (2008a), Stable intermediate-spin ferrous iron in lower mantle perovskite, *Nat. Geosci.*, *1*, 684–687.

McCammon, C. A., L. Dubrovinsky, I. Kantor, O. Narygina, X. Wu, A. Chumakov, and I. Sergeev (2008b), Elastic wave velocities of lower mantle perovskite with intermediate-spin iron and consequences for mantle properties and dynamics, *Eos Trans. AGU*, *89*(53), Fall Meet. Suppl., Abstract MR23A-07.

McCammon, C., L. Dubrovinsky, O. Narygina, I. Kantor, X. Wu, K. Glazyrin, I. Sergueev, and A. I. Chumakov (2010), Low-spin Fe^{2+} in silicate perovskite and a possible layer at the base of the lower mantle, *Phys. Earth Planet. Inter.*, *180*, 215–221.

Metsue, A. and T. Tsuchiya (2012), Thermodynamic properties of $(Mg,Fe^{2+})SiO_3$ perovskite at the lower-mantle pressures and temperatures: An internally consistent LSDA + U study, *Geophys. J. Int.*, *190*, 310–322.

Morra, G., D. A. Yuen, L. Boschi, P. Chatelain, P. Koumoutsakos, and P. J. Tackley (2010), The fate of the slabs interacting with a density/viscosity hill in the mid-mantle, *Phys. Earth Planet. Inter.*, *180*, 271–282.

Murakami, M., K. Hirose, K. Kawamura, N. Sata, and Y. Ohishi (2004), Post-perovskite phase transition in $MgSiO_3$, *Science*, *304*, 855–858.

Murakami, M., K. Hirose, N. Sata, and Y. Ohishi (2005), Post-perovskite phase transition and mineral chemistry in the pyrolitic lowermost mantle, *Geophys. Res. Lett.*, *32*, L03304, doi:10.1029/2004GL021956.

Murakami, M., Y. Ohishi, N. Hirao, and K. Hirose (2012), A perovskitic lower mantle inferred from high-pressure, high-temperature sound velocity data, *Nature*, *485*, 90–95.

Nagai, T., T. Ishido, Y. Seto, D. Nishio-Hamane, N. Sata, and K. Fujino (2010), Pressure-induced spin transition in $FeCO_3$-siderite studied by X-ray diffraction measurements, *J. Phys. Conf. Ser.*, *215*, 012002.

Narygina, O., M. Mattesini, I. Kantor, S. Pascarelli, X. Wu, G. Aquilanti, C. McCammon, and L. Dubrovinsky (2009), High-pressure experimental and computational XANES studies of $(Mg,Fe)(Si,Al)O_3$ perovskite and (Mg,Fe)O ferropericlase as in the Earth's lower mantle, *Phys. Rev. B*, *79*, 174175.

Narygina, O. V., I. Y. Kantor, C. A. McCammon, and L. S. Dubrovinsky (2010), Electronic state of Fe^{2+} in $(Mg,Fe)(Si,Al)O_3$ perovskite and $(Mg,Fe)SiO_3$ majorite at pressures up to 81 GPa and temperatures up to 800 K, *Phys. Chem. Miner.*, *37*, 407–415.

Narygina, O., L. S. Dubrovinski, H. Samuel, C. A. McCammon, I. Y. Kantor, K. Glazyrin, S. Pascarelli, G. Aquilanti, and V. B. Prakapenka (2011), Chemically homogeneous spin transition zone in Earth's lower mantle, *Phys. Earth Planet. Inter.*, *185*, 107–111.

Nellis, W., S. Weir, and A. Mitchell (1999), Minimum metallic conductivity of fluid hydrogen at 140 GPa (1.4 Mbar), *Phys. Rev. B*, *59*, 3434–3449.

Nishio-Hamane, D., and T. Yagi (2009), Equations of state for postpoervskite phases in the $MgSiO_3$-$FeSiO_3$-$FeAlO_3$ system, *Phys. Earth Planet. Inter.*, *175*, 145–150.

Nomura R., H. Ozawa, S. Tateno, K. Hirose, J. Hernlund, S. Muto, H. Ishii, and N. Hiraoka (2011), Spin crossover and iron-rich silicate melt in the Earth's deep mantle, *Nature*, *473*, 199–203.

Oganov, A. R. and S. Ono (2004), Theoretical and experimental evidence for a post-perovskite phase of $MgSiO_3$ in Earth's D″ layer, *Nature*, *430*, 445–448.

Oganov, A. R., R. Martoňák, A. Laio, P. Raiteri, and M. Parrinello (2005), Anisotropy of Earth's D″ layer and stacking faults in the $MgSiO_3$ post-perovskite phase, *Nature*, *438*, 1142–1144.

Ohta, K., K. Hirose, S. Onoda, and K. Shimizu (2007), The effect of iron spin transition on electrical conductivity of magnesiowüstite, *Proc. Jpn. Acad., Ser. B*, *83*, 97–100.

Ohta, K., S. Onoda, K. Hirose, R. Sinmyo, K. Shimizu, N. Sata, Y. Ohishi, and A. Yasuhara (2008), The electrical conductivity of post-perovskite in Earth's D″ layer, *Science*, *320*, 89–91.

Ohta, K., K. Hirose, K. Shimizu, N. Sata, and Y. Ohishi (2010a), The electrical resistance measurements of $(Mg,Fe)SiO_3$ perovskite at high pressures and implications for electronic spin transition of iron, *Phys. Earth Planet. Inter.*, *180*, 154–158.

Ohta, K., K. Hirose, M. Ichiki, K. Shimizu, N. Sata, and Y. Ohishi (2010b), Electrical conductivities of pyrolitic mantle and MORB materials up to the lowermost mantle conditions, *Earth Planet. Sci. Lett.*, *289*, 497–502.

Olsen, N. (1999), Long-period (30 days–1 year) electromagnetic sounding and the electrical conductivity of the lower mantle beneath Europe, *Geophys. J. Int.*, *138*, 179–187.

Osako, M. (1991), Thermal diffusivity of $MgSiO_3$ perovskite, *Geophys. Res. Lett.*, *18*, 29–242.

Persson, K., A. Bengtson, G. Ceder, and D. Morgan (2006), Ab initio study of the composition dependence of the pressure-induced spin transition in the (Mg1-x,Fex)O system, *Geophys. Res. Lett.*, *33*, L16306, doi:10.1029/2006GL026621.

Polyakov, V. B. (2009), Equilibrium iron isotope fractionation at core-mantle boundary conditions, *Science*, *323*, 912–914.

Richmond, N. C., and J. P. Brodholt (1998), Calculated role of aluminum in the incorporation of ferric iron into magnesium silicate perovskite, *Am. Miner.*, *83*, 947–951.

Ricolleau, A., et al. (2009), Density profile of pyrolite under lower mantle conditions, *Geophys. Res. Lett.*, *36*, L06302, doi:10.1029/2008GL036759.

Ringwood, A. E. (1982), Phase transformations and differentiation in subducted lithosphere: Implications for mantle dynamics basalt petrogenesis and crustal evolution, *J. Geol.*, *90*, 611–642.

Robert, A., J. Wagner, T. Autenrieth, W. Hartl, and G. Grubel (2004), Coherent X-rays as a new probe for the investigation of the dynamics of opaque colloidal suspensions, *J. Magn. Magn. Mater.*, *289*, 47–49.

Romanowicz, B. (2008), Using seismic waves to image Earth's internal structure, *Nature 451*, 266–268

Rustard, J. R., and Q.- Z. Yin (2009), Iron isotope fractionation in the Earth's lower mantle, *Nat. Geosci.*, *2*, 514–518.

Saha, S., A. Bengtson, K. L. Crispin, J. A. Van Orman, and D. Morgan (2011), Effects of spin transition on diffusion of Fe^{2+} in ferropericlase in Earth's lower mantle, *Phys. Rev. B*, *84*, 184102.

Saha, S., A. Bengtson, and D. Morgan (2013), Effect of anomalous compressibility on Fe diffusion in ferropericlase throughout the spin crossover in the lower mantle, *Earth Planet. Sci. Lett.*, *362*, 1–5.

Sakai, T., E. Ohtani, H. Terasaki, N. Sawada, Y. Kobayashi, M. Miyahara, N. Hirao, Y. Ohishi, and T. Kikegawa (2009), Fe-Mg partitioning between perovskite and ferropericlase in the lower mantle, *Am. Miner.*, *94*, 921–925.

Sakai, T., E. Ohtani, H. Terasaki, M. Miyahara, M. Nishijima, N. Hirao, Y. Ohishi, and N. Sata (2010), Fe-Mg partitioning between post-perovskite and ferropericlase in the lowermost mantle, *Phys. Chem. Minerals*, *37*, 487–496.

Sammis, C. G., J. C. Smith, and G. Schubert (1981), A critical assessment of estimation methods for activation volume, *J. Geophys. Res.*, *86*, 10,707–10,718.

Shannon, R. D. (1976), Revised effective ionic radii and systematic studies of interatomic distances in halides and chaleogenides, *Acta Cryst.*, *A32*, 751–767.

Shannon, R. D., and C. T. Prewitt (1969), Effective ionic radii in oxides and fluorides, *Acta Cryst.*, *B25*, 925–746.

Shi, H., W. Luo, B. Johansson, and R. Ahuja (2008), First-principles calculations of the electronic structure and pressure-induced magnetic transition in siderite $FeCO_3$, *Phys. Rev. B*, *78*, 155119.

Shieh, S. R., T. S. Duffy, A. Kubo, G. Shen, V. B. Prakapenka, N. Sata, K. Hirose, and Y. Ohishi (2006), Equation of state of the postperovskite phase synthesized from a natural (Mg,Fe)SiO3 orthopyroxene, *Proc. Natl. Acad. Sci. U.S.A.*, *103*, 3039–3043.

Shieh, S. R., S. M. Dorfman, A. Kubo, V. B. Prakapenka, and T. S. Duffy (2011), Synthesis and equation of state of post-perovskite in the $(Mg,Fe)_3Al_2Si_3O_{12}$ system, *Earth Planet Sci. Lett.*, *312*, 422–428.

Shim, S.H., K. Catalli, J. Hustoft, A. Kubo, V. B. Prakapenka, W. A. Caldwell, and M. Kunz (2008), Crystal structure and thermoelastic properties of $(Mg_{0.91}Fe_{0.09})SiO_3$ postperovskite up to 135 GPa and 2,700 K, *Proc. Natl. Acad. Sci.*, *105*, 7382–7386.

Sinmyo, R., and K. Hirose (2010), The Soret effect in laser-heated diamond-anvil cell, *Phys. Earth Planet. Inter.*, *180*, 172–178.

Sinmyo, R., K. Hirose, H. S. O'Neill and E. Okunishi (2006), Ferric iron in Al-bearing post-perovskites, *Geophys. Res. Lett.*, *33*, L12S13, doi:10.1029/2006GL025858

Sinmyo, R., H. Ozawa, K. Hirose, A. Yasuhara, N. Endo, N. Sata, and Y. Ohishi (2008), Ferric iron content in $(Mg,Fe)SiO_3$ perovskite and post-perovskite at deep mantle conditions, *Am. Mineral.*, *93*, 1899–1902.

Sinmyo, R., K. Hirose, S. Muto, Y. Ohishi, and A. Yasuhara (2011), The valence state and partitioning of iron in the Earth's lowermost mantle, *J. Geophys. Res.*, *116*, B07205, doi:10.1029/2010JB008179.

Sinmyo, R., and K. Hirose (2013), Iron partitioning in pyrolitic lower mantle, *Phys. Chem. Miner.*, *40*, 107–113.

Sinogeikin, S. V., and J. D. Bass (2000), Single-crystal elasticity of pyrope and MgO to 20 GPa by Brillouin scattering in the diamond cell, *Phys. Earth Planet. Inter.*, *120*, 43–62.

Skvortsova, V., N. Mironova-Ulmane, L. Trinkler, and L. Grigorieva (2008), Optical properties of hydrogen-containing MgO crystal, *Proc. of SPIE*, *7142*, 71420E.

Speziale, S., A. Milner, V. E. Lee, S. M. Clark, M. P. Pasternak, and R. Jeanloz (2005), Iron spin transition in Earth's mantle, *Proc. Natl. Acad. Sci. U.S.A.*, *102*, 17,918–17,922.

Speziale, S., V. E. Lee, S. M. Clark, J. F. Lin, M. P. Pasternak, and R. Jeanloz (2007), Effects of Fe spin transition on the elasticity of (Mg, Fe)O magnesiowüstite and implications for the seismological properties of the Earth's lower mantle, *J. Geophys. Res.*, *112*, B10212, doi:10.1029/2006JB004730.

Stacey, F. D., and P. M. Davis (2004), High pressure equations of state with applications to the lower mantle and core, *Phys. Earth Planet. Inter.*, *142*, 137–184.

Stackhouse, S., J. P. Brodholt, D. P. Dobson, and G. D. Price (2006), Electronic spin transitions and the seismic properties of ferrous iron-bearing $MgSiO_3$ post-perovskite, *Geophys. Res. Lett.*, *33*, L12S03, doi:10.1029/2005GL025589.

Stackhouse, S., J. P. Brodholt, and G. D. Price (2007), Electronic spin transitions in iron-bearing MgSiO3 perovskite, *Earth Planet. Sci. Lett.*, *253*, 282–290.

Stackhouse, S., L. Stixrude, and B. B. Karki (2010), Thermal conductivity of periclase (MgO) from first principles, *Phys. Rev. Lett.*, *104*, 208501.

Stixrude, L., and C. Lithgow-Bertelloni (2005), Thermodynamics of mantle minerals—1. Physical properties, *Geophys. J. Int.*, *162*, 610–632.

Sturhahn, W. (2004), Nuclear resonant spectroscopy, *J. Phys. Condens. Matter*, *16*, S497.

Sturhahn, W., J. M. Jackson, and J. F. Lin (2005), The spin state of iron in minerals of Earth's lower mantle, *Geophys. Res. Lett.*, *32*, L12307, doi:10.1029/.2005GL022802.

Tang, X., and J. Dong (2010), Lattice thermal conductivity of MgO at conditions of Earth's interior, *Proc. Natl. Acad. Sci. U.S.A.*, *107*, 4539–4543.

Tange, Y., Y. Nishihara and T. Tsuchiya (2009), Unified analyses for *P-V-T* equation of state of MgO: A solution for pressure-scale problems in high *P-T* experiments, *J. Geophys. Res.*, *114*, B03208, doi:10.1029/2008JB005813.

Tschauner, O., B. Kiefer, H. Liu, S. V. Sinogeikin, M. Somayazulu, and N. S. Lou (2008), Possible structural polymorphism in Al-bearing magnesium-silicate post-perovskite, *Am. Miner.*, *93*, 533–539.

Tsuchiya, T., and X. Wang (2013), Ab initio investigation on the high-temperature thermodynamic properties of Fe^{3+}-bearing $MgSiO_3$ perovskite, *J. Geophys. Res.*, *118*, 83–91, doi:10.1029/2012JB009696.

Tsuchiya, T., J. Tsuchiya, K. Umemoto, and R. M. Wentcovitch (2004), Phase transition in $MgSiO_3$ perovskite in the Earth's lower mantle, *Earth Planet. Sci. Lett.*, *224*, 241–248.

Tsuchiya, T., R. M. Wentzcovitch, C. R. S. da Silva, and S. de Gironcoli (2006), Spin transition in magnesiowüstite in Earth's lower mantle, *Phys. Rev. Lett.*, *96*, 198501.

Van Orman, J. A., C. Li, and K. L. Crispin (2009), Aluminum diffusion and Al-vacancy association in periclase, *Phys. Earth Planet. Inter.*, *172*, 34–42.

Wentzcovitch, R. M., J. F. Justo, Z. Wu, C. R. S. da Silva, D. A. Yuen, and D. Kohlstedt (2009), Anomalous compressibility of ferropericlase throughout the iron spin cross-over, *Proc. Natl. Acad. Sci. U.S.A.*, *106*, 8447–8452.

Wentzcovitch, R. M., H. Hsu, and K. Umemoto (2012), First-principles studies of spin-state crossovers of iron in perovskite, *Eur. J. Mineral.*, *24*, 851–862.

Wirth, R. (2009), Focused ion beam (FIB) combined with SEM and TEM: Advanced analytical tools for studies of chemical composition, microstructure and crystal structure in geometerials on a nanometer scale, *Chem. Geol.*, *261*, 217–229.

Wood, B. J. (2000), Phase transformations and partitioning relations in peridotitieunder lower mantle conditions, *Earth Planet. Sci. Lett.*, *174*, 341–354.

Wu, Z., J. F. Justo, C. R. S. da Silva, S. de Gironcoli, and R. M. Wentzcovitch (2009), Anomalous thermodynamic properties in ferropericlase throughout its spin crossover, *Phys. Rev. B*, *80*, 014409.

Yamanaka, T., K. Hirose, W. L. Mao, Y. Menge, P. Ganesh, L. Shulenburger, G. Shen, and R. J. Hemley (2012), Crystal structures of $(Mg_{1-X},Fe_X)SiO_3$ postperovskite at high pressures, *Proc. Natl. Acad. Sci. U.S.A.*, *109*, 1035–1040.

Yamazaki, D., and T. Irifune (2003), Fe-Mg interdiffusion in magnesiowüstite up to 35 GPa, *Earth Planet. Sci. Lett.*, *216*, 301–311.

Yoshino, T., E. Ito, T. Katsura, D. Yamazaki, S. Shan, X. Guo, M. Nishi, Y. Higo, and K. Funakoshi (2011), Effect of iron content on electrical conductivity of ferropericlase with implications for the spin transition pressure, *J. Geophys. Res.*, *116*, B04202, doi:10.1029/2010JB007801.

Yu, Y. G., H. Hsu, M. Cococcioni, and R. M. Wentzcovitch (2012), Spin states and hyperfine interactions of iron incorporated in $MgSiO_3$ post-perovskite, *Earth Planet. Sci. Lett.*, *331–332*, 1–7.